Non-Traditional Stable Isotope Variations: Applications for Biomedicine

by

Jennifer Lynn Louden Morgan

A Dissertation Presented in Partial Fulfillment
of the Requirements for the Degree
Doctor of Philosophy

Approved April 2011 by the
Graduate Supervisory Committee:

Ariel D. Anbar, Chair
Anne K. Jones
Everett Shock
Laura E. Wasylenki

ARIZONA STATE UNIVERSITY

May 2011

ABSTRACT

Applications of non-traditional stable isotope variations are moving beyond geosciences to biomedicine, made possible by advances in multiple collector inductively coupled plasma mass spectrometry (MC-ICP-MS) technology. Mass-dependent isotope variation can provide information about the sources of elements and the chemical reactions that they undergo. Iron and calcium isotope systematics in biomedicine are relatively unexplored but have great potential scientific interest due to their essential nature in metabolism.

Iron, a crucial element in biology, fractionates during biochemically relevant reactions. To test the extent of this fractionation in an important reaction process, equilibrium iron isotope fractionation during organic ligand exchange was determined. The results show that iron fractionates during organic ligand exchange, and that isotope enrichment increases as a function of the difference in binding constants between ligands.

Additionally, to create a mass balance model for iron in a whole organism, iron isotope compositions in a whole mouse and in individual mouse organs were measured. The results indicate that fractionation occurs during transfer between individual organs, and that the whole organism was isotopically light compared with food. These two experiments advance our ability to interpret stable iron isotopes in biomedicine.

Previous research demonstrated that calcium isotope variations in urine can be used as an indicator of changes in net bone mineral balance. In order to measure calcium isotopes by MC-ICP-MS, a chemical purification method was developed to quantitatively separate calcium from other elements in a biological matrix. Subsequently, this method was used to evaluate if calcium isotopes

respond when organisms are subjected to conditions known to induce bone loss: 1) Rhesus monkeys were given an estrogen-suppressing drug; 2) Human patients underwent extended bed rest. In both studies, there were rapid, detectable changes in calcium isotope compositions from baseline - verifying that calcium isotopes can be used to rapidly detect changes in bone mineral balance.

By characterizing iron isotope fractionation in biologically relevant processes and by demonstrating that calcium isotopes vary rapidly in response to bone loss, this thesis represents an important step in utilizing these isotope systems as a diagnostic and mechanistic tool to study the metabolism of these elements *in vivo*.

DEDICATION

This document and my overall PhD experience are dedicated to my family. Specifically, I want to acknowledge, my dad, my mom, and my wonderful husband, who was with me for every single moment.

Dad, your constant support while you were here has propelled me through this very challenging process. Education was so important to you, and you instilled that passion for knowledge in me. I wish more than anything that you could have watched me undertake this challenge and ultimately overcome it. I take comfort in the fact that you were a huge part of my success.

Mom, your support and love have been invaluable. Your sympathetic ear when things were not going my way means the world. I appreciate all your trips to Arizona to distract me from work, at least for a little while, and to spoil me. I love you.

Adam, you were there everyday, for the good days and for the bad. You kept me motivated and focused to reach my goal. I could not have done this without your love and support. Thank you. I love you so much and I am looking forward to the next step.

ACKNOWLEDGMENTS

Funding: The iron research of this dissertation was supported by NSF-EAR 0519347 to A.D.A. and L.E.W. Calcium research was supported by NASA Astrobiology institute. Funding provided by NASA's Human Research Project Grant number NNX08AQ36G (PI Anbar).

Help and Support: I want to take time to thank everyone who I have worked with throughout my graduate studies. First, I want to thank my advisor Dr. Ariel Anbar for his patience and support. I appreciate the guidance and advice that my graduate committee, Dr. Anne Jones, Dr. Everett Shock, and Dr. Laura Wasylenki provided. I also want to especially thank Dr. Gwyneth Gordon with the day-to-day issues and for always being so supportive. In addition, I would also like to thank Dr. Gail Arnold, Dr. Felisa Wolf-Simon, and Dr. Laura Wasylenki for the mentoring they provided me early on. I want to thank fellow graduate students Sarah Staton, Yun Duan, Katie Noonan, Jennifer Glass, Greg Brennecka, Chris Mead, Alex Hamilton, and Jessie Shipp. I would like to especially thank Stephen Romaniello for always being there to bounce ideas off of. I also want to thank Carrina Arrua and Christy Meza for their help in lab.

TABLE OF CONTENTS

LIST OF TABLES

LIST OF FIGURES

Chapter 1

REVIEW OF NON-TRADITIONAL STABLE ISOTOPE PRINCIPLES, MASS SPECTROMETRY, AND THE MEASUREMENTS OF IRON AND CALCIUM ISOTOPES IN BIOLOGICAL SAMPLES

Jennifer L. L. Morgan[1]

[1]Department of Chemistry and Biochemistry, Arizona State University, Tempe AZ 85287

1.1 Introduction

Frederick Soddy in 1914 was the first to introduce the concept of an isotope. He defined isotopes as atoms of a single element that have different atomic weights (Soddy, 1914). This definition changed the way scientists thought about atoms and provided an explanation for phenomena like radioactivity. J.J. Thomson confirmed the existence of neon isotopes (Thomson, 1913). Thompson used a “cathode ray tube”, an early version of today’s mass spectrometers that separated different charge to mass ratios. Using this instrument, he and others rapidly discovered isotopes for almost all atoms.

Isotopes can be subdivided into radioactive or stable isotopes depending on whether they decay into “daughter” atoms. Stable isotopes can be further subdivided into radiogenic and nonradiogenic stable isotopes based on their origin. The focus of this dissertation is nonradiogenic stable isotopes.

The atomic weights of elements given on the periodic table are the average of all the isotopes for that element, weighted by isotopic abundance. If the isotope composition of an atom in all materials were truly invariant, as is implied by the singular atomic weights on the periodic table, then there would be no utility in measuring the

isotope compositions of different materials. However, isotope compositions are not uniform, and these variations can be used to obtain information about the sources or the reaction mechanisms of a given element. The types of reactions that cause isotope variation or “fractionation” are described in the next section and are reviewed elsewhere (Criss, 1999).

1.2 Isotope Fractionation Principles

Mass-dependent stable isotope fractionation occurs when isotopes of a given element are enriched or depleted in different pools as a function of mass. Fractionation is most pronounced when the relative mass differences are large, as for light elements like hydrogen, carbon, or oxygen. Fractionation also occurs for larger elements with smaller relative mass differences like iron, molybdenum and uranium.

The isotope fractionation between pools can provide clues about the sources of an element to one or the other pool and about the chemical or physical processes that transfer an element between the pools. There are two main types of isotope effects: non-equilibrium and equilibrium isotope effects. The magnitude and direction of the isotope abundance can change depending on whether the reaction is controlled by kinetic, equilibrium or a combination of processes. For an isotope fractionation to be detectable, the reaction must be incomplete. If the reactant pool is exhausted, then the isotope composition of the product pool will be identical to the original reactant pool because of mass balance; reactions that go to completion leave no signature of any isotope variation.

Any process that is unidirectional and incomplete can express non-equilibrium or kinetic isotope effects. An example of a non-equilibrium effect is the fractionation that occurs during diffusion in a gas or liquid phase. Diffusion causes an isotope fractionation

because isotopes with smaller mass move faster according to Graham's law of diffusion (Equation 1), where υ_1 and υ_2 are velocities and m_1 and m_2 are the masses of the isotopes.

$$\frac{\upsilon_1}{\upsilon_2} = \sqrt{\frac{m_2}{m_1}} \qquad (1)$$

The lighter isotopes travel faster, leaving the starting material enriched in heavy isotopes.

A second type of non-equilibrium isotope effect is the kinetic isotope effect. Kinetic isotope effects can result from differences in dissociation energies between chemical bonds involving different isotopes of the same element. In this type of reaction, the bond-breaking step in a chemical reaction requires less energy when breaking a bond involving a light isotope than the same bond involving a heavier isotope. This preference enriches the product pool in light isotopes and in turn depletes the reactant pool of light isotopes.

Another type of isotope fractionation is an equilibrium isotope effect. In this case, the reaction continues until the overall system is at the lowest energy state. The potential energy is typically lower for bonds involving heavier isotopes. Therefore, in the lowest energy state the heavier isotopes will usually be enriched in the molecules that create the strongest bonds (Figure 1-1).

In biological systems, isotope fractionation is most likely a combination of multiple fractionation processes including equilibrium, diffusion and kinetic effects. The most common example is the difference in carbon isotope composition between C3 (vegetables and trees) and C4 (grasses and corn) plants. The diffusion of CO_2 into the plants causes both types of plants to be enriched in ^{12}C over the atmospheric carbon

isotope composition (Osmond et al., 1973). Preferential incorporation of the ^{12}C isotope into plant material causes C3 plants to be more enriched in ^{12}C compared to C4 plants. This variation extends up the food chain as higher organisms consume these plants. By measuring this variation, the dominant diet of extinct and modern animal species, ancient human migration patterns and even the sources of sugar in commercial products can be determined (DeNiro and Epstein, 1978a; DeNiro and Epstein, 1978b).

In this dissertation, biological fractionations of the isotopes of the elements Fe and Ca are investigated. The long-term goal – beyond the scope of this dissertation – is to use the stable isotope variations of these elements as diagnostic markers for diseases and to understand metal metabolism *in vivo*. Such applications have been limited because until recently mass spectrometers were unable to detect the small natural variations in isotope compositions that result from mass fractionation for elements heavier than sulfur. New mass spectrometry technology has made the measurements of these “non-traditional” stable isotopes possible.

1.3 Mass Spectrometry

There are many varieties of mass spectrometers. All have three basic components, but the details of design and operation are variable. All mass spectrometers have: 1) a source of ions; 2) a mass analyzer to separate ions based on mass-to-charge ratios; and 3) at least one ion detector. The mass spectrometers utilized for this dissertation are the Thermo Scientific X series quadrupole inductively coupled plasma mass spectrometer (Q-ICP-MS) and the Thermo Scientific Neptune multiple collector inductively coupled plasma mass spectrometer (MC-ICP-MS). The MC-ICP-MS was used for the high precision measurements of isotope compositions that are at the

core of the research. The Q-ICP-MS was used during methods development. A detailed description of each instrument follows.

Q-ICP-MS

A diagram of a generic quadrupole inductively coupled plasma mass spectrometer (Q-ICP-MS) is shown in Figure 1-2. Q-ICP-MS is primarily used to rapidly measure the concentrations of a variety of different elements in a sample. The X Series Q-ICP-MS uses an RF generator operating at 1400 W to generate an argon plasma which ionizes the analyte. The analyte is introduced as an aqueous solution using a nebulizer. To separate species with different mass to charge ratios, the quadrupole mass spectrometer uses four rods parallel to and surrounding the ion beam. An alternating voltage is applied to these four rods and, depending on the frequency and strength of the electromagnetic field, specific elemental masses are allowed to pass through the cavity between the four rods in a helical path. The single detector is an ion-counting electron multiplier, which is very sensitive in detecting charged particles; it can also measure voltages for excessively large signals. This property allows for large dynamic range of measurable concentrations.

The electric field in the instrument can be varied to separate and analyze almost all the elements from Na to U in less than a minute. The signal strength of known standards can be used to create calibration curves for concentration measurements of unknowns. Detection limits are element-dependant. For example, uranium and similar metals have detection limits as low as a few ppt (parts per trillion), while major elements have higher background levels and correspondingly higher detection limits.

While Q-ICP-MS has made it straightforward to measure a large number of elements in a sample rapidly, accurately and precisely, this type of instrument cannot

easily measure isotope ratios to a precision of better than ~ 1%. This precision is not adequate to resolve natural variations in isotope composition that result from mass fractionation in the case of elements like Fe and Ca.

MC-ICP-MS

A diagram of the Thermo Neptune multiple collector inductively coupled plasma mass spectrometer (MC-ICP-MS) is shown in Figure 1-3. As with the X Series Q-ICP-MS, the Neptune MC-ICP-MS uses an RF generator to produce an energetic argon plasma to ionize the sample. The Neptune uses a large magnetic sector to separate ions according to their charge-to-mass ratios. By using a magnet, multiple ion beams can travel through the flight tube, so that they can be detected simultaneously. The detectors consist of nine Faraday cups that can be mechanically moved to align with the ion beams of the multiple isotopes. Simultaneous measurement of multiple ion beams with an MC-ICP-MS provides an advantage over a single detector instrument in measuring isotope ratios because most variations in the intensities of the ion beams are correlated in time. If these ion beams were measured at different times, as required in a single collector instrument, the measurement of the isotope ratio would be affected by this variability. Therefore, multiple collector instruments allow more precise measurement of isotope ratios.

The Neptune is a pseudo-high resolution instrument. Resolution is the degree to which an instrument can resolve or separate peaks based on mass. High resolution is important to measurements of Fe and Ca isotopes because of isobaric polyatomic interferences. In order for an instrument to be a “true” high-resolution instrument, there must be narrow entrance and exit slits. The Neptune only has narrow entrance slits. However, Fe and Ca isotope composition can still be measured on the Neptune MC-

ICP-MS (Arnold et al., 2004a; Weyer and Schwieters, 2003a; Wieser et al., 2004). Measuring Fe and Ca isotopes on the Neptune MC-ICP-MS require the isotopes to be measured on peak shoulders because the instrument cannot fully resolve the isobaric interferences (Figure 1-4 and Figure 1-5). The medium and high-resolution slits on the Neptune MC-ICP-MS provide enough resolution so the low mass side of the Fe or Ca peak is free of isobaric interferences.

A critical challenge to high precision measurements of isotope composition by MC-ICP-MS is that ICP instruments induce a large mass-dependent isotope fractionation during measurement. This instrument fractionation or “mass bias” is substantially larger than the natural variations being measured. This instrument fractionation primarily occurs during transfer of the ions through the cones that separate the atmospheric pressure ion source from the vacuum of the mass analyzer. When the ions are accelerated through the cones, traveling from high pressure to low pressure, a zone of supersonic expansion is produced. In this region, the light isotopes expand outward preferentially relative to the heavier isotopes. The light isotopes on the outside of the ion cloud tend to get pumped away by the interface pump (Marechal et al., 1999).

There are three ways that this instrumental mass bias is corrected: standard-sample-standard bracketing; element doping; and the double spike method. The double spike method was not used in this dissertation and will not be reviewed here. Descriptions of the double spike method are be found elsewhere (Dideriksen et al., 2006; Ripperger and Rehkamper, 2007; Beard et al., 2003; Siebert et al., 2001; Russell et al., 1978).

1) Standard-Sample-Standard bracketing involves measuring a known standard before and after every sample. The sample’s isotope value is calculated relative to the

average of the two bracketing standards. This method offers a sufficiently precise correction as long as the matricies of samples and the standard are similar. Similar matricies are necessary because of the potential effects of non-isobaric organic or elemental contaminants in that are not removed by the sample purification procedures. A limitation of this technique is that it assumes that any change in mass bias during the course of analysis is linear over time, so that the average of the bracketing standards provides a good estimate of the standard value at the time of the sample measurement. This assumption is not always valid. Additionally, this method requires quantitative yield from any element purification procedures, such as column chromatography, because these procedures may fractionate isotopes to the same extent as the natural variations being measured.

2) Element Doping uses another element close in mass and ionization energy to the analyte element to monitor instrumental mass bias and to correct for it. This method is typically combined with standard-sample-standard bracketing. For example, when measuring Fe, a Cu solution of a known natural isotope composition is added to samples and standards, and the mass fractionation undergone by the Cu isotopes is used to determine and compensate for the instrumental fractionation undergone by Fe isotopes. This method monitors and corrects for time-dependent variations in mass bias. It can also compensate, to some extent, for differences in matricies between samples and standard. However, this method requires the use of more detector cups, which may require the magnet to rapidly switch its field strength (magnet jumping) and hence increase the analysis time. A magnet jump may also be needed if the mass dispersion between the two elements is larger than the Neptune can accommodate. For example, the Neptune cannot simultaneously measure ^{57}Fe and ^{63}Cu because these two ion

beams cannot simultaneously pass through the flight tube to the detectors. This technique also assumes that the relative mass bias for the analyte element and the doping element is constant during the course of the analysis and between samples and standard (Barling et al., 2001), assumptions that may not always hold in detail. Another disadvantage is that the sample has to be rigorously purified of the doping element, to ensure that the isotope composition of this element is identical for standards and samples. Quantitative yields during sample purification are also required for the element doping technique.

In this dissertation, standard-sample-standard bracketing alone was used for Ca isotope measurement because there is not an element with the same ionization properties that does not interfere with the Ca measurement. An element doping along with standard-sample-standard bracketing was used to measure Fe isotopes since utilization of Cu for this purpose are already well developed. Quality control was checked using both techniques to insure data quality.

The Neptune MC-ICP-MS offers several advantages over thermal ionization mass spectrometry (TIMS), which previously was the common mass spectrometric method used to measure high-precision isotope ratios for heavier elements. Many of the advantages center on higher sample throughput. The TIMS sample introduction system requires deposition of the purified sample on a filament, conversion to a solid state and a slow warm up to ionize the sample. Measurement of a single sample on TIMS can require hours of analysis time, versus several minutes for MC-ICP-MS. TIMS ionization is done in a vacuum and TIMS sample turrets are limited in the number of samples and standards that can be introduced without breaking the vacuum, further reducing sample throughput. In contrast, the sample throughput of MC-ICP-MS is only limited by the

willingness of operators to refill an auto sampler that sits outside the vacuum of the mass analyzer. This, the sample introduction system on the MC-ICP-MS allows between 20-80 samples to be analyzed per day without the need for a highly trained technician monitoring instrument progress. Sample-standard-sample bracketing on TIMS is ineffective because the analytical conditions for samples and standards loaded on different filaments are not consistent enough. Element doping is not possible because the ionization efficiencies among elements can be vastly different. Therefore, TIMS requires use of a double spike.

1.4 Iron Isotopes in Biomedicine

Iron is an essential element for all known life. It is the metal center in many critical enzymes and performs many tasks in biology including acting as an oxygen transporter, redox active center, and catalyst for biotransformations. The variety of coordination environments for Fe in biological systems gives rise to its rich and vital biochemistry; this same variety of binding environments holds the potential for significant isotope fractionation between biological reservoirs. Iron isotopes may be useful for studying Fe metabolism *in vivo* and may be used to gain information about Fe diseases like anemia and hemochromatosis.

Iron has four naturally occurring stable isotopes ^{54}Fe (5.85%), ^{56}Fe (91.76%), ^{57}Fe (2.12%) and ^{58}Fe (0.28%). Early studies proposed that Fe isotope variations in the rock record might be a useful biosignature because Fe reducing bacteria produced Fe isotope fractionation on the magnitude of what was observed in the rock record (Beard et al., 1999). This proxy has proved to be problematic because a number of abiotic reactions also substantially fractionate Fe [see reviews by (Anbar et al., 2000; Anbar and Rouxel, 2007b; Beard et al., 2003; Dauphas and Rouxel, 2006; Johnson et al., 2008;

Johnson et al., 2004)]. Measuring the Fe isotope fractionation in model abiotic experiments like reduction, separation chemistry and ligand exchange (Dideriksen et al., 2008; Johnson et al., 2002; Roe et al., 2003) helps us further understand the magnitude and direction of Fe fractionation for different reactions and can be useful in interpreting these signals in biology. In addition to experiments, several theoretical frameworks exist to predict the magnitude of Fe isotope fractionation based on vibrational frequencies and Mössbauer shifts (Domagal-Goldman and Kubicki, 2008; Domagal-Goldman et al., 2009; Polyakov, 1997; Polyakov and Mineev, 2000; Schauble et al., 2001). Performing controlled experiments and measuring the Fe isotope ratios can test these predictions, but on their own they are useful tools in estimating the fractionation in biology.

Several preliminary studies measured the Fe isotopic variation in biological samples:

- The isotope composition of human blood is offset lightward from dietary Fe values and light Fe is enriched along the food chain (Walczyk and von Blanckenburg, 2002; Walczyk and von Blanckenburg, 2005).
- Blood from males is enriched in light Fe isotopes compared to females indicating that females lose more light Fe compared with males, or absorb heavy Fe preferentially. Since blood is isotopically light, the loss of blood during menstruation is the most likely cause of the isotope offset between males and females. (Walczyk and von Blanckenburg, 2002; Walczyk and von Blanckenburg, 2005).
- The Fe isotope composition of blood from vegetarians and omnivores was measured, however, there was no significant difference between the two populations (Krayenbuehl et al., 2005).

- The isotope composition of patients with hemochromatosis, a genetic disease that is characterized by excessive Fe content in organs and tissue because Fe absorption, is poorly regulated. The Fe isotope composition of blood in patients with hemochromatosis was isotopically heavy compared to healthy individuals. Fractionation during import is not as strong for patients with hemochromatosis (Krayenbuehl et al., 2005).
- The Fe isotope composition of minipig intestine was found to be isotopically lighter than food indicating that this is the location where isotope fractionation occurs (Hotz et al., 2011).

While these studies have begun to investigate the application of Fe isotopes to biomedicine, more research is needed to move Fe isotopes from a series of interesting observations to an elucidation of biochemical mechanisms.

In this dissertation, two important experiments expanded this knowledge base. The first experiment assessed the equilibrium Fe isotope fractionation during organic ligand exchange (CHAPTER 2). The second experiment measured the Fe isotope composition of various organs in a mouse model and created an isotope mass balance model of the organism (CHAPTER 3). Both experiments were necessary steps to advance the use of Fe isotopes in biomedical applications.

1.5 Calcium Isotopes in Biomedicine

Calcium has many important functions in biology. In addition to forming the skeletal system in mammals, it also acts as a signaling element that regulates the heartbeat, controls osmotic pressure and allows nerve cells to communicate with each other. The main reservoir for Ca in the body is the skeleton, presenting a unique opportunity for using Ca isotopes to explore bone health and metabolism.

There are six stable or long-lived Ca isotopes: ^{40}Ca (96.941%), ^{42}Ca (0.647%), ^{43}Ca (0.135%), ^{44}Ca (2.086%), ^{46}Ca (0.004%), and ^{48}Ca (0.187%). Until recently, the Ca isotope composition of various materials was mainly been measured by Thermal Ionization Mass Spectrometry (TIMS) (DePaolo, 2004; Skulan et al., 2007; Skulan and Depaolo, 1999; Skulan et al., 1997). The measurement of Ca isotopes on MC-ICP-MS was recently introduced for Ca-rich samples like calcium carbonate rocks (Wieser et al., 2004). Despite the inability of MC-ICP-MS to measure the ^{40}Ca isotope because of the unresolvable ^{40}Ar interference from the argon plasma, the higher sample throughput of MC-ICP-MS offers an advantage that is especially important for biomedical studies which require a large number of samples and patients. However, prior to this dissertation research, only samples with high Ca content relative to other elements were measured for isotope variations by MC-ICP-MS (e.g., dissolved $CaCO_3$ rocks). The measurement of Ca isotopes in complex matrices like urine and blood that have much lower relative abundances of Ca presented new analytical challenges that are addressed in CHAPTER 4.

The biomedical applications of Ca isotopes are more established than are those of Fe isotopes. Previous studies have shown that there is a systematic isotope offset between bone and soft tissue in a variety of animals (Skulan and Depaolo, 1999). This observation led to the hypothesis that Ca isotopes are fractionated during bone formation, but that there is no fractionation during bone resorption because of the quantitative nature of resorption. A simple box model describing the bone and soft tissue isotope composition was established and is shown in Figure 1-6 (Skulan and Depaolo, 1999). This model led to the hypothesis that changes in the isotopic compositions of soft tissues like urine and blood could be used to monitor changes in bone mineral balance

in organisms. Bone mineral balance (BMB) is the rate of bone formation compared to bone loss.

An effective experimental model to examine bone loss is bed rest; during bed rest, reduced gravitational loading on the skeleton leads to a marked decreases in bone density. To test the usefulness of Ca isotopes to detect this change, a prior study tested archived urine samples from a 90-day bed rest experiment (Skulan et al., 2007). Patients in this study were placed into one of three groups: a control group, a group that exercised, and a group given the drug alendronate. Alendronate is a bone resorption inhibitor that can be used as a countermeasure to bone loss. It is commonly prescribed to slow the rate of bone loss associated with osteoporosis. Skulan et al. (2007) observed differences in the Ca isotope systematics between the three groups consistent with expectations (Figure 1-7). This research provided the first evidence that the Ca isotope composition of soft tissue can be used as in indicator of changes in bone mineral balance.

A more recent study examined the isotope composition of urine in two patients in significantly different states of bone mineral balance, a young boy (12 yrs) and an old woman (84 yrs). The isotope compositions of these two patients over a 30 day period were systematically different from each other (Heuser and Eisenhauer, 2010). The Ca isotope offset between these two patients was proposed to be a measure of age, gender and bone health status. This study discussed some of the complicating issues that may arise when attempting to use Ca isotopes to detect bone mineral balance including the fractionation during absorption in the intestines, the renal fractionation and dietary variation (Heuser and Eisenhauer, 2010).

This dissertation reports methods developed to achieve high sample throughput for Ca isotope measurements using MC-ICP-MS (CHAPTER 4). These methods were then applied in two biomedically relevant studies. First, the ability to use Ca isotopes to detect changes in BMB during estrogen-depleted bone loss in a non-human primate model, the female rhesus monkey, was tested (CHAPTER 5). Second, the rapidity of bone loss in a 30-day bed rest study was examined (CHAPTER 6). These studies constitute important steps in validating the use of Ca isotopes in biomedical research and indicate potential for clinical applications.

1.6 Layout of Dissertation

This dissertation is made up of five chapters. Each has been or will be submitted for publication in peer-reviewed journals. The co-authors of each chapter have given their permission for reprint in this dissertation. If the manuscript has been published, the reference information is provided below the title. If the manuscript is in review or submitted, no information about the journal will be provided in print due to the press embargo policies of certain journals.

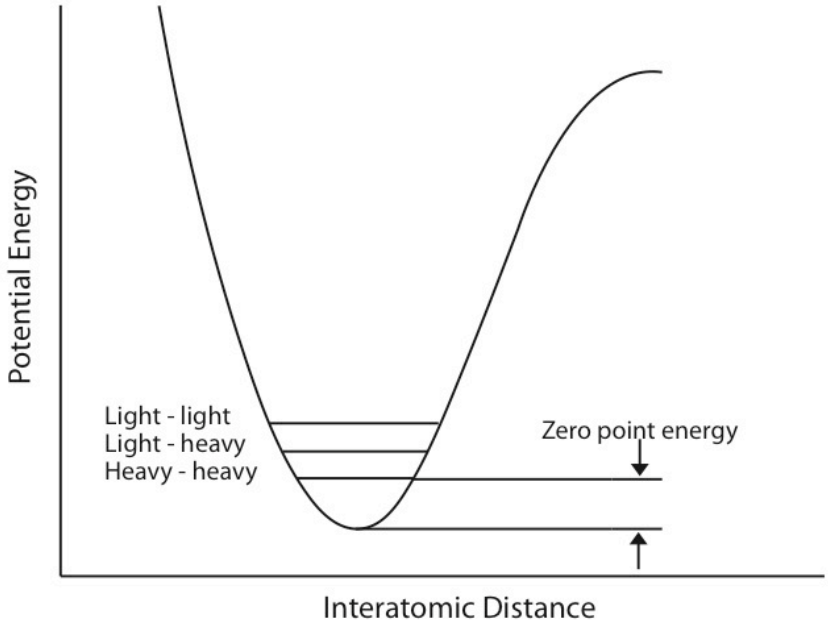

Figure 1-1 Potential energy diagram and zero point energies for different combinations of isotopes.
The zero point energy for heavier isotopes or molecules is lower than for lighter isotopes or molecules.

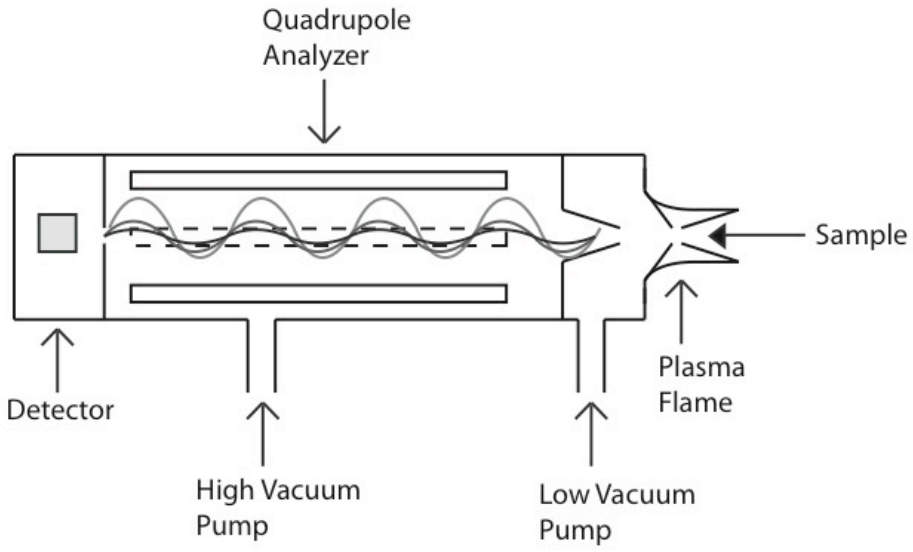

Figure 1-2 Schematic of quadrupole ICP-MS.
Modified from schematic in (Dawson, 1976).

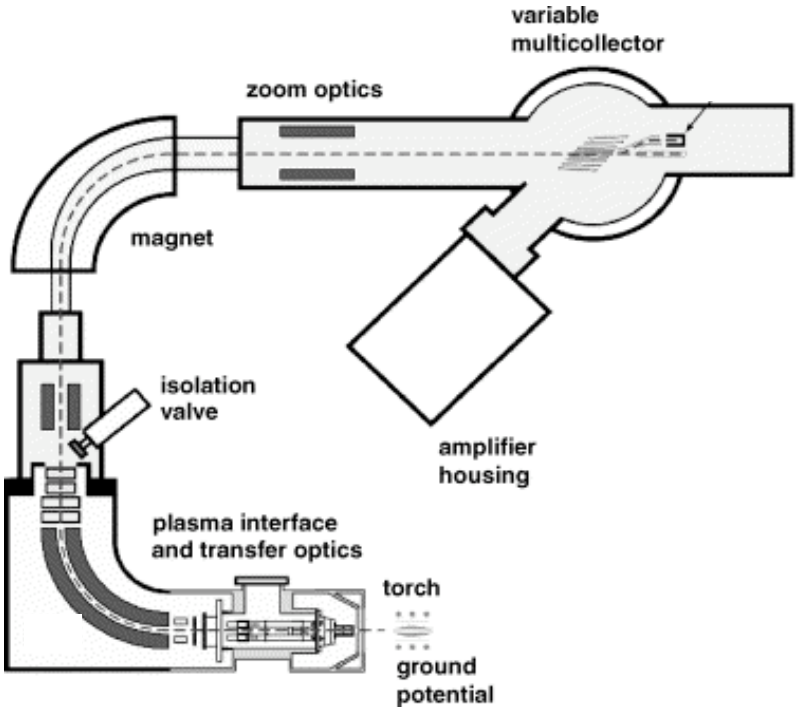

Figure 1-3 Schematic of Thermo Scientific Neptune MC-ICP-MS.
Reprinted with permission from Thermo Scientific and Elsevier (Weyer and Schwieters, 2003a).

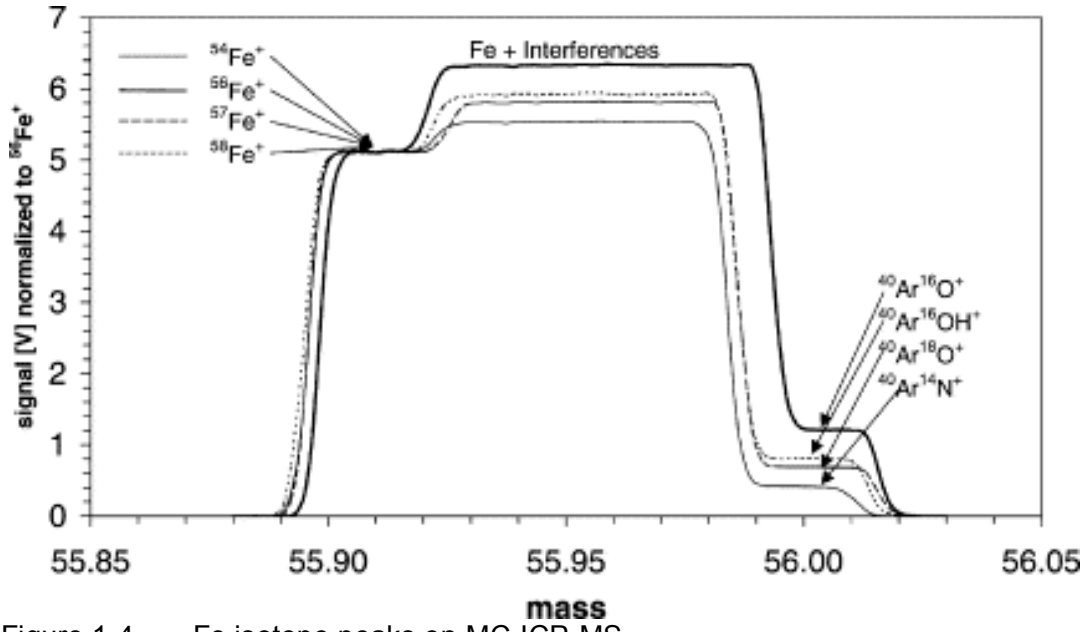

Figure 1-4 Fe isotope peaks on MC-ICP-MS.
Demonstrating Fe resolution and the need to measure Fe on peak shoulder (Weyer and Schwieters, 2003a). Reprinted with permission from Elsevier.

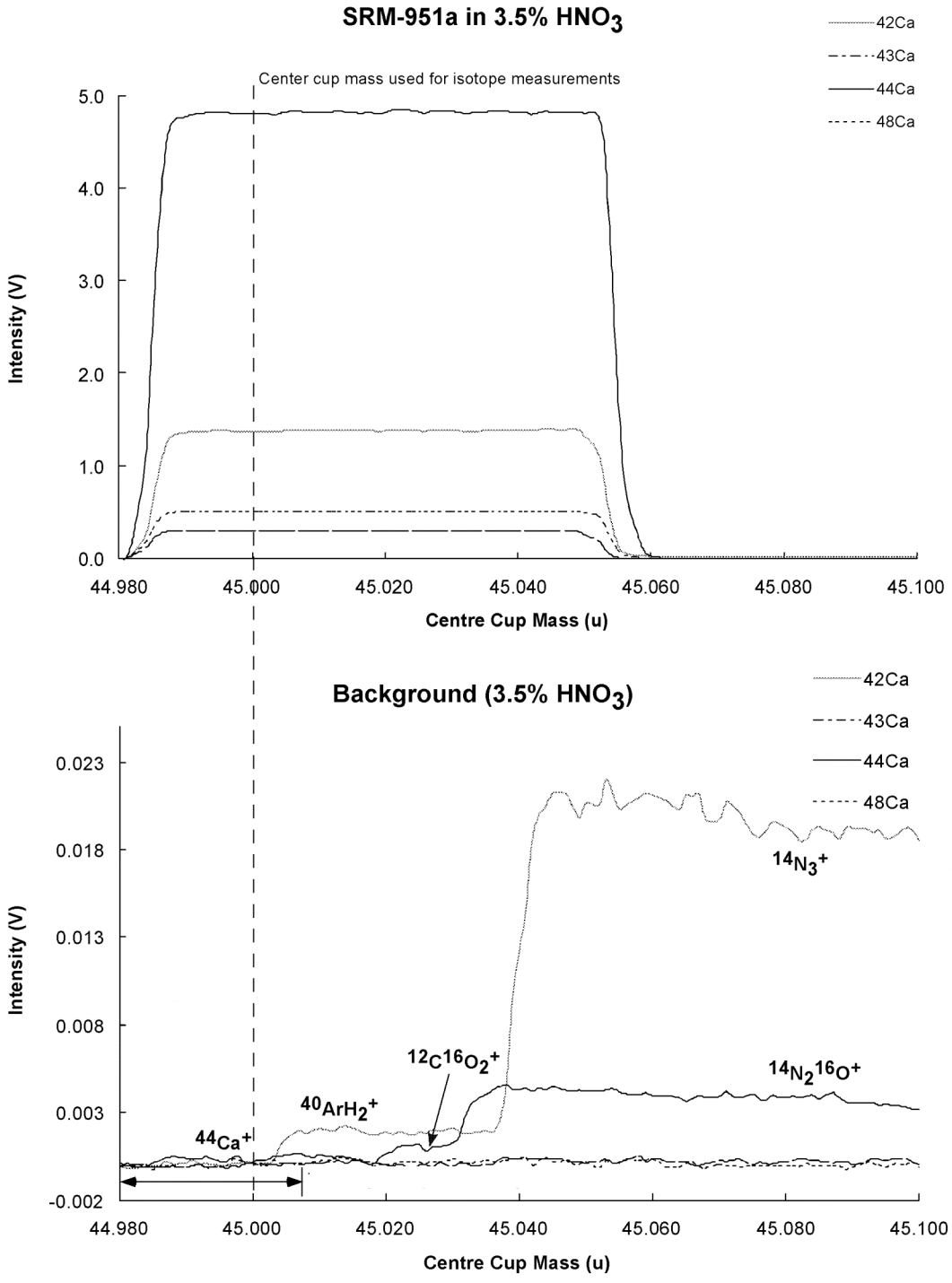

Figure 1-5 Ca peak and interferences on MC-ICP-MS.
Reproduced with permission of The Royal Society of Chemistry. (Wieser et al., 2004).

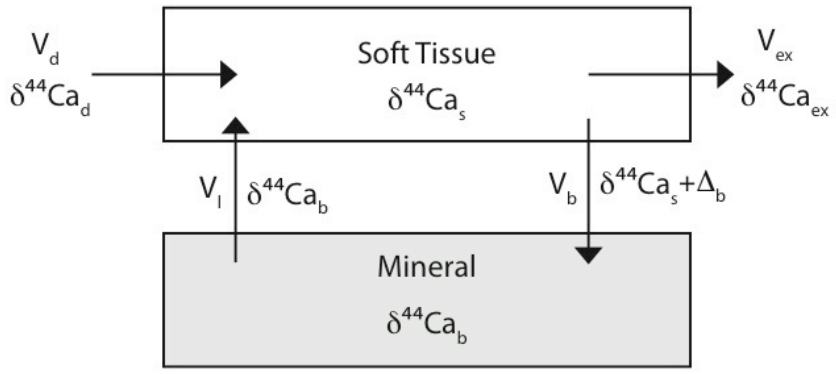

Figure 1-6 Box diagram of bone and soft tissue to monitor bone loss using Ca isotopes.
$\delta^{44}Ca$ is the isotope composition of a given reservoir. Δ_b is the fractionation into bone. V is the Ca flux. d, is diet; s is soft tissue, b is bone, and ex is excretion. Modified from (Skulan and Depaolo, 1999).

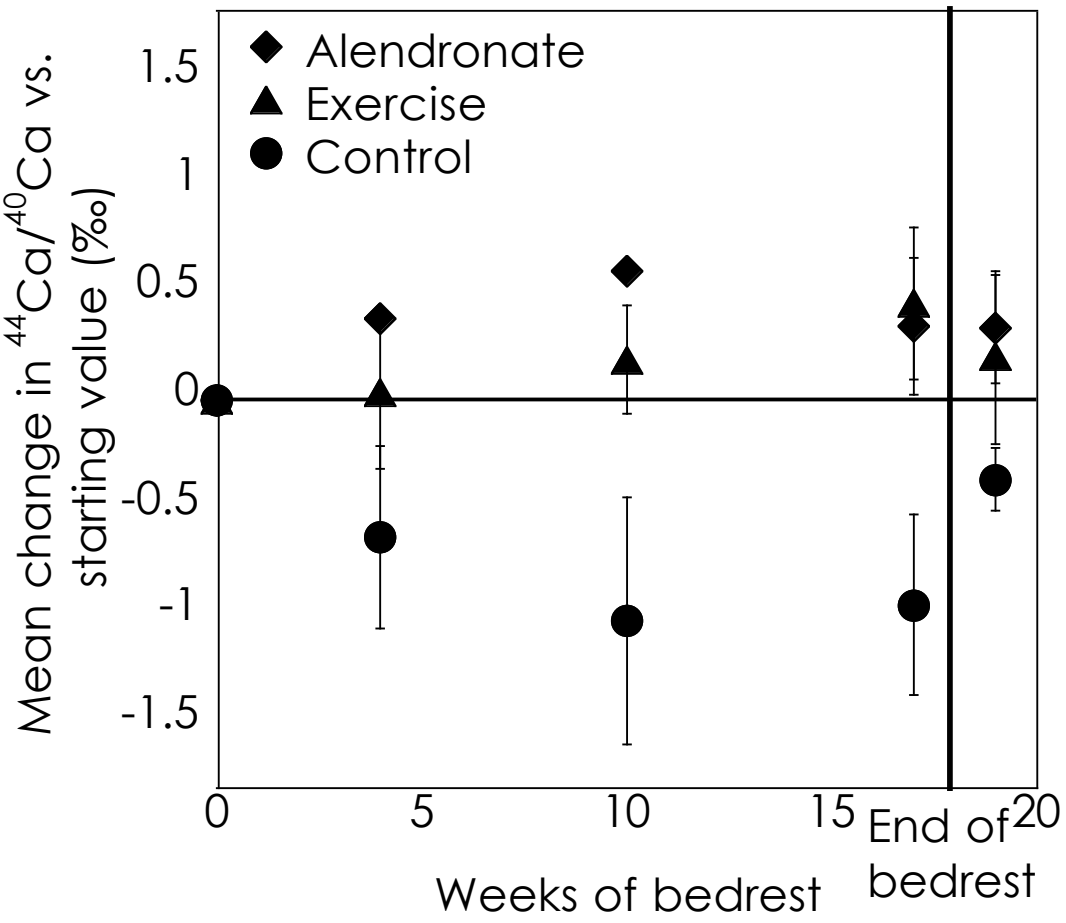

Figure 1-7 Results of previous bed rest study; Ca isotope vs. time. Modified from data presented in (Skulan et al., 2007).

1.7 References

Anbar, A. D., Roe, J. E., Barling, J., and Nealson, K. H. (2000). Nonbiological Fractionation of Iron Isotopes. Science *288*, 126-128.

Anbar, A. D., and Rouxel, O. (2007). Metal Stable Isotopes in paleoceanography. Annu Rev Earth Planet Sci *35*, 717-746.

Arnold, G., Weyer, S., and Anbar, A. D. (2004). Fe isotope variations in natural materials measured using high mass resolution multiple collector ICPMS. Anal Chem *76*, 322-327.

Barling, J., Arnold, G., and Anbar, A. D. (2001). Natural mass-dependent variations in the isotopic composition of molybdenum. Earth and Planetary Science Letters *193*, 447-457.

Beard, B. L., Johnson, C. M., Cox, L., Sun, H., Nealson, K. H., and Aguilar, C. (1999). Iron isotope biosignatures. Science *285*, 1889-1892.

Beard, B. L., Johnson, C. M., Skulan, J. L., Nealson, K. H., Cox, L., and Sun, H. (2003). Application of Fe isotopes to tracing the geochemical and biological cycling of Fe. Chem Geol *195*, 87-117.

Criss, R. E. (1999). Principles of Stable Isotope Distribution (New York: Oxford University Press).

Dauphas, N., and Rouxel, O. (2006). Mass spectrometry and natrual variations of iron isotopes. Mass Spectrom Rev *25*, 515-550.

Dawson, P. H. (1976). Quadrupole Mass Spectrometry and its Application: Elsevier).

DeNiro, M. J., and Epstein, S. (1978a). Carbon isotopic evidence for different feeding patterns in two hyrax species occupying the same habitat. Science *201*, 906-908.

DeNiro, M. J., and Epstein, S. (1978b). Influence of deit on distribution of carbon isotopes in animals. Geochimica et Cosmochimica Acta *42*, 495-506.

DePaolo, D. J. (2004). Calcium Isotopic Variations Produced by Biological, Kinetic, Radiogenic and Nucleosynthetic Processes, In Geochemistry of non-traditional stable isotopes, C. Johnson, B. Beard, and F. Albarede, eds. (Mineralogical Society of America), pp. 255-288.

Dideriksen, K., Baker, J. A., and Stipp, S. L. S. (2006). Iron isotopes in natural minerals determined by MC-ICP-MS with a 58Fe-54Fe double spike. Geochimica et Cosmochimica Acta *70*, 118-132.

Dideriksen, K., Baker, J. A., and Stipp, S. L. S. (2008). Equilibrium Fe isotope fractionation between inorganic aqueous Fe(III) and the siderophore complex, Fe(III)-desferrioxamine B. Earth and Planetary Science Letters *269*, 280-290.

Domagal-Goldman, S. D., and Kubicki, J. D. (2008). Density functional theory predictions of equilibrium isotope fractionation of iron due to redox changes and organic complexation. Geochimica Et Cosmochimica Acta *72*, 5201-5216.

Domagal-Goldman, S. D., Paul, K. W., Sparks, D. L., and Kubicki, J. D. (2009). Quantum chemical study of the Fe(III)-desferrioxamine B siderophore complex-Electronic structure, vibrational frequencies, and equilibrium Fe-isotope fractionation. Geochimica Et Cosmochimica Acta *73*, 1-12.

Heuser, A., and Eisenhauer, A. (2010). A pilot study on the use of natural calcium isotopes (44Ca/40Ca) fractionation in urine as a proxy for the human body calcium balance. Bone *46*, 889-896.

Hotz, K., Augsburger, H., and Walczyk, T. (2011). Isotopic signatures of iron in body tissue as a potential biomarker for iron metabolism. J Anal At Spectrom.

Johnson, C. M., Beard, B. L., and Roden, E. E. (2008). The iron isotope fingerprints of redox and biogeochemical cycling in modern and ancient Earth. Annu Rev Earth Pl Sc *36*, 457-493.

Johnson, C. M., Beard, B. L., Roden, E. E., Newman, D. K., and Nealson, K. H. (2004). Isotopic Constraints on Biogeochemical Cycling of Fe. Reviews in Mineralogy & Geochemistry *55*, 359-408.

Johnson, C. M., Skulan, J. L., Beard, B. L., Sun, H., Nealson, K. H., and Braterman, P. S. (2002). Isotopic fractionation between Fe(III) and Fe(II) in aqueous solutions. Earth Planet Sci Lett *195*, 141-153.

Krayenbuehl, P.-A., Walczyk, T., Schoenberg, R., von Blanckenburg, F., and Schulthess, G. (2005). Hereditary hemochromatosis is reflected in the iron isotope composition of blood. Blood *105*.

Marechal, C. N., Telouk, P., and Albarede, F. (1999). Precise analysis of copper and zinc isotopic compositions by plasma-source mass spectrometry. Chem Geol *156*, 251-273.

Osmond, C. B., Allaway, W. G., Sutton, B. G., Troughton, J. H., Queiroz, O., Luttge, U., and Winter, K. (1973). Carbon Isotope Discrimination in Photosynthesis of CAM Plants. Nature *246*, 41-42.

Polyakov, V. B. (1997). Equilibrium fractionation of iron isotopes: Estimation from Mossbauer spectroscopy data. Geochimica et Cosmochimica Acta *61*, 4213-4217.

Polyakov, V. B., and Mineev, S. D. (2000). The use of Mossbauer spectroscopy in stable isotope geochemistry. Geochimica et Cosmochimica Acta *64*, 849-865.

Ripperger, S., and Rhkamper, M. (2007). Precise determination of cadmium isotope fractionation in seawater by double spike MC-ICPMS. Geochimica et Cosmochimica Acta *71*, 631-642.

Roe, J. E., Anbar, A. D., and Barling, J. (2003). Nonbiological fractionation of Fe isotopes: evidence of an equilibrium isotope effect. Chem Geol *195*, 69-85.

Schauble, E. A., Rossman, G. R., and Taylor, H. P. (2001). Theoretical estimates of equilibrium Fe-isotope fractionations from vibrational spectroscopy. Geochimica et Cosmochimica Acta *65*, 2487-2497.

Siebert, C., Nagler, T. F., and Kramers, J. D. (2001). Determination of molybdenum isotope fractionation by double-spike multicollector inductively coupled plasma mass spectrometry. Geochemistry Geophysics Geosystems *2*, 1-16.

Skulan, J., Bullen, T., Anbar, A. D., Puzas, J. E., Shackelford, L., LeBlanc, A., and Smith, S. M. (2007). Natural Calcium Isotopic Composition of Urine as a Marker of Bone Mineral Balance. Clinical Chemistry *53*, 1155-1158.

Skulan, J., and Depaolo, D. J. (1999). Calcium Isotope Fractionation between Soft and Mineralized Tissue as a Monitor of Calcium Use in Vertebrates. Proceedings of the National Academy of Science *96*, 13709-13713.

Skulan, J., DePaolo, D. J., and Owens, T. L. (1997). Bilogical control of calcium isotopic abondances in the global calcium cycle. Geochimica et Cosmochimica Acta *61*, 2505-2510.

Soddy, F. (1914). Intra-atomic charge. Nature *92*, 399.

Thomson, J. J. (1913). Bakerian Lecture: Rays of Positive Electricity. Proceedings of the Royal Society of London *89*, 1-20.

Walczyk, T., and von Blanckenburg, F.. (2002). Natural iron isotope variations in human blood. Science *295*, 2065-2066.

Walczyk, T., and von Blanckenburg, F. (2005). Deciphering the iron isotope message of the human body. Int J Mass Spectrom *242*, 117-134.

Weyer, S., and Schwieters, J. (2003). High precision Fe isotope measurements with high mass resolution MC-ICPMS. Int J Mass Spectrom *226*, 355-368.

Wieser, M. E., Buhl, D., Bouman, C., and Schwieters, J. (2004). High precision calcium isotope ratio measurements using a magnetic sector multiple collector inductively coupled plasma mass spectrometer. J Anal At Spectrom *19*, 844-851.

Chapter 2

IRON ISOTOPE FRACTIONATION DURING EQUILIBRATION OF IRON-ORGANIC COMPLEXES

Jennifer L. L. Morgan*[1], Laura E. Wasylenki[2], Jochen Nuester[3], Ariel D. Anbar[1,2]

Published in Environmental Science and Technology, 2010, *44*, 6095-6101

[1]Arizona State University, Department of Chemistry and Biochemistry, PO Box 871604, Tempe, AZ 85287

[2]Arizona State University, School of Earth and Space Exploration, PO Box 871404, Tempe, AZ 85287

[3] Bigelow Laboratory for Ocean Science, PO Box 475, West Boothbay Harbor, ME 04575

2.1 Abstract

Despite the importance of Fe-organic complexes in the environment, few studies have investigated Fe isotope effects driven by changes in Fe coordination that involve organic ligands. Previous experimental (Dideriksen et al., 2008, *EPSL* 269:280-290) and theoretical (Domagal-Goldman et al., 2009, *Geochim. Cosmochim. Acta* 73:1-12) studies disagreed on the sense of fractionation between Fe-desferrioxamine B (Fe-DFOB) and $Fe(H_2O)_6^{3+}$. Using a new experimental technique that employs a dialysis membrane to separate equilibrated Fe-ligand pools, we measured the equilibrium isotope fractionations between Fe-DFOB and (1) Fe bound to ethylenediaminetetraacetic acid (EDTA) and (2) Fe bound to oxalate. We observed no significant isotope fractionation between Fe-DFOB and Fe-EDTA ($\Delta^{56/54}Fe_{Fe\text{-}DFOB/Fe\text{-}EDTA} \approx 0.02 \pm 0.11$ ‰) and a small but

significant fractionation between Fe-DFOB and Fe-oxalate ($\Delta^{56/54}Fe_{Fe\text{-}DFOB/Fe\text{-}Ox3}$ = 0.20 ± 0.11 ‰). Taken together, our results and those of Dideriksen et al. (2008) reveal a strong positive correlation between measured fractionation factors and the Fe-binding affinity of the ligands. This correlation supports the experimental results of Dideriksen et al. (2008). Further, it provides a simple empirical tool that may be used to predict fractionation factors for Fe-ligand complexes not yet studied experimentally.

2.2 Introduction

The relative abundances of the four stable isotopes of Fe (^{54}Fe, ^{56}Fe, ^{57}Fe and ^{58}Fe) vary in different environmental materials because the rates and equilibrium constants of many chemical reactions are sensitive to atomic mass (Anbar and Rouxel, 2007a; Johnson et al., 2008). With this discovery, the Fe stable isotope system emerged as a powerful new tool to study the sources and chemical transformations of Fe (Anbar, 2004; Beard et al., 1999; Fehr et al., 2008). It has proven useful in tracking many processes in the environment, including the dissolution of mineral phases, biotic and abiotic redox transformations in modern and ancient settings, and anthropogenic pollution sources (Beard et al., 2003; Brantley et al., 2001; Brantley et al., 2004; Flament et al., 2008; Johnson et al., 2002; Majestic et al., 2009; Walczyk and von Blanckenburg, 2005). The fractionation of Fe and other metal isotopes is strongly affected by the metal bonding environment. However, the relative importance of organic ligand binding for Fe isotope fractionation is not well known.

It is important to understand the effects of organic ligand binding on Fe isotope fractionation because interactions between Fe and organic ligands strongly influence the environmental chemistry and biogeochemistry of this element. In oceans, lakes and rivers, Fe-organic complexes dominate Fe speciation (Raymond and Carrano, 1979). In

aerobic environments where dissolved Fe^{2+} and Fe^{3+} are scarce, some organisms produce low molecular weight organic ligands (siderophores) that stabilize Fe^{3+} in solution and sequester it from other organisms (Hutchins et al., 1999). These siderophores have a high binding affinity for Fe^{3+} (log K ~ 20-50) (Albrecht-Gary and Crumbliss, 1998; Hernlem et al., 1996). In addition to siderophores, Fe is also commonly bound to humic and fulvic acids in estuaries, lakes, rivers and soils.

Ligand interactions unique to Fe may also induce isotope fractionation in biology. The diversity of Fe coordination environments in biomolecules gives rise to its rich biochemistry. Certain Fe motifs are found in many enzymes. These include heme-bound Fe and Fe-sulfur clusters, as well as non-heme Fe coordinated by protein. Differences in Fe-organic coordination among these motifs may induce Fe isotope fractionations manifested in the environment.

Some Fe isotope variations in nature have already been attributed to Fe-organic ligand complexation (Bergquist and Boyle, 2006; Fantle and DePaolo, 2004). For example, isotope fractionation associated with organic complexation may explain why dissolved Fe in the organic-rich tributaries of the Negro River is enriched in heavy Fe isotopes (Bergquist and Boyle, 2006). However, the validity of such interpretations is uncertain because there have been few experimental or theoretical studies of Fe isotope fractionation during interaction with organic ligands (Brantley et al., 2001; Brantley et al., 2004; Dideriksen et al., 2008; Domagal-Goldman and Kubicki, 2008; Domagal-Goldman et al., 2009; Ottonello and Zuccolini, 2008; Wiederhold et al., 2006). With over 500 known siderophore complexes (Raymond and Carrano, 1979) and numerous other Fe-binding molecules in the environment, a systematic understanding of Fe isotope fractionation during ligand binding is required.

Among the studies that do exist, there are significant discrepancies between experimental assessments and theoretical predictions of Fe isotope fractionation involving organic ligands. The first measurement of the equilibrium isotope fractionation between Fe^{3+} bound to the siderophore desferrioxamine B (DFOB) and the inorganic Fe complex $Fe(H_2O)_6^{3+}$ indicated a fractionation of ~0.6 ‰, (Equation 1) favoring heavier isotopes in the Fe^{3+}-DFOB complex (Dideriksen et al., 2008).

$$\delta^{56/54}Fe_{sample} = \left(\frac{(^{56}Fe/^{54}Fe)_{sample}}{(^{56}Fe/^{54}Fe)_{IRMM\text{-}014}} - 1\right) \times 1000 \qquad 1$$

This effect is significant compared to the total range of Fe isotope variation found in nature (~ 3 ‰) (Anbar, 2004). In contrast, theoretical calculations using molecular orbital/density functional theory (MO/DFT) for the same equilibrium reaction, including water solvation and at 25°C, predicted an isotope effect of 0.3 ‰ in the opposite direction, favoring lighter isotopes in the Fe^{3+}-DFOB complex (Domagal-Goldman et al., 2009). This disagreement between experimental and theoretical findings suggests shortcomings in either prior experiments or MO/DFT computations.

Here we present determinations of the magnitude and direction of equilibrium Fe isotope fractionation involving the Fe-organic complexes Fe^{3+}-DFOB, Fe^{3+}-oxalate (Fe^{3+}-Ox_3), and Fe^{3+}-ethylenediaminetetraacetic acid (Fe^{3+}-EDTA), using a new experimental method. We compare these data to prior experimental and theoretical results.

2.3 Experimental and Analytical methods

Experimental Design

We utilized a new method to measure equilibrium isotope fractionation. In the approach employed previously by Dideriksen et al. (Dideriksen et al., 2008), $Fe(H_2O)_6^{3+}$ was separated from Fe^{3+}-DFOB after equilibration by rapidly increasing pH, resulting in

rapid (<1 s) precipitation of $Fe(H_2O)_6^{3+}$ as Fe-oxyhydroxide. After separating the solution and precipitate by centrifugation, the isotope compositions of both Fe pools were measured. However, the precipitation of Fe-oxyhydroxides can induce an isotope effect of its own (Johnson et al., 2002). In order to check for this potential problem and to correct for its effects, it is necessary to measure the rate of precipitation, the isotope composition of the remaining $Fe(H_2O)_6^{3+}$ pool, and the rate of isotope exchange between $Fe(H_2O)_6^{3+}$ and Fe^{3+}-DFOB. This was accomplished via parallel sets of control experiments with an ^{57}Fe tracer. Further, this method of separation is only applicable when one of the equilibrating species is $Fe(H_2O)_6^{3+}$, limiting the utility when considering pairs of organic species.

Membrane separations offer an alternative to precipitation and centrifugation in isotope equilibration studies. For example, in a study of Zn isotopes, a Donnan membrane was used to separate Zn^{2+} from Zn^{2+} bound to purified humic acid (Jouvin et al., 2009). However, because the Donnan membrane requires that one of the equilibrating species be charged, it cannot be used for studies involving neutral organic species.

Dialysis membranes offer another possibility. In our study, dialysis bags with a nominal molecular weight cutoff of 100 g/mol were used to physically separate the Fe ligand pools by simple diffusion. We determined experimentally that the actual molecular weight cutoff was variable. In the experiments reported here, the bags allowed small ligand complexes of up to 350 g/mol to diffuse through, while ligand complexes heavier than 350 g/mol were unable to cross the membrane (Figure 2-1, Table 2-1). The exact molecular weight cutoff varied among bags purchased at different times either as a result of subtle manufacturing variations in different batches of bags or of pore size

changing with age. Control experiments involving one Fe-ligand complex in the dialysis bag were performed with new bag batches and for every Fe-ligand complex to ensure successful separation.

Two sets of experiments were conducted for each ligand pair: one with ^{54}Fe tracer to quantify the extent of isotope exchange, and one with "normal" Fe (~ 0 ‰) to measure isotope fractionation. In a typical experiment, two Fe-ligand stock solutions were prepared, mixed, allowed to equilibrate for at least 24 hours, then placed in a 3 mL dialysis bag. The bag was placed inside a 250 mL jar of 18 MΩ-cm water, which was agitated to facilitate diffusion of the smaller ligand through the bag and into the surrounding solution. Samples were taken from both the inside solution and the outside solution for isotope analyses.

The experiments were designed so that approximately half the Fe would be bound in the larger siderophore complex, DFOB, and half would be bound to the smaller ligand, EDTA or Ox_3, based on equilibrium constants obtained from the literature (Table 2-1). The Fe concentrations outside the bags were monitored in every experiment to ensure that the concentration reached the value expected if only the smaller Fe complex diffused out and attained uniform concentration on both sides of the membrane (Figure 2-1).

The advantages of the dialysis bag method over precipitation are: (a) there is no back reaction requiring correction; and (b) our separation method can be used even when $Fe(H_2O)_6^{3+}$ is not one of the equilibrating species (Dideriksen et al., 2008).

Experimental Details

Stock solutions were made for multiple experiments. The ^{54}Fe-DFOB stock solution was made by mixing 5.2 mM DFOB (Fisher Scientific desferrioxamine mesylate)

and 5.1 mM ^{54}Fe (Lot #166642, Oak Ridge National Labs, $FeCl_3$ in 2% HNO_3; ^{54}Fe (96.41%), ^{56}Fe (3.49%), ^{57}Fe (0.10%), ^{58}Fe (<0.03%)). The Fe-EDTA stock solution contained 5.10 mM EDTA (Acros Organics ethylenediaminetetraacetic acid, 99%) and 5.1 mM Fe (Fisher Scientific, $FeCl_3$ in 2% HNO_3)). The Fe-Ox_3 solution contained 15.4 mM oxalic acid (Fisher Chemical oxalic acid) and 5.1 mM Fe. The Fe-DFOB solution contained 5.1 mM DFOB and 5.2 mM Fe. All solutions were made with 18.2 MΩ-cm water and kept at room temperature.

The tracer experiments were performed by mixing 7.5 mL of $^{54}Fe^{3+}$-DFOB stock with 7.5 mL of Fe^{3+}-EDTA or Fe^{3+}-Ox_3. The equilibrium experiments were performed by mixing 7.5 mL of Fe^{3+}-DFOB stock with 7.5 mL of Fe^{3+}-EDTA or Fe^{3+}-Ox_3. For all experiments, the initial pH was 3. After 24 hours of equilibration, 3 mL was transferred to a dialysis bag (Spectrum Lab, 100D CE Float-A-Lyzer®). The bag and its contents were placed in a jar containing 250 mL of 18 MΩ-cm water freshly extracted from a DI system, with an initial pH of 7. In all experiments, pH decreased to 5. In the case of Fe^{3+}-Ox_3, the experiment was kept in an amber colored shaker while being agitated, or in a dark cabinet, to prevent photoreduction of Fe^{3+}-Ox_3 (Chen et al., 2007).

Once each experiment reached completion, as assessed in near real-time using UV-Vis spectrophotometry and Ferrozine® with hydroxylamine reagent (Stookey, 1970), the bag was removed from the surrounding solution. The concentration of Fe in the surrounding solution was then analyzed using ICP-MS to quantify mass balance (Table 2-2). The inside solution was diluted from 3 mL (initial volume) to 3.5-5 mL because of osmosis. The final volume was used to calculate the μg of Fe in the experiment to assess mass balance. Fe mass balance was achieved within analytical error (2σ = ± 5%) for all experiments (Table 2-3). This indicates that significant sorption to the dialysis

membrane did not occur. It also indicates that in the unlikely event of bacterial growth, there was no significant biotic removal of Fe from solution. While a small amount of the diffusing Fe-ligand complex remained inside the bag (~1%), its contribution to the Fe isotope composition of the inside solution was negligible. The high recovery of the smaller and less stable Fe-ligands also shows that significant quantities of Fe-oxyhydroxides, which would have remained in the bag, did not form.

Aliquots of the inside and outside solutions were taken to obtain 14 μg of Fe for each isotopic analysis: ~145 μL from the inside solution and ~11.8 mL from the outside solution. These aliquots were dried and digested using distilled HNO_3 and ultra-pure H_2O_2. Once digested, the samples were diluted in 0.32 M HNO_3 for analysis. Typically, for Fe isotope analysis samples must be chemically purified using anion exchange resin to isolate Fe from other elements. However, chemical purification of these experimental samples was not needed because the sample matrix only contains Fe and easily digested organic ligands.

Analytical Procedures

Precise Fe concentrations were measured by quadrupole ICP-MS (Thermo Scientific X Series). Sample and standard solutions were introduced in parallel with an internal standard solution containing yttrium for normalization of plasma variation. Uncertainties for replicate measurements were approximately ± 5% (2σ).

Fe isotope compositions were measured following the method of Arnold et al. using a multiple collector ICP-MS (Thermo Scientific Neptune)(Arnold et al., 2004a). Medium mass-resolution mode (50 μm slits) was used to resolve the polyatomic interferences $^{40}Ar^{16}O^+$, and $^{40}Ar^{14}N^+$ and $^{40}Ar^{16}OH^+$ from $^{54}Fe^+$, $^{56}Fe^+$ and $^{57}Fe^+$, respectively (Weyer and Schwieters, 2003a). We monitored mass 53 for ^{53}Cr to ensure

that there was no interference from ^{54}Cr, although our experimental system nominally contains no Cr. Some samples were measured using high mass-resolution mode (25 μm slits) when medium resolution slits were unavailable; other than reducing the ion beam intensities and hence requiring less diluted samples, the use of high mass-resolution slits had no effect on our data. The Fe concentrations of samples and standards were 600 ppb (10.74 μM) for medium resolution analyses and 1200 ppb (21.48 μM) for high resolution analyses. Sample and standard concentrations were checked during the analysis to ensure they were identical to within ± 5%. Instrumental mass bias, i.e., isotope fractionation produced by the mass spectrometer, was corrected using a combination of standard-sample bracketing and addition of Cu as an internal standard (Arnold et al., 2004a). Cu concentrations matched Fe concentrations in all standards and samples.

For each isotopic analysis, 20 cycles with 16.77 second integrations were averaged. Three isotope ratios were measured simultaneously: $^{56}Fe/^{54}Fe$, $^{57}Fe/^{54}Fe$, and $^{58}Fe/^{54}Fe$. All ratios were measured relative to the IRMM-014 standard (Institute of Reference Material and Measurement, Geel, Belgium). Values are reported as:

$$\delta^{56/54}Fe_{sample} = \left(\frac{(^{56}Fe/^{54}Fe)_{sample}}{(^{56}Fe/^{54}Fe)_{IRMM\text{-}014}} - 1\right) \times 1000 \qquad (1)$$

As a quality-control measure, we checked that all measured isotope values obeyed mass dependence by comparing $\delta^{56/54}Fe$ and $\delta^{57/54}Fe$ (the precision of $\delta^{58/54}Fe$ was typically too poor to be useful, due to the relative rarity of ^{58}Fe). Data were rejected if $\delta^{56/54}Fe/2$ differed from $\delta^{57/54}Fe/3$ by more than 0.05 ‰ (this check was not applicable to isotope tracer experiments). Data were also rejected if the magnitude of the mass bias correction exceeded 0.35 ‰. Good agreement between $\delta^{56/54}Fe/2$ and $\delta^{57/54}Fe/3$, as well

as small instrumental mass bias corrections, indicate that the isotope measurements were not significantly affected by interferences or other matrix effects. Data were rejected if the ion beam intensity from $^{56}Fe^{+}$ was < 6 V, because in such cases the contribution of instrument blank to the beam intensities measured for the less abundant Fe isotopes becomes significant.

Solutions containing extreme enrichments of ^{54}Fe, used in tracer experiments, were usually run at the end of an analytical session to avoid any chance of memory effects. However, no such effects were seen when running standards immediately after such samples.

Throughout the analytical runs, we measured the IRMM-014 standard, gravimetric standards of known isotope composition, and previously analyzed rock standards to ensure accuracy and reproducibility from session to session. Based on replicate measurements of each sample, the external precision was better than ± 0.11 ‰ (± 2σ) in $\delta^{56/54}Fe$.

2.4 Results and Discussion

Verification of Isotope Equilibration

We assessed the extent of isotope equilibration in ^{54}Fe tracer experiments. The isotope compositions of all solutions and mixtures were measured directly so as to not assume an isotope composition based on a mixing calculation. The initial isotope composition of $^{54}Fe^{3+}$-DFOB in these tracer experiments was $\delta^{56/54}Fe$ = -91.77 ± 0.03 ‰. The initial isotope compositions of Fe^{3+}-EDTA and Fe^{3+}-Ox_3 were 0.26 ± 0.09 ‰ and 0.20 ± 0.06 ‰ ($\delta^{56/54}Fe$). The isotope compositions of the Fe^{3+}-DFOB/ligand mixtures were -48.12 ± 0.08 ‰ and -48.26 ± 0.11 ‰ for Fe^{3+}-EDTA and Fe^{3+}-Ox_3, respectively.

After separating the complexes, the isotope composition of Fe inside the bag (Fe^{3+}-DFOB) was -48.39 ± 0.09 ‰ after exchange with Fe^{3+}-EDTA and -48.32 ± 0.11 ‰ after exchange with Fe^{3+}-Ox_3. The Fe isotope composition outside the bag for Fe^{3+}-EDTA was -47.86 ± 0.08 ‰. The Fe isotope composition for Fe^{3+}-Ox_3 was -48.27 ± 0.07 ‰ (Table 2-2).

The isotopes in both experiments converge toward a common value, indicating that the isotopes exchanged between the two Fe-ligand complexes. The isotope composition that should be attained after complete equilibration is easily predicted by mass balance. The isotope compositions of the separated ligands can be predicted using the following equations:

$$\delta^{56/54}Fe_{DFOB\text{-}final} = (1\text{-}M)\ \delta^{56/54}Fe_{DFOB\text{-}initial} + M\ \delta^{56/54}Fe_{unspikedligand\text{-}initial} \quad (2)$$

$$\delta^{56/54}Fe_{unspikedligand\text{-}final} = (1\text{-}M)\ \delta^{56/54}Fe_{unspikedligand\text{-}initial} + M\ \delta^{56/54}Fe_{DFOB\text{-}initial} \quad (3)$$

Here, M is the fraction of Fe in each complex that has exchanged with the other complex. Since no more than 52.7 % of the Fe came from $^{54}Fe^{3+}$-DFOB, M must be $0 \leq M \leq 0.527$. M can be converted to F, the percent exchanged, by dividing M obtained from Equation 2 and Equation 3 by the percent Fe that was initially added to the experiment from Fe^{3+}-unspikedligand and $^{54}Fe^{3+}$-DFOB, respectively. Equations 2 and 3 are approximations, but these approximations deviate from the actual equivalence by no more than 1% as long as $\delta^{56/54}Fe_{Spike}$-$\delta^{56/54}Fe_{Unspiked} < 400$ ‰ (Roe et al., 2003). The Fe isotope composition of each Fe-ligand complex is shown as a function of F in Figure 2-2A.

When the measured isotope values are substituted into Equation 1 and 2, the results indicate that > 99% of the Fe exchanged in all experiments (Figure 2-2B). These results demonstrate that despite the strong binding affinity of DFOB for Fe, Fe isotopes

exchange between DFOB and ligands with smaller Fe-binding affinities. The extent of exchange also indicates that the experiments closely approached equilibrium.

Equilibrium Isotope Fractionation

Isotope fractionation between pairs of organic Fe complexes was measured using the same procedures described above, but beginning with Fe^{3+}-DFOB, Fe^{3+}-EDTA, and Fe^{3+}-Ox_3 of the same initial Fe isotope composition (these experiments had no ^{54}Fe tracer). By measuring $d^{56/54}Fe$ in the separated ligand pools after equilibration, we found that the fractionation between Fe^{3+}-DFOB and Fe^{3+}-Ox_3 ($\Delta^{56/54}Fe_{Fe\text{-}DFOB/Fe\text{-}Ox3} = \delta^{56/54}Fe_{Fe\text{-}DFOB} - \delta^{56/54}Fe_{Fe\text{-}Ox3}$) is 0.20 ± 0.11 ‰, while the difference between Fe^{3+}-DFOB and Fe^{3+}-EDTA is 0.02 ± 0.11 ‰ (Figure 2-3). These values indicate that organic ligand binding affects the magnitude of Fe isotope fractionation.

We cannot directly compare our results with those of Dideriksen et al. (Dideriksen et al., 2008), because it was not possible to use our experimental method to directly measure the fractionation between Fe^{3+}-DFOB and $Fe(H_2O)_6^{3+}$; to avoid precipitation of hydrous ferric oxides from $Fe(H_2O)_6^{3+}$, pH would need to be < 3, causing the dialysis membrane to degrade. However, an indirect comparison is possible if we plot $\Delta^{56/54}Fe$ as a function of the affinity constants (log K) of the Fe-binding ligands. The assumption underlying this simple, first-order comparison is that Fe isotope fractionation in these systems is largely driven by differences in Fe-ligand binding affinity between the equilibrating complexes. Specifically, we plot $\Delta^{56/54}Fe$ versus Δlog K (Figure 2-4), where Δlog K is the difference in log K values between the two equilibrating species. In the case of isotope exchange between $Fe(H_2O)_6^{3+}$ and Fe^{3+}-DFOB, Δlog K is simply the binding affinity for the reaction Fe^{3+} + DFOB → Fe^{3+}-DFOB, because the value of this log

K was determined in an aqueous solution in which Fe^{3+} was presumably present as the hexaquo complex (Martell and Smith, 1989).

When our results are combined with those of Dideriksen et al. (Dideriksen et al., 2008) in this way, a linear trend emerges (Figure 2-4). This trend follows the expectation that heavier isotopes preferentially partition into stronger bonding environments and that the magnitude of this effect scales with differences in bond strengths (Bigeleisen and Mayer, 1947; Urey, 1947). (Note that this relationship only applies to ligands in equilibrium with each other and does not account for kinetic isotope effects.)

Our findings are consistent with other recent work. Ottonello and Zuccolini (Ottonello and Zuccolini, 2008) similarly suggested a positive correlation between Fe-ligand binding affinity and equilibrium isotope fractionation based on their MO/DFT study of consecutive binding of acetic acid molecules to Fe^{3+}. Wiederhold et al. (Wiederhold et al., 2006) and Brantley et al. (Brantley et al., 2004) observed light Fe bound to ligands with high Fe binding affinity in leaching experiments with goethite and hornblende, respectively, but these experiments were not at equilibrium, and thus an opposite sense of fractionation from our experiments is unsurprising. Wiederhold's long-duration experiments displayed an isotopically heavy product and therefore likely represent equilibrium exchange between goethite-bound Fe and oxalate-bound Fe with a fractionation of 0.5 ± 0.15 ‰ (Wiederhold et al., 2006). There is no simple Fe binding affinity constant for the goethite lattice, but this result suggests a stronger bonding environment for Fe in Fe^{3+}-Ox_3 than for Fe in goethite.

Reconciling Experiments and Theory

To assess the validity of the experimental trend of $\Delta^{56/54}$Fe versus Δlog K, we plotted the theoretically predicted $\Delta^{56/54}$Fe values for Fe^{3+}-Ox_3/Fe^{3+}-catecholate (Cat_3),

Fe^{3+}-DFOB/Fe^{3+}-Ox_3, and Fe^{3+}-DFOB/Fe^{3+}-Cat_3 (Domagal-Goldman and Kubicki, 2008) as a function of the difference in log K (Figure 2-4). Like the experimental results, these MO/DFT predictions form a linear trend. This trend in theoretical $\Delta^{56/54}$Fe versus Δlog K supports our observation that the extent of fractionation correlates directly with differences in binding affinity. However, the two trend lines are slightly offset and have different slopes. These differences suggest that MO/DFT calculations may systematically deviate from experimental fractionation factors, and that this problem may worsen with increasing difference in log K. Experiments that directly quantify the fractionation factors for Fe^{3+}-Ox_3/Fe^{3+}-Cat_3, and Fe^{3+}-DFOB/Fe^{3+}-Cat_3 could test this suggestion.

Our findings and interpretations shed new light on the mismatch between previous experimental and theoretical studies of fractionation between Fe^{3+}-DFOB and $Fe(H_2O)_6^{3+}$. The previous study that measured Fe in equilibrium between siderophore (Fe^{3+}-DFOB) and inorganic Fe complex ($Fe(H_2O)_6^{3+}$) reported a fractionation of ~0.6 ‰ ($\Delta^{56/54}$Fe), favoring heavier isotopes in the Fe^{3+}-DFOB complex (Dideriksen et al., 2008). The corresponding quantum chemical calculations for the same system predicted an isotope effect of 0.3 ‰ in the opposite direction (Domagal-Goldman et al., 2009). In an attempt to more accurately model speciation in experiments prior to and during precipitation, Domagal-Goldman et al. (Domagal-Goldman et al., 2009) modeled a mixture of inorganic species ($Fe(H_2O)_6^{3+}$, $Fe(H_2O)_8(OH)_2^{3+}$ and $Fe(H_2O)_6^{2+}$). This modification changed the isotope fractionation to -0.15 ‰, but did not fully resolve the disagreement with experiments. Neither of these calculated values for $Fe(H_2O)_6^{3+}$ in equilibrium with Fe^{3+}-DFOB falls on the linear trend defined by experiments, or on the trend defined by the other MO/DFT calculations (Figure 2-4).

Similar discrepancies were noted between experimental and theoretical fractionation factors observed between $Fe(H_2O)_6^{3+}$ and a series of mineral phases [20]. There is an average offset of 0.8 ‰ between the experimental and theoretical values for these systems. The theoretical calculations predict that $Fe(H_2O)_6^{3+}$ should be enriched in heavy isotopes compared to the mineral phase, but this is not observed in experiments (Domagal-Goldman and Kubicki, 2008). The discrepancies between experiments and theory are consistently of similar magnitude and in the same direction when $Fe(H_2O)_6^{3+}$ is involved. We hypothesize that there is a specific deficiency in MO/DFT models of $Fe(H_2O)_6^{3+}$.

Broader Implications

The linear trend we observe between $\Delta^{56/54}$Fe and Δlog K may prove particularly useful in predicting equilibrium isotope fractionation induced by ligands that have not been experimentally tested or theoretically modeled. For example, the equilibrium Fe isotope fractionation for Fe^{3+}-DFOB in equilibrium with Fe^{3+}-citrate has not been measured or modeled. The difference in binding affinity between Fe^{3+}-DFOB and Fe^{3+}-citrate is 19.2. Using the linear trend we predict a fractionation of $\Delta^{56/54}Fe_{Fe\text{-}DFOB/Fe\text{-}citrate}$ = 0.33 ± 0.26 ‰. Future experimental work could test this hypothesis.

More broadly, our results confirm that isotope fractionations generated from interactions between Fe and organic ligands can be significant and are therefore likely to be important in natural systems. Because many different types of ligands bind Fe in nature, improved understanding of the systematics of ligand-driven isotope effects may prove particularly useful in studying weathering, biological acquisition and metabolism of Fe. Iron cycling in these systems often involves Fe redox changes, which cause some of the largest known Fe isotope fractionations (Bullen et al., 2001; Welch et al., 2003). The

presence of organic ligands, especially those that have high affinity for only one redox state of Fe, could be important in governing Fe isotope signatures in natural systems.

Table 2-1: Binding affinities and formula weights for organic ligands[a]

Ligand	log (K)	Formula Weight
Fe-Desferrioxamine-B (DFOB)	31	617 g/mol
Fe-Ethylenediaminetetraacetic acid (EDTA)	25	348 g/mol
Fe-Oxalate (Ox_3)	19	326 g/mol (for 3 ligands)

[a]Smith and Martell (Martell and Smith, 1989)

Table 2-2: Iron concentrations and $\delta\,^{56/54}Fe$ in experimental solutions.

Solution	Measured [Fe, ppm] 2σ = ± 5%	$\delta^{56/54}$Fe (‰) ± 2σ, n=3-4
Stock		
$^{54}Fe^{3+}$-DFOB	300.0	-91.77 ± 0.03
Fe^{3+}-EDTA	281.2	0.26 ± 0.09
Fe^{3+}-Ox_3	299.9	0.20 ± 0.06
Fe^{3+}-DFOB	272.4	0.23 ± 0.13
Spike Fe		
$^{54}Fe^{3+}$-DFOB/Fe^{3+}-Ox_3 Mixture	299.9	-48.26 ± 0.11
Inside (Fe^{3+}-DFOB)	120.9	-48.32 ± 0.11
Outside (Fe^{3+}-Ox_3)	1.6	-48.27 ± 0.07
$^{54}Fe^{3+}$-DFOB/Fe^{3+}-EDTA Mixture	290.6	-48.12 ± 0.08
Inside (Fe^{3+}-DFOB)	147.8	-48.39 ± 0.09
Outside (Fe^{3+}-EDTA)	1.7	-47.86 ± 0.08
Normal Fe		
Fe^{3+}-DFOB/Fe^{3+}-Ox_3 Mixture	286.2	0.24 ± 0.03
Inside (Fe^{3+}-DFOB)	87.6	0.25 ± 0.10
Outside (Fe^{3+}-Ox_3)	1.6	0.05 ± 0.06
Fe^{3+}-DFOB/Fe^{3+}-EDTA Mixture	276.8	0.25 ± 0.05
Inside (Fe^{3+}-DFOB)	82.8	0.17 ± 0.07
Outside (Fe^{3+}-EDTA)	1.4	0.15 ± 0.09

Table 2-3: Added and measured iron quantities in the experiments.
μg Fe in experiment (2σ = ± 5%)

Solution	μg Fe added	μg Fe Measured (inside and outside bag)
Spike Fe		
$^{54}Fe^{3+}$-DFOB/Fe^{3+}-Ox_3 Mixture	757	724
$^{54}Fe^{3+}$-DFOB/Fe^{3+}-EDTA Mixture	815	848
Normal Fe		
Fe^{3+}-DFOB/Fe^{3+}-Ox_3 Mixture	839	804
Fe^{3+}-DFOB/Fe^{3+}-EDTA Mixture	803	806

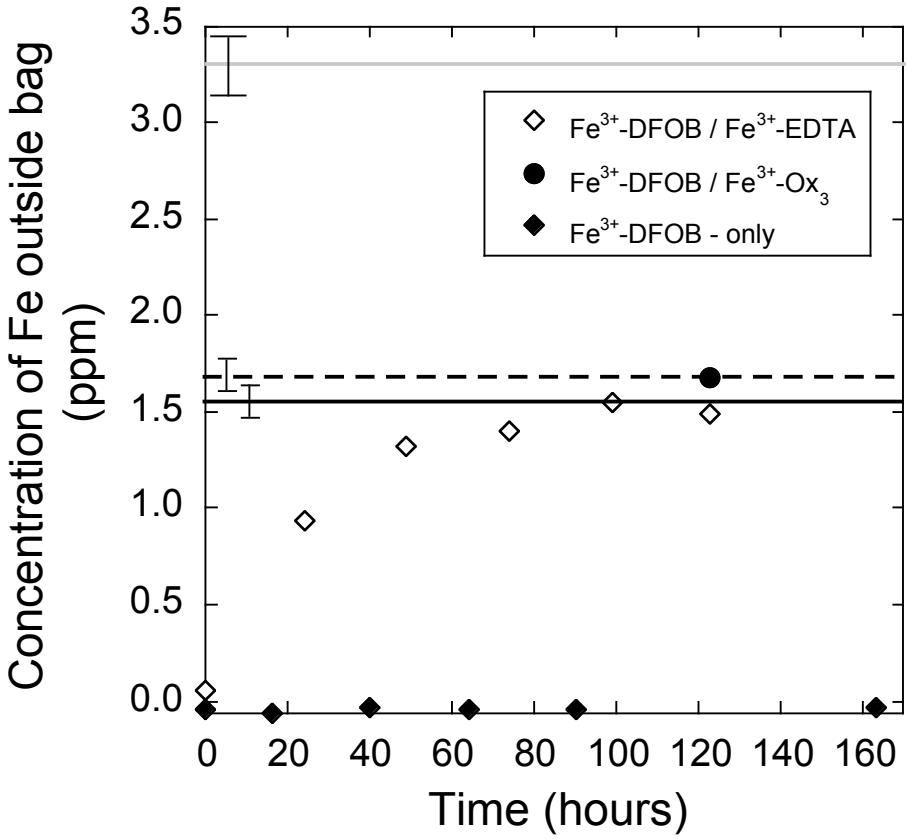

Figure 2-1 Concentration of Fe outside dialysis bag vs. time.
The horizontal lines shown represent the expected Fe concentrations outside the bag if either one ligand (solid black line, and dashed black line), or both ligands (solid gray line), escaped the bag from the two mixed-ligand experiments. The error bars on the horizontal lines represent 5% standard deviation as defined by replicate measurements of standards. Three separate dialysis bag experiments were performed. In experiment 1, 3 mL of 5 mM Fe (280 ppm Fe) as Fe^{3+}-DFOB/Fe^{3+}-EDTA were added to a dialysis bag (solid black line, open diamonds). In experiment 2, 3 mL of 5 mM Fe as Fe^{3+}-DFOB/Fe^{3+}-Ox_3 were placed into a dialysis bag (dashed black line, closed circle). In experiment 3, 3 mL of 5 mM Fe as Fe^{3+}-DFOB were added (closed diamonds). Each bag was placed in 250 mL jars of 18 MΩ cm^{-1} water, and the Fe concentration outside the bag was measured over time using the Ferrozine® method. Concentrations in all cases indicate that Fe^{3+}-DFOB was trapped by the membrane, while Fe^{3+}-EDTA and Fe^{3+}-Ox diffused to the outside. For the time series concentration measurements, the error bars are smaller than the symbols.

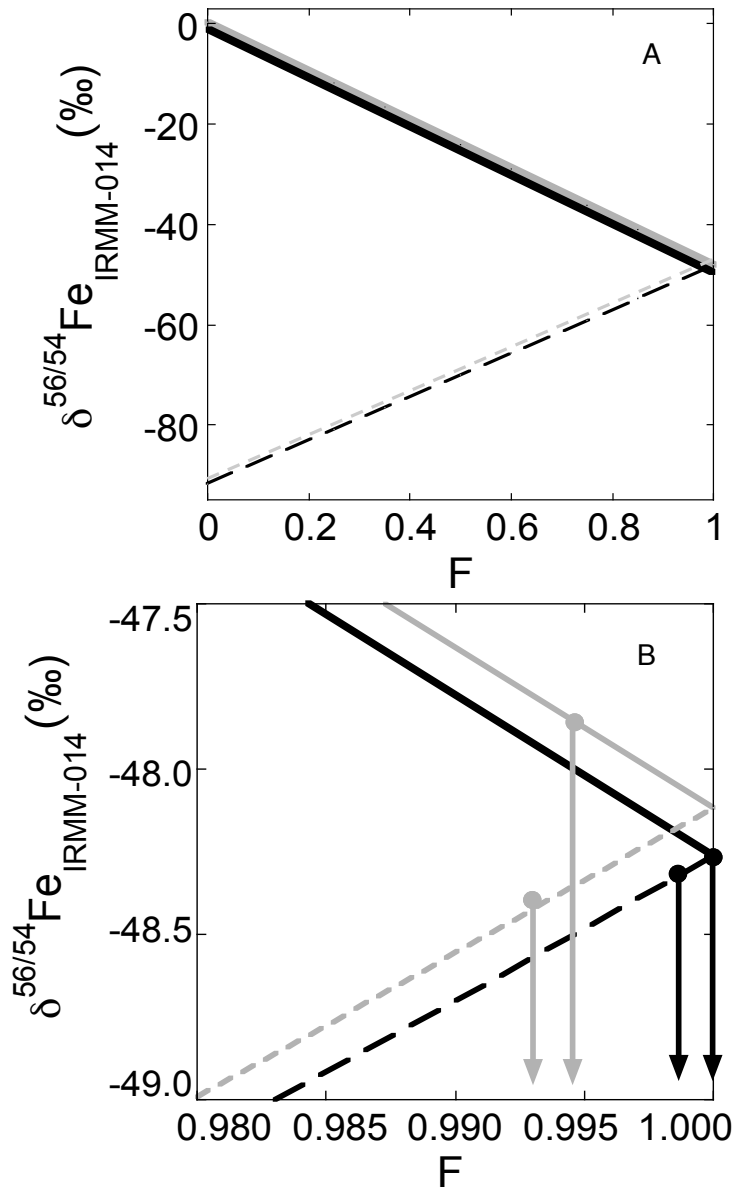

Figure 2-2 Mixing lines to determine extent mixed.
A) Expected isotope composition as a function of isotope exchange progress. The lines were calculated using equations 2 and 3 then converted to F. F is the fractional extent to which exchange has approached completion. F=0 indicates no exchange occurs. F=1 indicates complete exchange between pools. The black solid line is Fe^{3+}-Ox_3, and the dashed black line is $^{54}Fe^{3+}$-DFOB mixed with Fe^{3+}-Ox_3. The solid gray line is Fe^{3+}-EDTA, and the dashed gray line is $^{54}Fe^{3+}$-DFOB mixed with Fe^{3+}-EDTA. B) Magnified view of F > 0.980. The points on the line show the measured isotope composition of each ligand after the experiment. The arrows show the extent to which the ligands mixed in each experiment. Each was > 99% mixed.

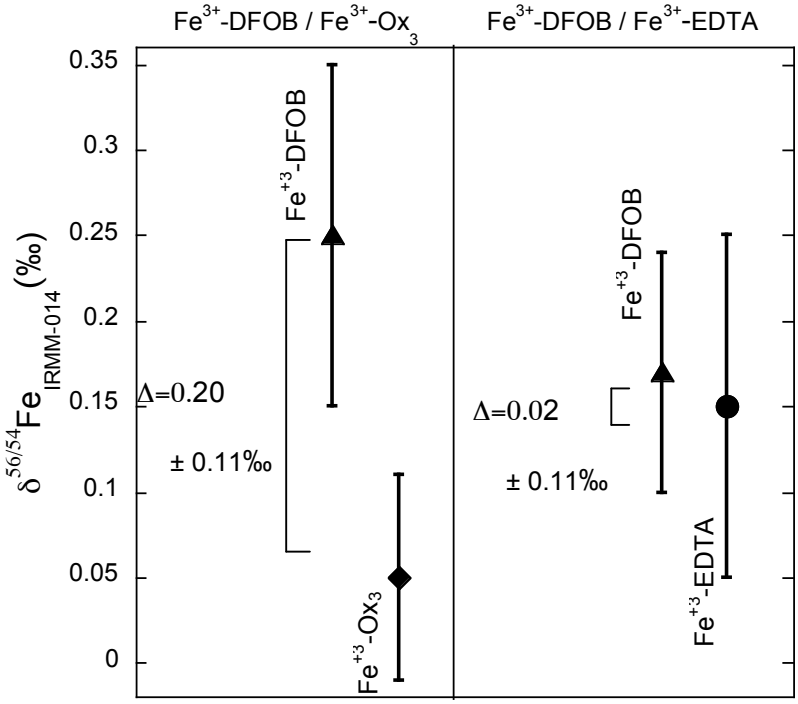

Figure 2-3 Measured fractionation for each experiment.
Measured $\delta^{56/54}$Fe for each sample. Fe^{3+}-DFOB and Fe^{3+}-Ox_3 were significantly different with $\Delta^{56/64}$Fe = 0.20 ± 0.11 ‰. Fe^{3+}-DFOB and Fe^{3+}-EDTA were within analytical error of each other, indicating that $\Delta \approx 0.02 \pm 0.11$ ‰. Error bars represent $\pm 2\sigma$ uncertainty on replicate measurements of samples.

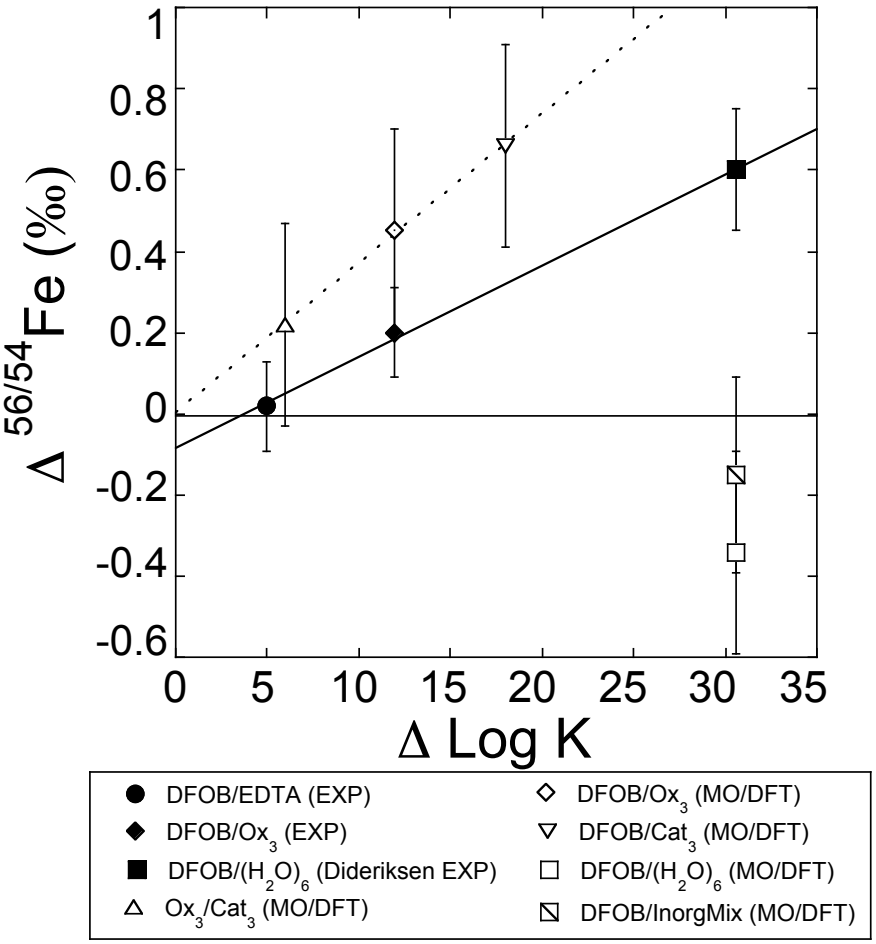

Figure 2-4 Fractionation between ligands vs difference in binding affinity.
Plot of isotope fractionation as a function of the difference in log K for each ligand pair. The linear trend based on experiments has a slope of 0.02 ± 0.005. The y-intercept is 0.08 ± 0.08. The uncertainties on the slope and y-intercept were calculated using Isoplot (Ludwig, 2008). The experimental results fall on a line with an R^2 value of 0.99. The error bars are propagated 2σ uncertainties on replicate measurements. The MO/DFT predictions for Fe^{3+}-Ox_3/Fe^{3+}-Cat_3, Fe^{3+}-DFOB/Fe^{3+}-Ox_3, and Fe^{3+}-DFOB/Fe^{3+}-Cat_3 are plotted as a function of the difference in log K. The MO/DFT predictions form a linear trend that is offset and has a different slope from the experimental trend (see text on Reconciling Experiments and Theory).

2.5 References

Albrecht-Gary, A. M., and Crumbliss, A. L. (1998). Coordination chemistry of siderophores: Thermodynamics and kinetics of iron chelation and release, In Metal ions in biological systems, A. Sigel, and H. Sigel, eds. (CRC Press), pp. 239-316.

Anbar, A., and Rouxel, O. (2007). Metal stable isotopes in paleoceanography. Annu Rev Earth Pl Sci *35*, 717-746.

Anbar, A. D. (2004). Iron stable isotopes: beyond biosignatures. Earth Planet Sci Lett *217*, 223-236.

Arnold, G., Weyer, S., and Anbar, A. D. (2004). Fe isotope variations in natural materials measured using high mass resolution multiple collector ICPMS. Anal Chem *76*, 322-327.

Beard, B. L., Johnson, C. M., Cox, L., Sun, H., Nealson, K. H., and Aguilar, C. (1999). Iron isotope biosignatures. Science *285*, 1889-1892.

Beard, B. L., Johnson, C. M., Skulan, J. L., Nealson, K. H., Cox, L., and Sun, H. (2003). Application of Fe isotopes to tracing the geochemical and biological cycling of Fe. Chem Geol *195*, 87-117.

Bergquist, B. A., and Boyle, E. A. (2006). Iron isotopes in the Amazon River system: Weathering and transport signatures. Earth Planet Sci Lett *248*, 54-68.

Bigeleisen, J., and Mayer, M. G. (1947). Calculation of equilibrium constants for isotopic exchange reactions. J Chem Phys *15*, 261-267.

Brantley, S. L., Liermann, L., and Bullen, T. D. (2001). Fractionation of Fe isotopes by soil microbes and organic acids. Geology *29*, 535-538.

Brantley, S. L., Liermann, L. J., Guynn, R. L., Anbar, A., Icopini, G. A., and Barling, J. (2004). Fe isotopic fractionation during mineral dissolution with and without bacteria. Geochimica et Cosmochimica Acta *68*, 3189-3204.

Bullen, T. D., White, A. F., Childs, C. W., Vivit, D. V., and Schulz, M. S. (2001). Demonstration of significant abiotic iron isotpe fractioant in nature. Geology *29*, 899-702.

Chen, J., Zhang, H., Tomuv, I., Ding, X., and Rentzepis, P. M. (2007). Electron transfer and dissocaition mechanism of ferrioxalate: A time resolved optical and EXAFS study. Chemical Physics Letters *437*, 50-55.

Dideriksen, K., Baker, J. A., and Stipp, S. L. S. (2008). Equilibrium Fe isotope fractionation between inorganic aqueous Fe(III) and the siderophore complex, Fe(III)-desferrioxamine B. Earth and Planetary Science Letters *269*, 280-290.

Domagal-Goldman, S. D., and Kubicki, J. D. (2008). Density functional theory predictions of equilibrium isotope fractionation of iron due to redox changes and organic complexation. Geochimica Et Cosmochimica Acta *72*, 5201-5216.

Domagal-Goldman, S. D., Paul, K. W., Sparks, D. L., and Kubicki, J. D. (2009). Quantum chemical study of the Fe(III)-desferrioxamine B siderophore complex-Electronic structure, vibrational frequencies, and equilibrium Fe-isotope fractionation. Geochimica Et Cosmochimica Acta *73*, 1-12.

Fantle, M. S., and DePaolo, D. J. (2004). Iron isotopic fractionation during continental weathering. Earth Planet Sci Lett *228*, 547-562.

Fehr, M. A., Andersson, P. S., Halenius, U., and Morth, C. (2008). Iron isotope variations in Holocene sediments of the Gotland Deep, Baltic Sea. Geochimica et Cosmochimica Acta *72*, 807-826.

Flament, P., Mattielli, N., Aimoz, L., Choel, M., Deboudt, K., de Jong, J., Rimetz-Planchon, J., and Weis, D. (2008). Iron isotopic fractionation in industrial emissions and urban aerosols. Chemosphere *73*, 1793-1798.

Hernlem, B., Vane, L., and Sayles, G. (1996). Stability constants for complexes of the siderophore desferrioxamine B with selected heavy metal cations. Inorganica chimica acta *244*, 179-184.

Hutchins, D., Witter, A., Butler, A., and Luther III, G. (1999). Competition among marine phytoplankton for different chelated iron species. Nature *400*, 858-861.

Johnson, C. M., Beard, B. L., and Roden, E. E. (2008). The iron isotope fingerprints of redox and biogeochemical cycling in modern and ancient Earth. Annu Rev Earth Pl Sc *36*, 457-493.

Johnson, C. M., Skulan, J. L., Beard, B. L., Sun, H., Nealson, K. H., and Braterman, P. S. (2002). Isotopic fractionation between Fe(III) and Fe(II) in aqueous solutions. Earth Planet Sci Lett *195*, 141-153.

Jouvin, D., Louvat, P., Juillot, F., Marechal, C. N., and Benedetti, M. F. (2009). Zinc isotopic fractionation: why organic matters. Environ Sci Technol *43*, 5747-5754.

Ludwig, K. R. (2008). Isoplot 3.6 (Berkeley Geochronology Center Spec. Pub).

Majestic, B. J., Anbar, A. D., and Herckes, P. (2009). Stable Isotopes as a Tool to Apportion Atmospheric Iron. Environ Sci Technol *43*, 4327-4333.

Martell, A., and Smith, R. (1989). Critical Stability Constants, Vol 1-6 (New York: Plenum).

Ottonello, G., and Zuccolini, M. V. (2008). The iron-isotope fractionation dictated by the carboxylic functional: An ab-initio investigation. Geochimica Et Cosmochimica Acta *72*, 5920-5934.

Raymond, K. N., and Carrano, C. J. (1979). Coordination chemistry and microbial iron transport. Accounts Chem Res *12*, 183-190.

Roe, J. E., Anbar, A. D., and Barling, J. (2003). Nonbiological fractionation of Fe isotopes: evidence of an equilibrium isotope effect. Chem Geol *195*, 69-85.

Stookey, L. (1970). Ferrozine-a new spectrophotometric reagent for iron. Anal Chem *42*, 779–781.

Urey, H. C. (1947). The thermodynamic properties of isotopic substances. J Chem Soc, 562-581.

Walczyk, T., and von Blanckenburg, F. (2005). Deciphering the iron isotope message of the human body. Int J Mass Spectrom *242*, 117-134.

Welch, S. A., Beard, B. L., Johnson, C. M., and Braterman, P. S. (2003). Kinetic and equilibrium Fe isotope fractionation between aqueous Fe(II) and Fe(III). Geochimica et Cosmochimica Acta *67*, 4231-4250.

Weyer, S., and Schwieters, J. (2003). High precision Fe isotope measurements with high mass resolution MC-ICPMS. Int J Mass Spectrom *226*, 355-368.

Wiederhold, J., Kraemer, S. M., Teutsch, N., Borer, P., Halliday, A., and Kretzschmar, R. (2006). Iron isotope fractionation during proton-promoted, ligand-controlled, and reductive dissolution of goethite. Environ Sci Technol *40*, 3787-3793.

Chapter 3

WHOLE ORGANISM IRON ISOTOPE MASS BALANCE: IMPLICATIONS FOR THE STUDY OF IRON METABOLISM IN VIVO

Jennifer L. L. Morgan*[1], Stephen J. Romaniello[2], Joseph L. Skulan[3], Gwyneth W. Gordon[2], Daniel E. Bütz[4] , Ariel D. Anbar[1,2]

[1]Arizona State University, Department of Chemistry and Biochemistry, PO Box 871604, Tempe, AZ 85287

[2]Arizona State University, School of Earth and Space Exploration, PO Box 871404, Tempe, AZ 85287

[3]University of Wisconsin, Geology Museum, 1215 W. Dayton St. Madison, WI 53706

[4]University of Wisconsin-Madison, Department of Zoology, 1117 W. Johnson St. Room 211 Madison, WI 53706

3.1 Abstract

In mammals, iron balance is maintained by regulating Fe absorption, Fe storage, red blood cell formation and Fe loss. Disruptions to the regulators of these processes greatly affect Fe homeostasis, leading to diseases like anemia and hemochromatosis. Here we present preliminary data demonstrating the potential for stable Fe isotope fractionation to yield new insight into Fe metabolism. For the first time, the Fe isotopic composition of an entire organism was measured, as well as the isotopic compositions of various organs. In order to identify where Fe isotope fractionation occurs, individual mouse organs and a whole mouse were dissolved, and the Fe isotope ratios were measured. Results show that distinct isotope reservoirs exist in the small intestines, the

red blood cells, the serum and the liver. The entire organism was isotopically light compared with the sole food source. Our research supports the hypothesis that light Fe is absorbed preferentially in the small intestines. Using the Fe isotope composition of each reservoir, we estimate the fractionation between reservoirs and explore how Fe isotopes could be used as a tool to study Fe metabolism *in vivo*.

3.2 Introduction

Iron is an essential element for all living organisms; it is the metal center in many critical enzymes and biomolecules including hemoglobin, myoglobin, cytochrome P450, and all components of the electron transport chain. In mammals, iron balance is maintained by closely regulating Fe absorption, Fe storage, red blood cell formation and Fe loss; proteins mediate the distribution of Fe between these reservoirs. By measuring Fe isotope ratios *in vivo,* we hope to gain information that will improve our understanding of Fe metabolism and potentially be the first step in developing a new tool to evaluate the progression of disease states like anemia and hemochromatosis.

Fe has four stable isotopes: ^{54}Fe, ^{56}Fe, ^{57}Fe, and ^{58}Fe, with average natural abundances of 5.845 %, 91.754 %, 2.119 %, and 0.282 %, respectively. Isotopes of different masses of the same element have slightly different properties during chemical reactions. In an equilibrium reaction, the vibrational frequency is a function of the atomic weights of the constituent atoms; more energy is required to break this bond for heavier elements. In a kinetic reaction, bonds form and break at a faster rate for lighter elements. In chemical reactions, these mechanisms cause the ratio of isotopes in the reactants and products to differ. Depending on the type of reaction, either light or heavy isotopes can be enriched, as long as the reaction is incomplete. If the reaction is complete, the product's isotope composition will be identical to the reactant's isotope

composition. Isotopic fractionation can occur in all elements with multiple isotopes and has been quantified for light elements such as hydrogen, oxygen, carbon and nitrogen for many decades(Yang, 2009; Zhu et al., 2002). The range of isotope ratio variation between reservoirs is smaller in heavy elements like Fe than in light elements because the relative difference in the masses between isotopes is smaller. However, with technological advances such as multiple collector inductively coupled plasma mass spectrometry (MC-ICP-MS), the differences in isotope ratios for heavy elements can be routinely measured (Anbar and Rouxel, 2007a; Johnson et al., 2008).

Recent applications and advances in Fe isotope measurements have focused on applications to environmental weathering, microbial biomarkers in the rock record, and redox indicators of ancient earth (Anbar, 2004; Beard et al., 1999; Fehr et al., 2008; Johnson et al., 2002). In addition, experimental results and theory have shown that redox changes from Fe^{2+} to Fe^{3+} induce large natural isotope fractionations during reactions (Anbar et al., 2005; Domagal-Goldman and Kubicki, 2008; Domagal-Goldman et al., 2009; Johnson et al., 2002). Equilibrium exchange of Fe between organic ligands also fractionates Fe isotopes, if the difference in binding affinities of the two ligands is large (Dideriksen et al., 2008; Morgan et al., 2010). These types of reactions occur in biological systems aided by enzymes and so isotope fractionations of similar magnitude are possible. With further investigation, Fe isotopes could be used to understand details about Fe uptake pathways and utilization *in vivo*.

Studies have begun to investigate Fe isotope measurements as a way of detecting disease states. For example, blood samples from patients with hereditary hemochromatosis were characterized for their Fe isotope composition and were found to be significantly different compared to age matched controls (Krayenbuehl et al., 2005).

In addition to monitoring disease states, questions still remain about the Fe isotope composition in healthy populations. Previous research has explored the stable Fe isotopic signatures in human blood (Ohno et al., 2004; Walczyk and von Blanckenburg, 2002; Walczyk and von Blanckenburg, 2005). The isotopic composition of human blood is enriched in light Fe compared to nonspecific dietary Fe sources, including edible plants and herbivores. Three possible mechanisms for this fractionation have been proposed: 1) preferential absorption of light Fe in the intestines, 2) isotope-selective incorporation into organs, or 3) preferential excretion of heavy Fe (Walczyk and von Blanckenburg, 2005). To begin to address these hypotheses, researchers dissected and measured the Fe isotope composition of specific organs in a female Göttingen minipig. They measured the isotope composition of rinsed intestinal sections and found that all intestinal sections were isotopically light compared with food. In addition, by measuring select Fe containing organs they estimated the Fe isotope composition of the whole organism and determine it was isotopically light compared to diet. This lead the authors to conclude that preferential absorption of light Fe in the intestines caused the organism and its blood to be isotopically light (Hotz et al., 2011).

Our research aims to further distinguish between these three hypotheses by, for the first time, assessing Fe mass balance in a whole organism. Individual mouse organs and a whole mouse were dissolved, and the Fe isotope ratios measured to identify where Fe isotope fractionation occurs. Results show that distinct isotope reservoirs exist in the small intestines, the red blood cells, the serum and the liver, and that the entire organism was isotopically light compared with the sole food source. Our research supports the hypothesis that light Fe is absorbed preferentially in the small intestines. Using the Fe isotope composition of each reservoir, we estimate the fractionation

between reservoirs and start to explore how Fe isotopes could be used as a tool to study Fe metabolism *in vivo*.

3.3 Methods

Mouse status and age

All procedures on live animals were approved by the institutional animal care and use committee of the Collage of Letters and Sciences at the University of Wisconsin at Madison the site of these experiments. Two twelve-week-old ICR (imprinting control region) male mice, bred from an in house colony, were maintained on a 12-hour light dark cycle and fed following weaning the same standard rodent chow diet. At twelve-weeks of age, one mouse (A) was euthanized by CO_2 asphyxiation and the other individual (B) was deeply anesthetized with Isoflurane and exsanguinated via brachial arterial vein puncture. Whole blood from mouse B was allowed to clot at room temperature for 30-minutes, then centrifuged for 10 minutes at 10,000g. Serum was transferred to a new tube and both serum and blood pellet were saved for later analysis. Dissection of mouse B was done at the University of Wisconsin. Briefly, a midline incision was made in the peritoneum and extended through the thoracic cavity. The heart, lungs, liver, kidney, spleen, stomach, small intestines, cecum, colon, one femur bone, and one leg muscle were removed and immediately placed on dry ice. All the dissected organs, the remaining carcass and the intact euthanized mouse were sent to Arizona State University on dry ice.

Sample Digestion and Purification

The samples were defrosted, weighed, and digested using modified aqua regia (1:1 distilled nitric acid and distilled hydrochloric acid) at ~130°C. Sequential rounds of modified aqua regia digestion and nitric acid with 20% ultra pure H_2O_2 were added to the

samples until low surface tension indicated that the organic matrix was removed and the samples were completely dissolved.

Iron was purified from samples using an anion exchange column chromatography procedure utilizing Bio-Rad AG MP-1 resin and following the procedure outlined in Arnold et al. (2004b). Briefly, Fe is loaded onto the resin in 7M HCl. Under these conditions, Fe is tightly bound to the resin with a high distribution coefficient, while other matrix elements pass through the column. Once the matrix elements have been removed, the acid is changed to 0.5 M HCl and the Fe is eluted for collection.

3.4 Analytical Procedures

Iron concentrations and yields were measured by quadrupole ICP-MS with a 7% H_2-in-He collision cell gas (Thermo Scientific X Series). Sample and standard solutions were introduced in parallel with an internal standard solution containing yttrium for normalization of plasma variation. For replicate measurements of select samples, there was a 2σ error of ± 5%. Full recovery of Fe from the ion exchange column is required because the purification chemistry can induce an isotope fractionation of its own. Therefore, all samples measured for Fe isotopes had at least a 95% recovery of Fe off the column.

Iron isotopic compositions were measured using a MC-ICP-MS (Thermo Scientific Neptune) following the method of Arnold et al.(2004b). Medium mass-resolution mode was used to resolve the polyatomic interferences ArN^+, ArO^+, and $ArOH^+$ from $^{54}Fe^+$, $^{56}Fe^+$ and $^{57}Fe^+$, respectively (Weyer and Schwieters, 2003b). Some samples were measured using high mass-resolution mode when medium resolution slits were unavailable. The change in slits induced no change in the data quality or procedure other than requiring more concentrated solutions. Samples and standards were

introduced at concentrations of either 600 ppb Fe (medium resolution) or 1200 ppb Fe (high resolution). In addition to standard-sample bracketing, Cu was added at 600 ppb (medium resolution) or 1200 ppb (high resolution) to each standard and sample to monitor the instrumental mass bias. Each analysis averaged thirty, 8.16-second cycles measuring three Fe ratios simultaneously: $^{56}Fe/^{54}Fe$, $^{57}Fe/^{54}Fe$, and $^{58}Fe/^{54}Fe$. All ratios were measured relative to IRMM-014 (Institute of Reference Materials and Measurement, Geel, Belgium). Values are expressed as:

$$\delta^{56/54}Fe_{sample} = \left[\frac{\left(\frac{^{56}Fe}{^{54}Fe}\right)_{sample} - \left(\frac{^{56}Fe}{^{54}Fe}\right)_{standard}}{\left(\frac{^{56}Fe}{^{54}Fe}\right)_{standard}} \right] \times 1000 \quad (1)$$

Valid measurements must be mass dependent, so if the variation per amu ($\delta^{56/54}Fe/2$ and $\delta^{57/54}Fe/3$) differed by more than 0.05 ‰, the datum was rejected. Data were also rejected if the magnitude of the copper normalization of the mass bias correction exceeded |0.35| ‰ (indicating a significant difference in the sample matrix between samples and standards) or if the intensity of ^{56}Fe was less than 4.5 V. The intensities of the other less abundant isotopes did not sufficiently exceed the blank when ^{56}Fe was less than 4.5 V. The instrumental quality control criteria were relaxed for the serum sample because of the limited amount of Fe in the sample. The ^{56}Fe voltage for the serum measurement was 3.5 V and the variation per amu ($\delta^{56/54}Fe/2$ and $\delta^{57/54}Fe/3$) differed by 0.35 ‰. This relaxation of these quality control criteria is reflected in the larger error bar associated with the serum sample. Throughout analytical runs, the IRMM-014 standard, gravimetric isotope standards and rock standards were measured to ensure reproducibility from session to session. Based on replicate measurements of each sample, the internal precision is given for each sample in Table 3-1.

In general, the magnitude of the offset between two pools is known as the fractionation ($\Delta^{56/54}$Fe). Here we are specifically interested in the isotope fractionation as Fe moves from any one organ to another organ (A to B). Typically the fractionation factor, α, is used to describe these types of mass sensitive transfers. However, in order to keep the units in delta notation, we will utilize the following approximation:

$$\Delta^{56/54}Fe_{A\text{-}B} \cong 1000x\ln(\alpha^{56/54}Fe_{A\text{-}B}) \quad (2)$$

where $\Delta^{56/54}Fe_{A\text{-}B}$ is the isotope fractionation as Fe moves from reservoir A to reservoir B.

3.5 Results and Discussion

Fe Isotope Composition of Whole Organism

The Fe concentration and isotopic composition of the whole mouse and individual mouse organs from a pair of littermates were measured (Table 3-1). The isotopic composition of the whole mouse (-1.72 ± 0.16 ‰) was lighter compared to its sole food source (-0.17 ± 0.20 ‰). These values are consistent with previous estimates of a whole minipig Fe isotope composition (-1.5 ‰) (Hotz et al., 2011). The range of Fe isotope values for different organs within one individual is almost as large as the entire natural range of isotope variation found in nature (~3 ‰, (Anbar, 2004)). The Fe isotope composition of samples varies from the isotopically heavy value for food, (-0.17 ± 0.20 ‰) to the lightest value for blood (-2.23 ± 0.23 ‰; Figure 3-1). The large variation in isotopic composition of organs suggests the isotopic composition of individual organs is strongly controlled by the combination of mechanisms by which Fe enters and exits the organ. The known pathways by which Fe enters cells are 1) via transferrin and the transferrin receptor protein (TFR1), 2) reduction followed by transport via the divalent metal transporter 1 (DMT1) or 3) Fe-heme is absorbed via the heme carrier protein 1

(HCP1) (Andrews, 2008; Donovan et al., 2006). Measurements of Fe isotope ratios in one or more organs may provide a unique, naturally-occurring tracer for studying the physiology of Fe in biology.

In order to verify that all major Fe reservoirs in the dissected mouse were properly assessed, an isotope mass balance model for the dissected mouse was compared against the overall isotopic composition of its sacrificed littermate. The weighted average isotope composition of all of the organs plus the remaining carcass of the dissected mouse was calculated as follows:

$$\delta^{56/54}\mathrm{Fe}_{\text{weighted ave}} = \frac{\sum \delta^{56/54}\mathrm{Fe}_{\text{organ}-1} \times \mu\mathrm{gFe}_{\text{organ}-1} + \delta^{56/54}\mathrm{Fe}_{\text{organ}-n} \times \mu\mathrm{gFe}_{\text{organ}-n} \cdots}{\sum \mu\mathrm{gFe}_{\text{organ}-1} + \mu\mathrm{gFe}_{\text{organ}-n} \cdots} \quad (3)$$

We find that $\delta^{56/54}_{\text{weighted avg , mouse}}$ = -1.64 ± 0.10 ‰. This value can be compared to the isotope composition of the mouse digested in bulk, -1.72 ± 0.16 ‰. The two values are within error of each other, confirming that the dissected mouse includes all the major Fe reservoirs. These results also suggest that there is little variation between organisms when both specimens are healthy and have the same age and life history. These values can also be compared to the estimate for the minipig Fe isotope composition in the literature -1.5 ‰ (Hotz et al., 2011). The isotope composition of our mouse model is offset by about -0.18 ‰ from the minipig model, which is the same offset as the isotope composition difference in the two food values (-0.17 ± 0.20 ‰ mouse diet and ~0.0 ‰ for minipig diet). This offset indicates that the mechanisms that cause the isotope fractionation in both organisms are the same.

Determining the Fractionation Between Organs

The fundamental principles of isotope fractionation can be applied to biology just as they can be applied to environmental or geological processes. Isotope fractionation

during the transfer of Fe between organs can be calculated and used to track Fe fluxes. The isotope fractionation during the transfer of Fe from any one organ, A, to another organ, B, ($\Delta^{56/54}Fe_{A\text{-}B}$) was calculated using a mass balance model incorporating the measured isotope compositions of the organs and Fe fluxes obtained from literature values (Bothwell et al., 1979; Lopes et al., 2010; Walczyk and von Blanckenburg, 2005). This formalism was applied to each possible Fe transfer step in a system of simultaneous equations (Appendix A). Monte Carlo sensitivity analysis has shown that the calculated fractionations are only weakly dependent on the exact value of the fluxes, with the majority of the uncertainty limited by the precision of the Fe-isotope measurements (Appendix A).

For our model of biological Fe isotope fractionation in mice, we consider fluxes in and out of six major Fe reservoirs: serum, bone, red blood cell (RBC), spleen, liver, and "other organs" (Figure 3-2). The isotope composition of the "other organs" reservoir was determined by calculating the weighted average of the remaining carcass, muscle, bones, kidney, lungs and heart (Equation 3). The isotope composition of the Fe in the digestion track was not used in the model because the Fe in this reservoir is not metabolically active inside the mouse. We assume that Fe cycling in the mice was in steady-state, such that the Fe content and isotopic composition of each organ was not changing at the time of dissection. This implies that rates and isotopic compositions of Fe entering and leaving each organ are exactly balanced.

In cases where Fe is released by bulk processes there can be no mass-dependent fractionation and in these cases $\Delta^{56/54}Fe_{A\text{-}B}$ values were set to zero. These cases are: 1) the incorporation and destruction of red blood cells by the spleen ($\Delta^{56/54}Fe_{RBC\text{-}Spleen}$), 2) the release of Fe out of the liver ($\Delta^{56/54}Fe_{liver\text{-}serum}$), 3) cellular

sloughing ($\Delta^{56/54}Fe_{other\text{-}out}$), 4) phagocytosis ($\Delta^{56/54}Fe_{other\text{-}serum}$), and 5) bleeding ($\Delta^{56/54}Fe_{bleed}$) (Hentze et al., 2004).

The model was programmed in MATLAB™ with the equations in Appendix A. The fractionations between organs are presented in Figure 3-2.

Iron Cycling in Vivo

Iron is recycled very efficiently in mammals. Fe is absorbed in the intestine and transferred to serum. Only about 1 % of the Fe ingested daily is absorbed into the body (Hentze et al., 2004). In an adult human, this adds up to about 1 mg of Fe per day (Hentze et al., 2004). Once Fe is absorbed, it is taken up by transferrin in serum for transport throughout the body. Serum Fe makes up a very small percent of the total Fe in the body, but the flux of Fe is very high because all Fe transport between tissues passes through serum. Approximately 2.8 % of the total body Fe circulates through serum every day but at any given time the amount of Fe in serum only represents 0.06 % of the total Fe in the body. Hence the mean residence time of Fe in serum is only two to three hours.

Serum shuttles Fe into the red blood cell cycle where Fe is used to form functional RBCs. In the first step in the RBC cycle, Fe is transferred from serum to bone (Figure 3-2). The bone is the main location where RBCs are formed (Andrews, 2008). Bone makes up about 3.5 % of the Fe in the body and RBCs make up about 53 % (Bothwell et al., 1979; Donovan et al., 2006; Walczyk and von Blanckenburg, 2005). In RBC, most Fe is in the metal center in hemoglobin, which is used to transport oxygen to all the organs. RBCs have a lifetime of approximately 120 days in humans (Shemin and Rittenberg, 1946) but 20 to 54 days in mice (Lopes et al., 2010). Some RBCs are taken up constantly by the spleen, where reticuloendothelial macrophages capture and destroy

RBC in bulk. The Fe reenters the serum where it can be recycled into RBC, transported to other organs for use, or stored in the liver.

Fe loss occurs via two types of processes, a ligand selective process, which excretes Fe binding ligands via urine and bile and a bulk process through bleeding and cell sloughing. Currently, there is no known regulatory mechanism, which controls Fe loss (Andrews and Schmidt, 2007). This passive loss is approximately equal to the Fe absorption every day and in adult humans adds up to about 1 mg (0.02% total Fe) Fe per day but in mice is approximately 3.2 μg/day (0.32%) (Lopes et al., 2010).

Compared with other Fe reservoirs in the body, blood serum is unique because it has a very short residence time (about 30 min) (Lopes et al., 2010). The Fe isotopic composition of serum is -0.99 ± 0.40 ‰. Since this reservoir only contains small amounts of Fe and it is constantly being exchanged, it may be a useful reservoir to measure when attempting to evaluate Fe metabolism *in vivo*.

Isotope Fractionation Between Organs

Our measurements and modeling indicate that Fe isotopes are fractionated in distinct ways during transfer into and out of each organ. The largest fractionation occurs during intestinal absorption, where $\Delta^{56/54}Fe_{food\text{-}serum}$ = 1.93 ± 0.28 ‰ (Figure 3-2). As a result, the isotope composition of the Fe entering the mouse is -2.10 ± 0.28 ‰ ($\delta^{56/54}Fe_{IRMM}$) when ingested food is $\delta^{56/54}$Fe = -0.17 ± 0.2 ‰ as was the case here. Food and feces are isotopically similar because only a small fraction of dietary Fe is absorbed. Therefore, the isotope composition of feces (-0.18 ± 0.10 ‰) will always be similar to that of the diet.

Digestion Track

We measured the isotope composition of the stomach, small intestines, cecum and colon with food still inside the organ. The Fe concentrations and isotope compositions of these organs generally match that of food, indicating that most of the Fe in these reservoirs is likely from partially digested food. The residual food in the digestive prevented us from cleanly measuring the isotopic composition of these reservoirs. In order to accurately obtain the isotope composition of each section in the digestion track, the food would need to be removed and the organ washed with a clean solution of a suitable ionic strength. The small intestine was not cleaned of digested food, but happened to be mostly empty (as indicated by the much lower Fe concentration). Therefore, the isotope value of the small intestine (-0.99 ± 0.12 ‰) may be the best direct measure of fractionation that occurs during Fe absorption in this study and is much lighter than food (Table 3-1 and Figure 3-1). The isotope composition of small intestine measured in this study matched the measured isotope composition of cleaned intestinal cells in a minipig (-0.97 ‰ to -1.69 ‰) (Hotz et al., 2011). However, these values are nonetheless significantly heavier than the absorption value calculated from the model (-2.10 ± 0.28 ‰). One reason for this offset may be because the calculated absorption value represents the Fe flux from food to serum meaning that Fe is fractionated during absorption into entrocytes (intestinal absorptive cells) then further fractionated during excretion out of entrocytes into serum.

Red Blood Cells Cycle (RBC)

The red blood cell (RBC) cycle involves about 2.8 % of the Fe in the body per day. Serum brings Fe to bone; this transfer has a fractionation of 1.24 ± 0.46 ‰ ($\Delta^{56/54}Fe_{serum\text{-}bone}$). In the bone, RBCs are formed and released into the blood, with a fractionation of 0.57 ± 0.35 ‰ ($\Delta^{56/54}Fe_{bone\text{-}RBC}$), with the isotopically light Fe sequestered

into RBC. RBCs circulating in blood are eventually destroyed and the Fe in them is recycled. This occurs mainly in the spleen where reticuloendothelial macrophages capture and destroy RBC in bulk. It is unlikely that this process would induce an isotope fractionation, since the RBCs are captured in bulk, and so we fix $\Delta^{56/54}Fe_{RBC\text{-}spleen} \equiv 0$. Fixing this value also avoids parameter ambiguity in the model, allowing the remaining fractionations to be uniquely determined (Lopes et al., 2010). Fe is released from the spleen back into serum to be utilized again for RBC formation or transported to other reservoirs. The fractionation between spleen and serum is 0.62 ± 0.26 ‰ ($\Delta^{56/54}Fe_{spleen\text{-}serum}$). At steady state, the isotope composition of each flux in the RBC cycle must be the same. In our model, the isotopic composition of this flux is -2.23 ± 0.23 ‰, matching that of RBC. The reason that the isotope composition of the fluxes matches RBC is because the Fe moving from RBC into the spleen is not fractionated. If a system is in steady state, the isotope composition entering an organ must equal that exiting the organ. This defines the isotope composition of each flux - but in order to obtain that value, each flux in the RBC cycle has a unique fractionation.

Liver

The liver is another major reservoir of Fe; it includes ~ 20% of the Fe in the whole organism, mostly in the form of the iron storage protein ferritin. Ferritin stores Fe in several mineral phases including magnetite, hematite and ferrihydrite in the center of the ferritin protein casing (Galvez et al., 2008). Isotopically, the liver is very similar to serum (-1.04 ± 0.08 ‰, -0.99 ± 0.40 ‰ respectively). While a small portion of Fe in serum (2-7)% can be found as ferritin, the vast majority of Fe in serum is bound as transferrin, ruling out a single molecular environment as the reason for this isotopic similarity. However, both ferritin and transferrin proteins bind Fe^{3+}, suggesting that no redox

change is required for Fe to transfer between these proteins. Redox changes in Fe are usually accompanied by large isotope fractionation (Domagal-Goldman and Kubicki, 2008; Johnson et al., 2002). There is no evidence that supports that transferrin and ferritin directly exchange Fe *in vivo* (Harris, 1978). There are two hypotheses for the mechanism by which Fe is transferred between these two pools. 1) The ferritin reduction and chelation model in which Fe^{3+} is reduced to Fe^{2+} and then bound to a ligand on the outside of the ferritin molecule for release from ferritin or the Fe is oxidized for incorporation into ferritin. 2) The ferritin non-reductive process where no redox chemistry occurs and Fe^{3+} is bound to a ligand for transport to and from ferritin (Watt et al., 2010). The isotopic similarity of the liver and serum pools supports the hypothesis that there is no Fe redox change during the multiple ligand transfer of Fe from transferrin to ferritin. The predicted fractionation into the liver, 0.05‰, is smaller than the analytical uncertainty on the isotope measurement, 0.1 ‰, and so it is indeed possible that there is no fractionation. To constrain the model, the fractionation out of the liver is assigned to be zero ($\Delta^{56/54}Fe_{liver\text{-}serum} \equiv 0$), since any release of Fe out of liver would most likely be done in bulk via endocytosis of liver cells (Hentze et al., 2004). Overall, it appears that the transfer of Fe in and out of the liver does not fractionate.

Other Organs

The “other organs” reservoir includes muscle, heart, lungs and remaining carcass from the dissected mouse. The muscle isotope composition was similar to whole organism. Heart, lung and kidney contained Fe with similar isotope composition to blood. All these organs were lumped into the same reservoir for simplicity, and because they all had approximately the same isotope value. The fractionation into this reservoir was calculated to be 1.01 ± 0.42 ‰ ($\Delta^{56/54}Fe_{serum\text{-}other}$). Fe can be released from this reservoir

two different ways: either it can be excreted out of the body through cell sloughing, or return to serum via phagocytosis. Both fluxes' fractionations were set to zero ($\Delta^{56/54}Fe_{other\text{-}out} \equiv 0$, $\Delta^{56/54}Fe_{other\text{-}serum} \equiv 0$) since both these mechanisms are unlikely to express an isotope fractionation due to the quantitative nature of the transfer.

Distinguishing Hypotheses

This research aimed to distinguish between the three possible mechanisms for the presence of isotopically light Fe in blood. These hypotheses are: 1) preferential absorption of light Fe in the intestines, 2) isotope-selective incorporation into organs, or 3) preferential excretion of heavy Fe (Walczyk and von Blanckenburg, 2005).

We can immediately discount hypothesis 2. The entire organism is isotopically light compared to dietary input, eliminating the possibility that the isotopically light Fe value for blood could result from the partitioning of dietary iron into heavy and light pools within the body.

We can also discount hypothesis 3 and the possibility that the excretion of heavy Fe alone causes the organism to be isotopically distinct from food. The bulk excretion of Fe by either bleeding or cell sloughing is the main mechanism for Fe removal (64% of the Fe removed per day); since neither of these reservoirs is heavy, these bulk processes cannot remove heavy Fe from the organism. There is a ligand selective process to excrete Fe bound to low molecular weight organic ligands through urine and bile. It is estimated about 36% of the total Fe excreted per day is lost via ligand selective mechanisms with the majority being lost to bulk processes (Green et al., 1968; Hunt et al., 2009). Since the whole Fe-ligand complex is filtered by the liver and kidneys this process is most likely not sensitive to differences in the mass of the Fe being filtered. Our results cannot measure or calculate the fractionation in urine or bile. The isotope

composition of the bladder has been reported in the literature and is -1.38 ± 0.2 ‰ (Hotz et al., 2011) representing at least in part a urine sample. The feces isotope composition reported in this study to a small extent represent the Fe excreted with bile. These samples do not perfectly represent that of urine or bile because the contribution of Fe from urine or bile into the sample is small compared to total Fe measured. However, the fact that the samples are the same or lighter than the whole organism indicates that the urine or bile pool is not significantly heavier than the bulk organism. Therefore the majority of the Fe fractionation that offsets the organism from its food sources is occurring during absorption.

Our results support the hypothesis that preferential absorption of light Fe is the mechanism by which the Fe isotope composition of an organism comes to differ from that of its diet. This was also the hypothesis supported by previous research (Hunt et al., 2009; Walczyk and von Blanckenburg, 2002; Walczyk and von Blanckenburg, 2005). We constrain the fractionation during absorption and in our mouse model we estimate that fractionation to be $\Delta^{56/54}Fe_{food\text{-}serum}$ = 1.93 ± 0.28 ‰. In addition we outline a detailed model of the fractionation mechanism that cause RBC Fe to be isotopically light. RBCs are isotopically light because there is an incremental fractionation during absorption, transfer to bone and ultimately Fe's incorporation into RBC.

Causes of Fractionation Between Organs

The metabolism of Fe in the body is tightly regulated and mitigated by enzymes that catalyze most of the important transfers. As such, the reactions that control the transfer of Fe are most likely under kinetic control and not allowed to reach thermodynamic equilibrium. The fractionations that we predict in our model are all positive indicating that the product reservoir is sequestering light Fe isotopes. This is

consistent with a kinetic fractionation mechanism. Most transfers of iron occur via one of the three main pathways by which Fe enters cells: 1) via transferrin and the transferrin receptor protein (TFR1); 2) reduction of Fe^{3+} followed by transport via the divalent metal transporter 1 (DMT1); 3) Fe-heme is absorbed via the heme carrier protein 1 (HCP1) (Andrews, 2008; Donovan et al., 2006). Other proteins are involved in the transport of Fe intracellularly, and functional analogs of the proteins listed above have been discovered in specialized cell types, but the basic transport mechanisms are the same.

Based on what we know about abiotic Fe isotope fractionation, the reduction of Fe^{3+} to Fe^{2+} followed by transport via DMT1 should cause the largest fractionation. We suggest this because Fe isotopes are well-known to fractionate during both Fe reduction and oxidation (Anbar, 2004; Johnson et al., 2008; Johnson et al., 2002). During these processes, Fe^{3+} is typically enriched by as much as 3 ‰ relative to Fe^{2+}, which is the magnitude of the equilibrium Fe isotope fractionation between Fe^{3+} and Fe^{2+} aquo complexes (Anbar et al., 2005; Domagal-Goldman and Kubicki, 2008; Domagal-Goldman et al., 2009; Johnson et al., 2002). In addition, the binding of Fe to organic ligands causes an isotope fractionation but is smaller in magnitude (Dideriksen et al., 2008; Morgan et al., 2010). The isotope fractionation of Fe in cells is consistent with the type of fractionation suggested by abiotic experiments. For example, entrocytes (intestinal absorptive cells) mainly produce DMT1 in order to transport any divalent metal needed in the body. The main location where Fe^{3+} is reduced and transported via DMT1 is in the intestinal lumen. Therefore, based on the abiotic experiments, this mechanism should produce the largest Fe fractionation, and, since entrocytes mainly absorb Fe via this mechanism, they should be most fractionated from the reactant reservoir. Entrocytes also absorb Fe via HCP1. Heme-Fe is obtained mainly from animal meat but can also be

obtained from plants. We expect there to be no Fe isotope fractionation during the uptake of heme-Fe via HCP1 because the porphyrin ring prevents the transfer from being sensitive to variations in the mass of the Fe. However, the isotopic composition of the heme-Fe reservoir may be significantly different than dietary Fe^{3+}. The heme-Fe reservoir can shift the isotope composition of the entrocyte even if no fractionation occurs.

Fe fractionation can also occur when Fe is transported out of the entrocyte into the serum. Transferrin, the main Fe transport protein in the serum, transports Fe^{3+} therefore the Fe that was reduced to Fe^{2+} needs to be re-oxidized. The cumulative fractionations during absorption from food to serum is modeled to be $\Delta^{56/54}Fe_{food\text{-}serum}$ = 1.93 ± 0.28 ‰. The magnitude and direction of the fractionation calculated in this study is consistent with the generally accepted idea that reduction and binding by DMT1 is the main mechanism by which Fe is transported into the body.

3.6 Conclusion

Here we have measured the isotope composition of organs in a mouse; we calculated the fractionation between organs, and we have further verified the hypothesis that light Fe is preferentially absorbed in the intestine specifically during the reduction of Fe and transport via DMT1. This study represents a significant step forward in our understanding that mass dependant fractionation of Fe occurs in all organs throughout the body. It also provides insight into locations where transport of Fe is well controlled. With further experiments that investigate the fractionation between specific proteins, we can develop this tool to be used to monitor Fe metabolism *in vivo*.

Future work will focus on examining the fractionation that occurs between specific Fe proteins like ferritin and transferrin.

Table 3-1: Values for mouse organs and whole mouse				
	Weight (g)	Fe Concentration (ppm)	Amount Fe (μg)	$\delta^{56/54}$Fe ± 2σ (‰), n
Food	0.30	127.9	38.1	-0.17 ± 0.20, 4
Feces	0.05	317.7	17.4	-0.18 ± 0.10, 3
Stomach	0.40	102.3	41.2	-0.42 ± 0.17, 3
Small Intestine	1.42	32.4	46.2	-0.99 ± 0.12, 2
Cecum	0.43	132.1	56.4	-0.16 ± 0.12, 4
Colon	0.51	172.5	88.2	-0.15 ± 0.22, 4
Serum	0.20	3.9	0.8	-0.99 ± 0.40, 1
Liver	1.33	87.3	116.4	-1.04 ± 0.08, 4
Blood	0.87	537.9	467.6	-2.23 ± 0.23, 4
Heart	0.17	103.5	17.7	-2.16 ± 0.02, 3
Lungs	0.16	81.0	13.3	-2.23 ± 0.22, 4
Kidney	0.48	36.0	17.2	-2.26 ± 0.25, 3
Spleen	0.08	191.9	15.2	-1.61 ± 0.13, 4
Muscle	0.46	10.5	4.9	-1.81 ± 0.03, 4
Femur	0.08	33.9	2.9	-1.66 ± 0.27, 2
Mouse Carcass	16.96	10.7	181.2	-1.95 ± 0.02, 3
Other organs	18.23	12.8	234.3	-2.00 ± 0.10, NA
Dissected mouse*	23.57	45.36	1069.1†	-1.60 ± 0.10, NA
Whole Mouse	25.77	21.3	549.4†	-1.72 ± 0.16, 3

* sum of dissected organs and weighted average to used to calculate $\delta^{56/54}$Fe. † During digestion the whole mouse sample was spilled, causing a loss of Fe but had no effect on the Fe isotope composition

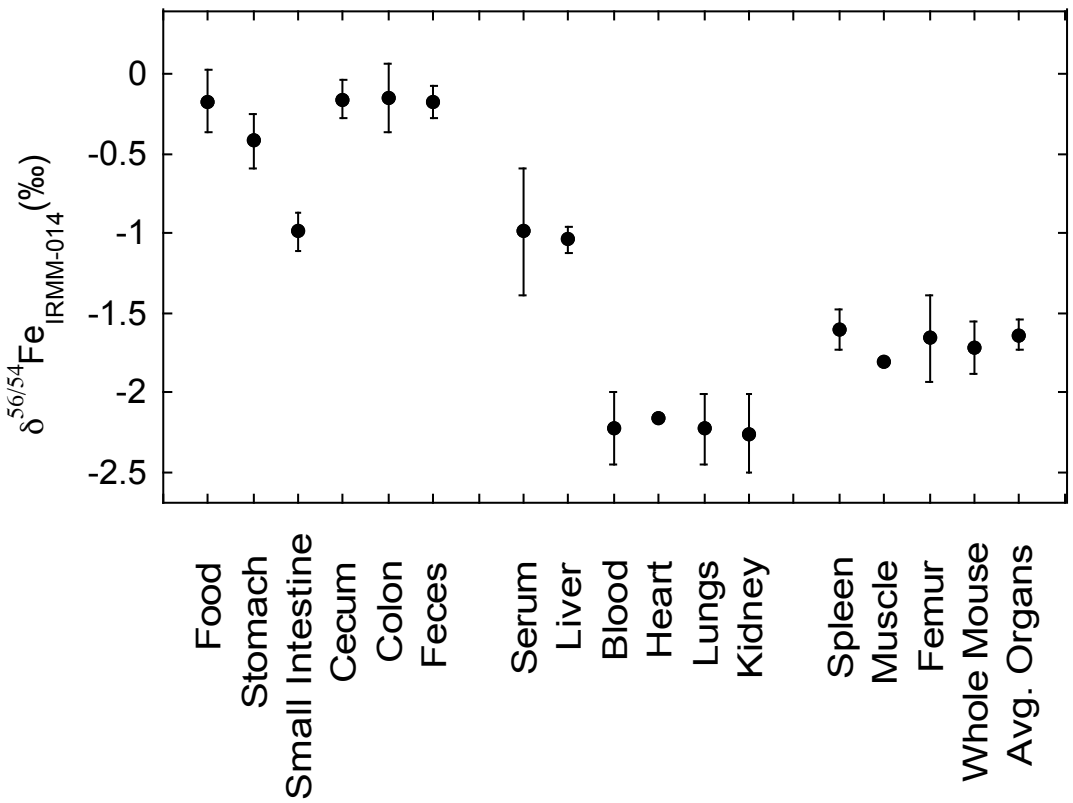

Figure 3-1 Fe isotope values of each organ.
$\delta^{56/54}Fe_{IRMM}$, 2σ error on individual replicates, n=1-4. Serum n=1 so error is approximate error on a single measurement. Concentration values are accurate within ± 5%.

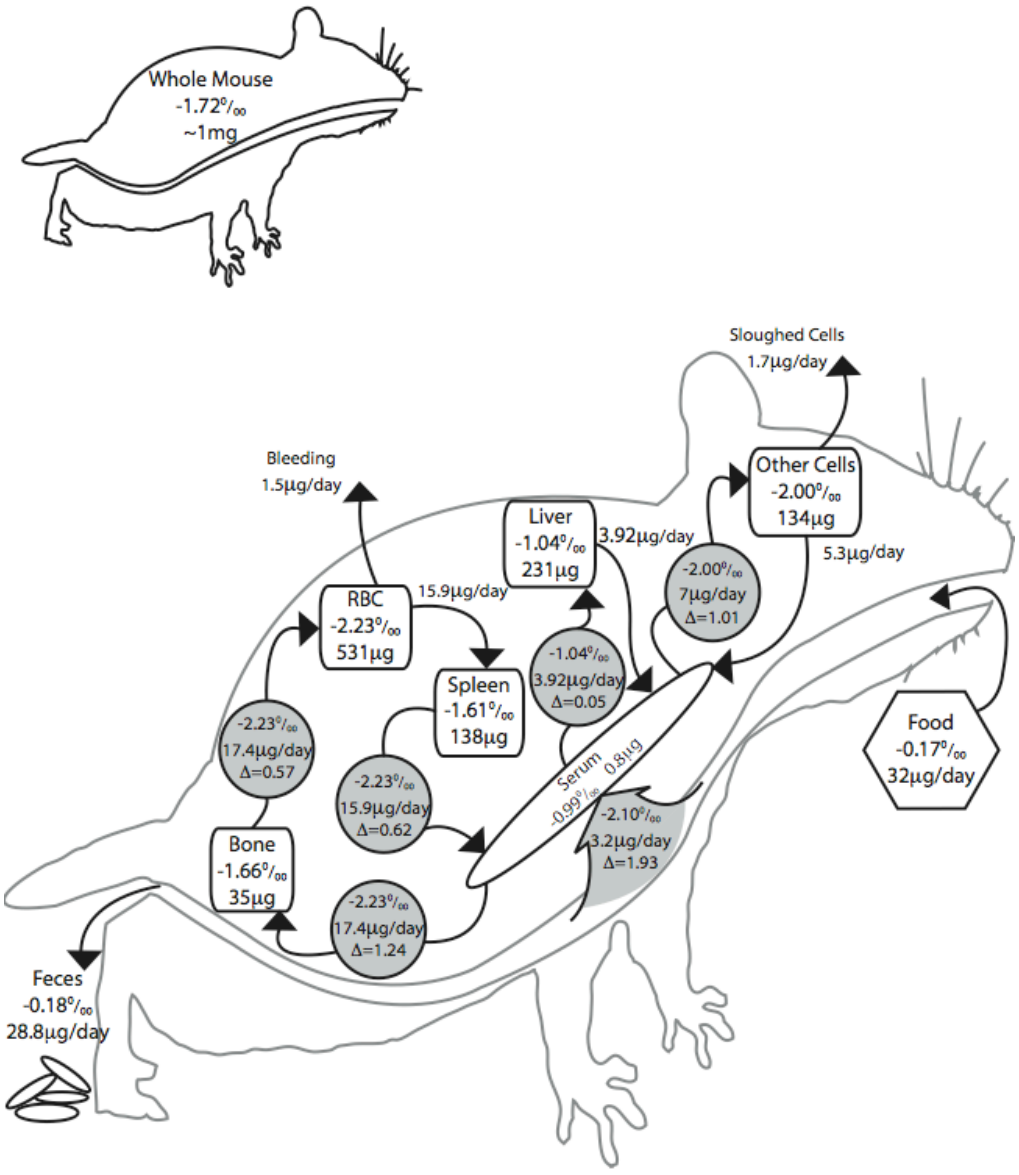

Figure 3-2 Fe fluxes into and out of major Fe stores in an organism. Fluxes are estimated from literature values see text for references. This figure is modeled after (Bothwell et al., 1979; Walczyk and von Blanckenburg, 2005).

3.7 References

Anbar, A., Jarzecki, A. A., and Spiro, T. G. (2005). Theoretical investigation of iron isotope fractionation between $(H_2O)_6^{3+}$ and $Fe(H_2O)_6^{2+}$: implications for iron stable isotope geochemistry. Geochimica et Cosmochimica Acta *69*, 825-837.

Anbar, A., and Rouxel, O. (2007). Metal stable isotopes in paleoceanography. Annu Rev Earth Pl Sci *35*, 717-746.

Anbar, A. D. (2004). Iron stable isotopes: beyond biosignatures. Earth Planet Sci Lett *217*, 223-236.

Andrews, N. C. (2008). Forging a field: the golden age of iron biolgy. Blood *112*, 219-230.

Andrews, N. C., and Schmidt, P. J. (2007). Iron Homeostasis. Annu Rev Physiol *69*.

Arnold, G. L., Weyer, S., and Anbar, A. D. (2004). Fe isotope variations in natural materials measured using high mass resolution multiple collector ICPMS. Anal Chem *76*, 322-327.

Beard, B. L., Johnson, C. M., Cox, L., Sun, H., Nealson, K. H., and Aguilar, C. (1999). Iron isotope biosignatures. Science *285*, 1889-1892.

Bothwell, T. H., Charlton, R. W., Cook, J. D., and Finch, C. A. (1979). Iron metabolism in man (Oxford: Blackwell Scientific).

Dideriksen, K., Baker, J. A., and Stipp, S. L. S. (2008). Equilibrium Fe isotope fractionation between inorganic aqueous Fe(III) and the siderophore complex, Fe(III)-desferrioxamine B. Earth and Planetary Science Letters *269*, 280-290.

Domagal-Goldman, S. D., and Kubicki, J. D. (2008). Density functional theory predictions of equilibrium isotope fractionation of iron due to redox changes and organic complexation. Geochimica Et Cosmochimica Acta *72*, 5201-5216.

Domagal-Goldman, S. D., Paul, K. W., Sparks, D. L., and Kubicki, J. D. (2009). Quantum chemical study of the Fe(III)-desferrioxamine B siderophore complex-Electronic structure, vibrational frequencies, and equilibrium Fe-isotope fractionation. Geochimica Et Cosmochimica Acta *73*, 1-12.

Donovan, A., Roy, C. N., and Andrews, N. C. (2006). The ins and outs of iron homeostasis. Physiolgy *21*, 115-123.

Fehr, M. A., Andersson, P. S., Halenius, U., and Morth, C. (2008). Iron isotope variations in Holocene sediments of the Gotland Deep, Baltic Sea. Geochimica et Cosmochimica Acta *72*, 807-826.

Galvez, N., Fernandez, B., Sanchez, P., Cuesta, R., Ceolin, M., Clemente-Leon, M., Trasobares, S., Lopez-Haro, M., Calvino, J. J., Stephan, O., and Dominguez-Vera, J. M. (2008). Comparative Structural and Chemical Studies of Ferritin Cores with Gradual Removal of their Iron Contents. J Am Chem Soc *130*, 8062-8068.

Green, R., Charlton, R., Seftel, H., and Bothwell, T. (1968). Body Iron Excreation in Man. Am J Med *45*, 336-353.

Harris, D. C. (1978). Iron exchange between ferritin and transferrin in vitro. Biochemistry *17*, 3071-3078.

Hentze, M. W., Muckenthaler, M. U., and Andrews, N. C. (2004). Balancing Acts: Molecular Control of Mammalian Iron Metabolism. `Cell *117*, 285-297.

Hotz, K., Augsburger, H., and Walczyk, T. (2011). Isotopic signatures of iron in body tissue as a potential biomarker for iron metabolism. J Anal At Spectrom.

Hunt, J. R., Zito, C. A., and Hohnson, L. K. (2009). Body iron excretion by healthy men and women. American Journal of Clinical Neutrition *89*, 1792-1798.

Johnson, C. M., Beard, B. L., and Roden, E. E. (2008). The iron isotope fingerprints of redox and biogeochemical cycling in modern and ancient Earth. Annu Rev Earth Pl Sc *36*, 457-493.

Johnson, C. M., Skulan, J. L., Beard, B. L., Sun, H., Nealson, K. H., and Braterman, P. S. (2002). Isotopic fractionation between Fe(III) and Fe(II) in aqueous solutions. Earth Planet Sci Lett *195*, 141-153.

Krayenbuehl, P.-A., Walczyk, T., Schoenberg, R., von Blanckenburg, F., and Schulthess, G. (2005). Hereditary hemochromatosis is reflected in the iron isotope composition of blood. Blood *105*.

Lopes, T. J., Luganskaja, T., Spasie, M. V., Hentze, M. W., Muckenthaler, M. U., Schumann, K., and Reich, J. G. (2010). Systems analysis of iron metabolism: the network of iron pools and fluxes. BMC System Biology *4*, 1-18.

Morgan, J. L. L., Wasylenki, L. E., Neuster, J., and Anbar, A. D. (2010). Fe isotope fractionation during equilibration of Fe-organic complexes. Environ Sci Technol *44*, 6095-6101.

Ohno, T., Shinohara, A., Kohge, I., Chiba, M., and Hirata, T. (2004). Isotopic Analysis of Fe in Human Red Blood Cells by Multiple Collector-ICP-Mass Spectrometry. Analytical Science *20*, 617-621.

Shemin, D., and Rittenberg, D. (1946). The lifespan of the human red blood cell. J Biol Chem *166*, 627-626.

Walczyk, T., and von Blanckenburg, F. (2002). Natural iron isotope variations in human blood. Science *295*, 2065-2066.

Walczyk, T., and von Blanckenburg, F. (2005). Deciphering the iron message in the human body. International Journal of Mass Spectrometry *242*, 117-134.

Watt, R. K., Hilton, R. J., and Graff, M. (2010). Oxido-reduction is not the only mechanism allowing ions to traverse the ferritin protein shell. Biochemica et Biophysica Acta *1800*, 745-759.

Weyer, S., and Schwieters, J. B. (2003). High precision Fe isotope measurements with high mass resolution MC-ICPMS. International Journal of Mass Spectrometry *226*, 355-368.

Yang, L. (2009). Accurate and Precise Determination of Isotopic Ratios by MC-ICP-MS: A Review. Mass Spectrometry Reviews *28*, 990-1011.

Zhu, X. K., Guo, Y., Williams, R. J. P., O'Nions, R. K., Matthews, A., Belshaw, N. S., Canters, G. W., Waal, E. C. d., Weser, U., Burgess, B. K., and Salvato, B. (2002). Mass fractionation process of transition metal isotopes. Earth Planet Sci Lett *200*, 47-62.

Chapter 4

HIGH PRECISION MEASUREMENTS OF VARIATIONS IN CALCIUM ISOTOPE RATIOS IN BIOMEDICAL MATERIAL BY MULTIPLE COLLECTOR INDUCTIVELY COUPLED PLASMA MASS SPECTROMETRY (MC-ICP-MS)

Jennifer L. L. Morgan[1]; Gwyneth W. Gordon[2]; Ruth C. Arrua [2]*; Joseph L. Skulan[3]; Ariel D. Anbar[1,2]

[1]Arizona State University, Department of Chemistry and Biochemistry, PO Box 871604, Tempe, AZ 85287

[2]Arizona State University, School of Earth and Space Exploration, PO Box 871404, Tempe, AZ 85287

[3]University of Wisconsin, Geology Museum, 1215 W. Dayton St. Madison, WI 53706

* now at Universidad Nacional de Córdoba – CONICET, Facultad de Ciencias Químicas, Dpto. de Quimica Organica, Medina Allende esq. Haya de la Torre, Ciudad Universitaria,

5000 Córdoba, Argentina.

4.1 Abstract

We describe a new chemical separation method to isolate calcium (Ca) from other matrix elements in biological samples, developed with the goal of making measurement of natural stable Ca isotope variations a clinically applicable tool to assess bone mineral balance. A new two-column procedure achieves the purity required to measure two ratios of Ca isotopes ($^{44}Ca/^{42}Ca$ and $^{44}Ca/^{43}Ca$) on a Neptune multi-collector inductively coupled plasma mass spectrometer (MC-ICP-MS). The matrix element limits for Ca/Sr (10,000), Ca/Ti (10,000,000) and Ca/K (10) were determined using element spikes in Ca standards of known isotopic composition. The precision of $\delta^{44/42}Ca$ measurements for purified samples is no worse than ± 0.2 ‰ (2σ). Accuracy was determined by comparing samples and standards run on thermal ionization mass spectrometry (TIMS), standards run through chemistry and sample-standard mixing.

4.2 Introduction

Calcium (Ca) isotope variations in biological fluids such as urine and blood can be used to assess bone mineral balance (BMB) in humans (Heuser and Eisenhauer, 2010; Skulan et al., 2007), raising the possibility that Ca isotopic analyses could be employed clinically to detect and assess treatments for diseases that affect BMB, such as osteoporosis and multiple myeloma (Yeh and Berenson, 2006). X-ray bone scans or histological biopsies are the only method

of measuring BMB currently in widespread clinical use. In contrast, a natural Ca isotopic biomarker would pose no radiological hazard, is noninvasive and could detect changes in BMB quickly before these have resulted in significant reduction in bone density and resulting clinical outcomes such as fracture (Damilakis et al., 2010a; Kanis et al., 2008; Skulan et al., 2007). Biomarkers of the bone formation and resorption processes have been developed as useful measures of the relative rates of their respective processes, but the Ca isotope technique can prove a helpful compliment since it measures net bone mineral balance directly (Leeming et al., 2006; Sorensen et al., 2007).

The Ca isotope technique is based on small but measurable differences in the partitioning of Ca isotopes between bone and soft tissues. During bone formation, light isotopes of Ca are preferentially incorporated into bone. This isotopic fractionation leaves soft tissue with an excess of heavy Ca isotopes relative to dietary Ca. Bone resorption involves a bulk dissolution of small volumes of bone, so there is no isotope fractionation. Bone resorption releases the isotopically light Ca that was stored in bone back into soft tissue. When the rate of bone formation and resorption are equal these two effects cancel and bone has no net effect on the Ca isotope composition of soft tissue, while net bone formation and net bone resorption causes heavy and light excursions in soft tissue Ca isotope composition, respectively. These natural isotope variations in soft tissues are reflected in urine and can be quantified by precise mass spectrometric measurements. This relationship between soft tissue Ca isotope composition and BMB has been empirically confirmed in several studies (Skulan et al., 2007; Skulan and Depaolo, 1999; Skulan et al., 1997). However, clinical

application of the Ca isotope technique demands the rapid analyses of large numbers of samples, which in turn requires a methodology capable of high sample throughput.

Traditionally, Ca isotope compositions are measured using thermal ionization mass spectrometry (TIMS) (DePaolo, 2004; Russell et al., 1978). The clinical utility of TIMS is limited because of its low sample throughput, typically 10-20 samples per day. Sample preparation and instrument operations for TIMS can also be time-consuming and require a highly trained operator to monitor instrument quality. Multiple collector inductively coupled plasma mass spectrometry (MC-ICP-MS) offers the potential for much higher rates of sample throughput, and can be set up with an on-line, automated chromatographic sample preparation system. TIMS offers the advantage of being able to measure the ^{40}Ca isotope, the major isotope of Ca, because thermal ionization does not use an argon plasma. MC-ICP-MS uses an argon plasma and the ^{40}Ar isotope interferes with ^{40}Ca such that resolution of signals from them is impossible. Despite only being able to measure the minor Ca isotopes, MC-ICP-MS requires sample sizes that are comparable to TIMS. An automated purification system for Ca measurement by TIMS has been developed for sample sizes < 5 μg using a commercially available HPLC system, but this automation did not substantially increase the sample throughput for TIMS as the bottleneck is downstream (Schmitt et al., 2009).

MC-ICP-MS has been successfully used for high-precision Ca isotope determinations in calcium carbonate rocks for geoscience research (Chu et al., 2006; Fietzke et al., 2004; Halicz et al., 1999; Wieser et al., 2004). However, few

stable Ca isotope studies in biological materials have employed MC-ICP-MS (Skulan et al., 2007; Skulan and Depaolo, 1999; Skulan et al., 1997). MC-ICP-MS measurement of Ca isotopes requires greater separation of Ca from other matrix elements than is necessary for TIMS. High-energy plasma ionizes many elements simultaneously and with high efficiency, generating isobaric interferences for ICP-MS that are not produced in the thermal range used for ionizing Ca in TIMS. Liquid chromatography that efficiently separates Ca from matrix elements is required to reduce these interferences. This chromatography must also have a nearly quantitative yield of Ca because chromatography itself fractionates Ca isotopes (Andren et al., 2004; Oi et al., 1993; Russell et al., 1978). Incomplete recovery could result in an isotope effect greater than the naturally occurring variations in the samples.

Here we report new liquid chromatography procedures that separate Ca from matrix elements in complex samples to the extent needed for MC-ICP-MS Ca isotope analyses. We determined the thresholds of separation efficiency required to obtain accurate and precise Ca isotope data by doping standard solutions with potential interferents. Our new chemical purification protocol produces consistent, quantitative yields. These procedures are appropriate for preparing Ca isotope samples in biological matrices for either TIMS or MC-ICP-MS methods. Unlike TIMS, MC-ICP-MS measurement can continue 24 hours a day with an autosampler, significantly reducing personnel costs, and dramatically increasing sample throughput. In addition, MC-ICP-MS offers the prospect of online, high-throughput methods in the future.

4.3 Methods

Digestion Procedure

All samples and standards were processed in a biosafety level 2, class 100, trace-metal-free clean lab with class 10 laminar airflow exhaust hoods. All plastics were single-use and acid washed by soaking in 3.2 M reagent grade nitric acid for one week, 2.4 M reagent grade hydrochloric acid for one week, washed in 18 MΩ cm^{-1} water and dried under a ULPA (ultra low particulate air) filtered air prior to use. Teflon screw top vials were cleaned in a heated (100 °C) 8 M nitric acid for 24 hours, followed by heated (100 °C) in 6 M hydrochloric acid for 24 hours and then leached in heated (100 °C) 18 MΩ cm^{-1} water. Acids used for chemical reagents were trace metal grade or better.

Concentrated nitric acid (2 mL) and ultra pure 30% fresh hydrogen peroxide (2 mL) was added to weighed samples in Teflon microwave digestion vessels. The MARS microwave system was set to ramp to 200 °C over 15 min then hold at 200 °C for 15 min. The samples were transferred to Teflon reaction vessels, and dried on a hotplate in a metal-free laminar airflow exhaust hood. Once dry, 1:1 concentrated nitric acid and concentrated hydrochloric acid (modified aqua regia) were added and the vessel was sealed and heated to 160 °C for 12 hrs. The sample solution was dried down, cooled, and 16 M nitric acid and 10% hydrogen peroxide were added to the sample. Alternating rounds of modified aqua regia and nitric acid plus peroxide digestions were performed until low aqueous surface tension indicated the samples were free of organic material. The samples were dissolved in 2.5 M HCl and placed in a storage container,

4 mL HDPE containers. Aliquots of the digested sample stocks equivalent to ~1 mL urine were weighed and purified on ion exchange columns.

Column Chemistry

Samples and standards were run through cation exchange resin (Biorad AG50-WX-12 200-400 mesh). Bio-Rad Econocolumns (0.7 x 30cm) were filled with 2 mL of clean resin, to a height of 8.6 cm. The column was equilibrated and stored in 2.5 M HCl. The sample was loaded onto the column with 1 mL of 2.5 M HCl, and an additional 1 mL of 2.5 M HCl was used to rinse the sample container. The following acids were added to the column, in order: 6 mL of 8 M HBr, 5 mL of 0.1 M HF, 10 mL of 0.1 M HF, 3 mL of 2.5 M HCl, and 10 mL of 2.5 M HCl. Ca was eluted in 5 mL of 6 M HCl, followed by two 10 mL aliquots of 6 M HCl (Table 4-1). This 25 ml of 6 M HCl contains all of the sample Ca and some Sr. The 25 mL sample was dried and dissolved in 0.25 mL 5 M HNO_3 and loaded onto 2 mm ID columns of Eichrom Sr-Spec Sr specific resin to separate Sr from Ca. At this acid concentaion, Sr binds to the resin and Ca passes through without interaction. The column was rinsed three times with 0.25 mL of 5 M HNO_3 to ensure complete recovery of Ca. After the column purification, samples were redigested with 16 M nitric acid and 30% hydrogen peroxide to degrade organic material eluted from the columns.

To ensure accuracy, ICP or carbonate standards and a blank were run in parallel to samples for each batch of column chemistry. The performance of the columns was verified for five samples; there were no significant changes to the position of the Ca elution peak, the resulting sample purity or sample recovery.

After samples were eluted the resin was cleaned with 20 mL of 6 M HCl and equilibrated with 20 mL of 2.5 M HCl.

Yields and elution curves were measured by quadrupole ICP-MS (Thermo Scientific X Series). Samples and calibration standard solutions were introduced in parallel with an internal standard solution containing Sc, Ge, Y and In for normalization of instrumental sensitivity. Uncertainties for replicate measurements were approximately ± 5-10% (2σ), depending on the element.

MC-ICP-MS Measurement

Ca isotopes were measured using a multiple collector ICP-MS (Thermo Scientific Neptune) following the method of Wieser et al. (Wieser et al., 2004). Standard-sample-standard bracketing was used with NIST X-10-39Ca (ICP1) as the standard solution since there is no internationally certified Ca isotope standard. For comparison to literature values, the $\delta^{44/42}Ca_{ICP1}$ value for IAPSO measured relative to ICP1 is 0.76 ± 0.15 ‰ and for 915a, a carbonate standard, is -0.15 ± 0.13 ‰; all Ca isotope measurements are reported relative to ICP1. Standard-sample-standard bracketing was chosen over a ^{42}Ca-^{48}Ca double spike employed in TIMS measurements (Skulan et al., 1997) because there are significant barriers to using a similar double spike in MC-ICP-MS from ^{48}Ti interferences, discussed in the Results/Discussion section. Standard-sample-standard is used to correct for instrumental mass bias, such as that caused by space-charge effect, which causes heavy isotopes to preferentially arrive at the detector (Andren et al., 2004). Standard-sample-standard bracketing assumes the mass bias drift is linear over time. This is not always the case, particularly if significant ionic or organic matrix remains in the sample solution, but replicate

measurements of the same sample on different analytical sessions and keeping analysis time short so bracketing standards are measured close in time to the samples reduces the effect of non-linear mass bias. To evaluate the impact of the assumption of linear mass bias change with time, and "memory effects" from incomplete sample washed out during rinse and uptake, we calculated the $\delta^{44/42}$Ca value for the standards, neglecting the intervening samples. Non-linear variations in mass bias were suggested if the standard value was offset from zero by more then 0.15 ‰. The sum of the absolute values for the bracketing standards and the 2σ errors on the value of the bracketing standards were calculated for each sample. If the sum of the two bracketing standards was greater than 0.3 ‰ ($\delta^{44/42}$Ca) or 2σ errors is greater than 0.3, then the sample is excluded.

Medium and high mass resolution modes were used to partially resolve the polyatomic interferences such as ArH_2^+, CO_2^+, N_2O^+ and N_3^+. The polyatomic interferences cannot be completely resolved from Ca, so isotope measurement were made on the shoulder of the calcium peak, avoiding the overlapping peak of calcium and polyatomic interferences (see Wieser et. al, Fig. 2). High resolution requires more concentrated samples, but there was no other effect on the data. Ca concentrations in samples and standards in medium-resolution mode varied widely depending on instrument performance but generally were between 1.5 ppm and 5 ppm, with most samples being run at 2.5 ppm. High-resolution mode was used only when medium resolution slits were worn through. High-resolution mode requires sample concentrations of ca. 20 ppm, increasing matrix effects and causing a buildup of sample on the cones and reduces sensitivity. Buildup

reduces the amount of sample that can be measured before cone cleaning is required.

For each analysis, 30 measurement cycles with 4.194 second integration times were averaged into a single measured value after exclusion of ratios >2 sigma from the average. Six masses were measured: ^{42}Ca, ^{43}Ca, ^{44}Ca, ^{46}Ca, ^{47}Ti and ^{48}Ca; intensity of ^{46}Ca (0.004%) was too low to produce reliable data. Values are reported as:

$$\delta^{44/4x}\mathrm{Ca} = \left[\frac{\left(\frac{^{44}\mathrm{Ca}}{^{4x}\mathrm{Ca}}\right)_{\mathrm{Sample}} - \left(\frac{^{44}\mathrm{Ca}}{^{4x}\mathrm{Ca}}\right)_{\mathrm{Standard}}}{\left(\frac{^{44}\mathrm{Ca}}{^{4x}\mathrm{Ca}}\right)_{\mathrm{Standard}}} \right] \times 1000 \qquad (1)$$

Although measured, the isotope ratios that used ^{48}Ca were rejected because of Ti and other interferences, as discussed below. Agreement between $\delta^{44/42}$Ca and $\delta^{44/43}$Ca per AMU were used to monitor mass dependence. If the two values differed by more than 0.11 ‰ per AMU, the value was excluded.

Throughout the experiment, secondary standards including SRM 915a, SRM 915b, IAPSO, and the house standard NIST X-10-39Ca (ICP1) were purified, analyzed and used to monitor for instrumental performance. Based on replicate measurements of each sample, the external precision was no worse than 0.2 ‰ ($\delta^{44/42}$Ca, 2σ) for replicate measurements of the standards.

4.4 Results and Discussion

Improvements in Matrix Separation

Chromatography column procedures can change depending on sample type. The previously published chromatography column separation method uses

a volumetric elution of HCl to separate Ca from other matrix elements in carbonates using cation exchange resin (Wieser et al., 2004). However, the ratio of Ca to other elements in biological samples is significantly lower than that in carbonates. Figure 4-1 shows an elution curve using the published carbonate method on a synthetic urine sample; the Ca aliquot collected contains approximately 10% K, 30% Rb, 10% P, 10% Sr and 10-20% Ti from the original sample. This degree of purification is sufficient to make accurate Ca isotope measurements in carbonates, but samples with lower relative amounts of Ca require significant improvements in the purity of the calcium eluate. In addition to the overlapping elemental elution peaks, the Ca elution peak can shift by ± 5 mL depending on the column height, sample concentration and age of the resin. All these factors make obtaining reliable and quantitative yields in urine or serum more problematic than in carbonates. We developed a new purification protocol that a) provides a higher degree of elemental separation between Ca and other elements and b) elutes Ca after an eluent molarity change, making the purification more reliable.

The HBr Ca elution chemistry described in this work is designed to purify complex biological materials. The HBr Ca elution chemistry removes most matrix elements in the HBr eluent and is more efficient than HCl at removing potassium (Figure 4-2). To reduce the impact of isobaric ^{48}Ti on ^{48}Ca, the 0.1 M HF eluent step removes additional titanium from the sample and 2.5 M HCl is used to remove the remaining sodium. HBr chemistry presented here is more robust than the HCl chemistry over a variety of sample types. As the Ca elution peak does not contain any matrix elements other than Sr, the ratio of matrix elements to Ca

in the initial sample can be higher without affecting the Ca purity after the column procedure. The new method is no more difficult than the HCl method. Both methods require an additional Sr specific resin column to remove the Sr. In addition to obtaining more highly purified samples, the HBr Ca elution chemistry achieves elution curves of consistent shape, which result in quantitative yields of Ca to within a measurement uncertainty of 10%.

Non-quantitative yields in chromatography can lead to isotope fractionation similar to that occurring in nature (e.g.,(Anbar et al., 2000; Oi et al., 1993; Roe et al., 2003)). We found that Ca isotopes are not measurably fractionated by the HBr elution chemistry if yields are > 85%. However, systematic effects may be possible for yields below this value. To determine how Ca isotopes fractionate during elution, Ca-containing aliquots were collected and their isotope compositions measured. We found that Ca isotopes exhibit a unique elution pattern unlike those seen in other published purification procedures (Figure 4-3). In a typical elution seen before, isotope compositions shift progressively from heavy to light (or from light to heavy) as the element elutes off the column (Anbar et al., 2000; Duan et al., 2010; Roe et al., 2003). Such behavior can result from equilibrium isotope fractionation between mobile and stationary phases (Roe et al., 2003). In contrast, the Ca isotope elution pattern we observed shifts from isotopically heavy to light, and back to heavy isotope compositions (Figure 4-3). When the isotope compositions of all the aliquots were integrated, $\delta^{44/42}$Ca was ≈ 0 ‰, similar to the isotope composition of the standard put on the column. Hence, the pattern is not an artifact of incomplete mass balance. To explain this unique pattern, we hypothesize that two or more

Ca species exist in this system, and that they fractionate differently during elution. In 6 M HCl, Ca speciation should be dominated by two species, $CaCl_2$, and $CaCl^+$, with abundances of 67% and 25%, respectively (Sverjensky et al., 1997). A “U” shaped isotope elution pattern would result if one of these species elutes off the column slightly ahead of the second species and if the equilibrium fractionation factor between the mobile and stationary phases is different for each species (specifically, the first species must exhibit the heavy to light pattern while the second species exhibits the light to heavy trend). If the reaction rates are high, so that these two species are always in isotope and concentration equilibrium with each other, as well as with the resin, then the two species can never be fully separated and will elute together. More experiments are needed to validate this hypothesis.

Assessing the Effect of Isobaric Interferences

Reliable and highly efficient sample purification is essential because isobaric interferences can affect all isotopes of Ca (Table 4-2). Modifications to published chemical purification protocols were required because they were found to be insufficiently rigorous in purifying biological samples like urine. Some of these isobaric interferences, such as those from isotopes of Sr, Ti and K, cannot be resolved by current technology. Therefore, they require either mathematical correction by measurement of a different isotope of the interferent element or sufficient chemical separation to reduce the effect of the interferent isotope below the measurement error. In order to determine the effect of interferences from isotopes of Sr, Ti and K, we spiked Ca standards with varying amounts of each potentially interfering element and compared the measured Ca isotope ratios in

the spiked sample with the known values of the pure standard. These experiments allowed us to determine the threshold of Ca/elemental ratios required for the purification protocol to minimize the introduced error.

Sr^{++} ions interfere with $^{42}Ca^{+}$, $^{43}Ca^{+}$ and $^{44}Ca^{+}$ from the contributions of $^{84}Sr^{++}$, $^{86}Sr^{++}$ and $^{88}Sr^{++}$, respectively. Offline correction of interfering Sr isotopes on the Ca isotope measurements can be made if the samples are not free of Sr (Hirata et al., 2008); this correction requires $^{87}Sr^{++}$ (m/z 43.5 u) production to be monitored and corrections to be made on ^{42}Ca, ^{43}Ca and ^{44}Ca for the contributions from Sr^{++}. This Sr correction assumes that the $^{87}Sr/^{86}Sr$ ratio and Sr^{++} production efficiencies are constant between samples. To avoid this correction and the need to monitor $^{87}Sr^{++}$, Ca was purified of Sr in a second column. To determine the threshold ratio of Ca/Sr that is required, we doped Ca standard with Sr to produce a range of Ca/Sr ratios and characterized $d^{44/42}Ca$ and $\delta^{44/43}Ca$ in these doped standards (Figure 4-4A). For a Ca/Sr ratio of 50, the measured effect is -3.69 ± 0.04 ‰ per AMU ($\delta^{44/43}Ca$) and 2.21 ± 0.08 ‰ per AMU ($\delta^{44/42}Ca$), much larger than the natural variation of interest. We modeled this effect by assuming Sr^{++} production efficiencies of 0.003 % and $^{87}Sr/^{86}Sr$ = 0.720; the modeled values were within error of the measurements (Figure 4-4A open and closed symbols, respectively), demonstrating that this large effect can be attributed solely to Sr^{++} interferences. Results from these experiments also indicate that the Ca/Sr ratio needs to be >10,000 in order for the Sr^{++} contribution to be smaller than analytical error of 0.1 ‰ per AMU on $\delta^{44/42}Ca$ and $\delta^{44/43}Ca$ (Figure 4-4A). This threshold is easily achievable using Sr specific resin, which reliably produces Ca/Sr >100,000.

There is also an isobaric interference from ^{48}Ti on ^{48}Ca. In theory, its effect could be corrected by monitoring ^{47}Ti. However, this correction has a large error because the natural abundance of ^{48}Ti is 73.8%, while the abundance of the monitored ^{47}Ti is only 7.44%, and ^{48}Ca to be corrected is only 0.187%. This means that for even small amounts of Ti contamination, a large amount of the signal on ^{48}Ca is the ^{48}Ti interference. The correction uses a relatively low abundance isotope of the interferent (^{47}Ti) to make a large correction on the abundance of the very low abundance ^{48}Ca signal (a very low abundance signal). A Ca/Ti of 500 leaves the uncorrected $\delta^{48/42}$Ca and $\delta^{48/43}$Ca offset by > 163 ‰.

The HBr chemistry described above reliably obtains Ca/Ti > 10,000. Using the known isotope abundances and assuming reasonable ionization efficiencies and instrumental sensitivities of Ca and Ti, we can predict a Ca/Ti of > 10,000,000 is required for the ^{48}Ti contribution to measured $\delta^{48/42}$Ca and $\delta^{48/43}$Ca to be less than analytical error. This level of purity would be very difficult to achieve or even assess. A 1 ppm Ca solution would need 1 ppt (parts per trillion) Ti, whereas the Ti detection limit by Q-ICP-MS is 10 ppb due to high background from polyatomic gas interferences. Therefore, it is not possible to reliably measure isotope abundance ratios that include ^{48}Ca. This error magnification is far too large to make an accurate correction to within our desired precision of ~0.1‰/amu on $\delta^{48/42}$Ca and $\delta^{48/43}$Ca, and we do not report ^{48}Ca ratios in our data. In addition, the Ti interference on ^{48}Ca makes it extremely challenging to successfully employ a double spike technique using a ^{42}Ca-^{48}Ca dopant with MC-ICP-MS (Skulan and Depaolo, 1999). In order for the double spike data reduction routines to converge on accurate sample Ca isotope values,

at least three ratios (four isotopes) need to be reliably measured. The major Ca isotope, ^{40}Ca (96.941%) cannot be measured by MC-ICP-MS because of the Ar plasma and the overwhelming ^{40}Ar isotope interference on ^{40}Ca. Hence, with our existing sample type, cleaning protocols and instrumentation, we were only able to measure two ratios: $\delta^{44/42}$Ca and $\delta^{44/43}$Ca.

The other important matrix element that could affect Ca isotopic measurement is K. When Ca/K in the samples is ≤ 1, $\delta^{44/42}$Ca and $\delta^{44/43}$Ca are offset from zero (Figure 4-4B). $^{41}K^{1}H^{+}$ could interfere with ^{42}Ca (Table 4-2). However, this interference does not explain the offset in the $d^{44/43}$Ca. $^{41}K^{1}H^{+}$ is also restricted by the relatively low abundance of ^{41}K (6.7%) and the low efficiency of hydride formation. K induced offsets in $\delta^{44/42}$Ca and $\delta^{44/43}$Ca are more likely produced as a matrix effect. Matrix effects such as differential ionic strength between samples and standards (due to different concentrations of K) may change the instrumental mass bias in an unsystematic manner, an effect that cannot be corrected for using standard-sample-standard bracketing. Offsets of similar magnitude and direction are seen when Na and Mg are added to the Ca standard. Therefore, for all alkali earth metals we require Ca/metal > 5; the chemical purification method reported here reliably purifies samples to the requisite thresholds.

Assessing the Accuracy of Standards and Samples

In addition to the precision of the analytical results reported above from replicate measurements of the same sample through chemistry (“external error”), the accuracy of the measurements was evaluated. Samples previously measured by TIMS were processed and analyzed in our laboratory for comparison with

published values (Figure 4-4). These included subsamples of the same bone and carbonate materials analyzed by Skulan et. al (1997) (Skulan et al., 1997), and new samples of milk. No previously measured milk samples were available, but most milk has similar isotope values (Chu et al., 2006). For both sample types, our measurements are within error of reported values (Chu et al., 2006; Skulan et al., 1997).

There are no urine samples previously analyzed by TIMS to which we can compare our results. To assess the accuracy of the isotopic compositions measured in a urine matrix, we collected the eluted matrix of a human urine sample purified of Ca. This matrix was then spiked with a Ca standard of known isotopic composition. This synthetic sample was re-processed through Ca and Sr columns and analyzed on the MC-ICP-MS. The measured Ca isotope value was within error of the standard value (Figure 4-5).

In a second experiment, we spiked a known standard (0.00 ‰ ± 0.1, $\delta^{44/42}$Ca) with different amounts of a urine sample. Similar to the method of standard addition to determine concentration independent of matrix effects, this procedure can be used to determine the isotope composition of a urine sample (Tipper et al., 2008). The y-intercept (0% urine sample) represents the isotope composition of the standard, while the value at y = 100% represents the isotopic composition of the pure urine sample. The urine-standard mixtures were processed and measured (Figure 4-6). A best-fit line was created for the urine-standard mixture samples (y=-.0049x+0.063, r^2=0.936). The y-intercept (0% urine, 100% standard) is within error of the standard 0.063 ‰ ± 0.1 ($\delta^{44/42}$Ca) and crosses y= 100% (100% urine, 0% standard) at -0.427 ‰ ± 0.1 ($\delta^{44/42}$Ca). Three

separate aliquots of the pure urine sample were processed through column chemistry, measured and the results averaged to be -0.43 ‰ ± 0.1 ($\delta^{44/42}$Ca) (Figure 4-6). The fact that the line crosses the y-intercept (Ca Standard) and 100% urine within error of the measured value is strong evidence that we are able to accurately measure Ca isotopes in complex matrix samples like urine.

4.5 Conclusion

With further investigation, the measurement of Ca isotope variation is a promising clinical technique for detection of disorders effecting BMB and the effectiveness of treatments for those disorders in individual patients. Previously, progress on developing this technique clinically has been limited by analytical processing. The Ca purification method described her greatly accelerates sample throughput and quality. In addition, we have quantified the degree of sample purity required to obtain accurate and precise Ca isotope values using MC-ICP-MS.

Table 4-1: Elution Step for new HBr chemistry			
mL	Molarity	Acid	Comment:
2	2.5	HCl	Load sample
6	8	HBr	Elute matrix elements (Na, K, Mg, Rb, K)
15	0.1	HF	Elute Ti
13	2.5	HCl	Elute Na
25	6	HCl	Elute Ca and Sr

Table 4-2: Potential isobaric interferences and their abundances (%) (Becker et al., 2008; Simpson et al., 2005; Sturup et al., 1997)					
^{40}**Ca** (96.941)	^{42}**Ca** (0.647)	^{43}**Ca** (0.135)	^{44}**Ca** (2.086)	^{46}**Ca** (0.004)	^{48}**Ca** (0.187)
^{40}**K**$^{+}$(0.01) ^{39}**K**(93.3)^{1}**H**$^{+}$ (99.9) ^{24}**Mg**(78.99) ^{16}**O**$^{+}$(99.7) ^{40}**Ar**$^{+}$(99.6)	^{84}**Sr**$^{++}$(9.8) ^{41}**K**(6.7)^{1}**H**$^{+}$(99.9) ^{25}**Mg**(10) ^{16}**O**$^{+}$(99.7) ^{30}**Si**(3.1)^{12}**C**$^{+}$(98.9) ^{28}**Si**(92.2)^{14}**N**$^{+}$(99.6) ^{40}**Ar**(99.6)^{1}**H**$_2^{+}$(99.9) ^{40}**Ar**(99.6)^{2}**H**$^{+}$(0.01)	^{86}**Sr**$^{++}$(7.0) ^{27}**Al**(100)^{16}**O**$^{+}$(99.7)	^{88}**Sr**$^{+-}$(82.6) ^{26}**Mg**(11.0)^{1}**H**$^{+}$(0.2) ^{28}**Si**(92.2)^{16}**O**$^{+}$(99.7) ^{30}**Si**(3.1)^{14}**N**$^{+}$(99.6) ^{12}**C**(98.9)^{16}**O**$_2^{+}$(99.7) ^{32}**S**(95.0)^{12}**C**$^{+}$(98.9)	^{46}**Ti**$^{+}$(8.0) ^{30}**Si**(3.1)^{16}**O**$^{+}$(99.7) ^{14}**N**(99.6)^{16}**O**$_2^{+}$(99.7) ^{92}**Mo**$^{++}$ (14.8)	^{48}**Ti**$^{+}$(73.8) ^{24}**Mg**(78.9)^{24}**Mg**$^{+}$(78.9) ^{36}**Ar**(0.337)^{12}**C**$^{+}$(98.9) ^{32}**S**(95.0)^{16}**O**$^{+}$(99.7) ^{96}**Mo**$^{++}$(16.7)

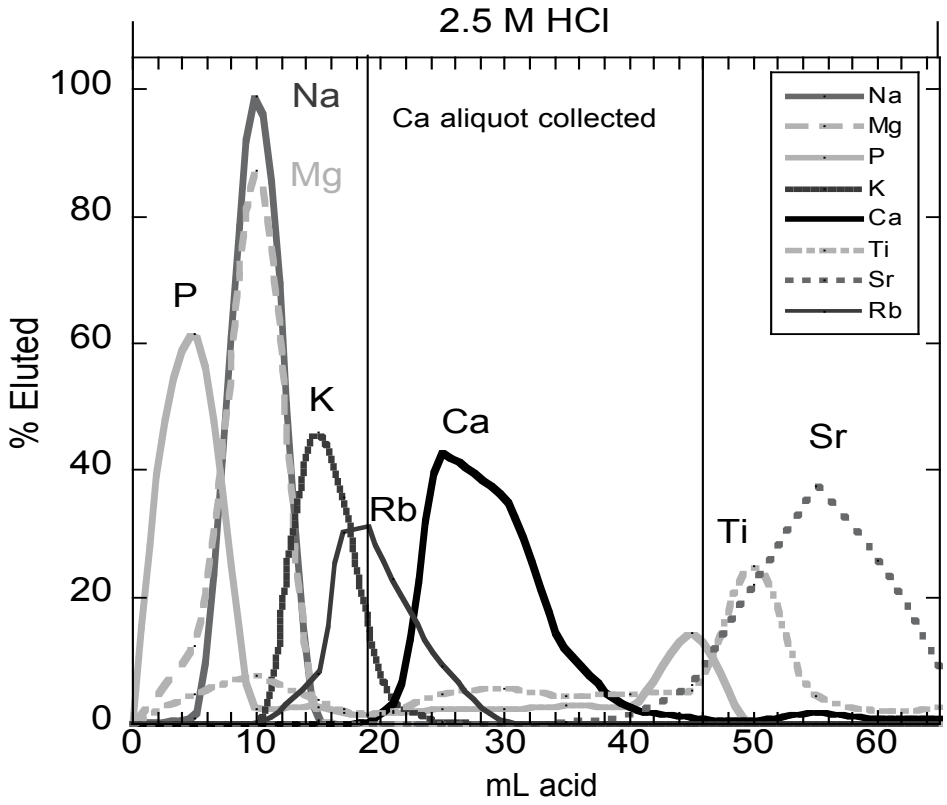

Figure 4-1 Elution curve of synthetic urine with old HCl Ca chemistry**.** Element concentrations were measured by Q-ICP-MS in aliquots that eluted off the column. Vertical lines represent Ca aliquot collected. Percent eluted was determined by adding up all aliquots and dividing that value by the value in a single aliquot. Yields were verified by measuring the elemental composition of the sample before and after chemistry. All samples and elements had at least 85% yield.

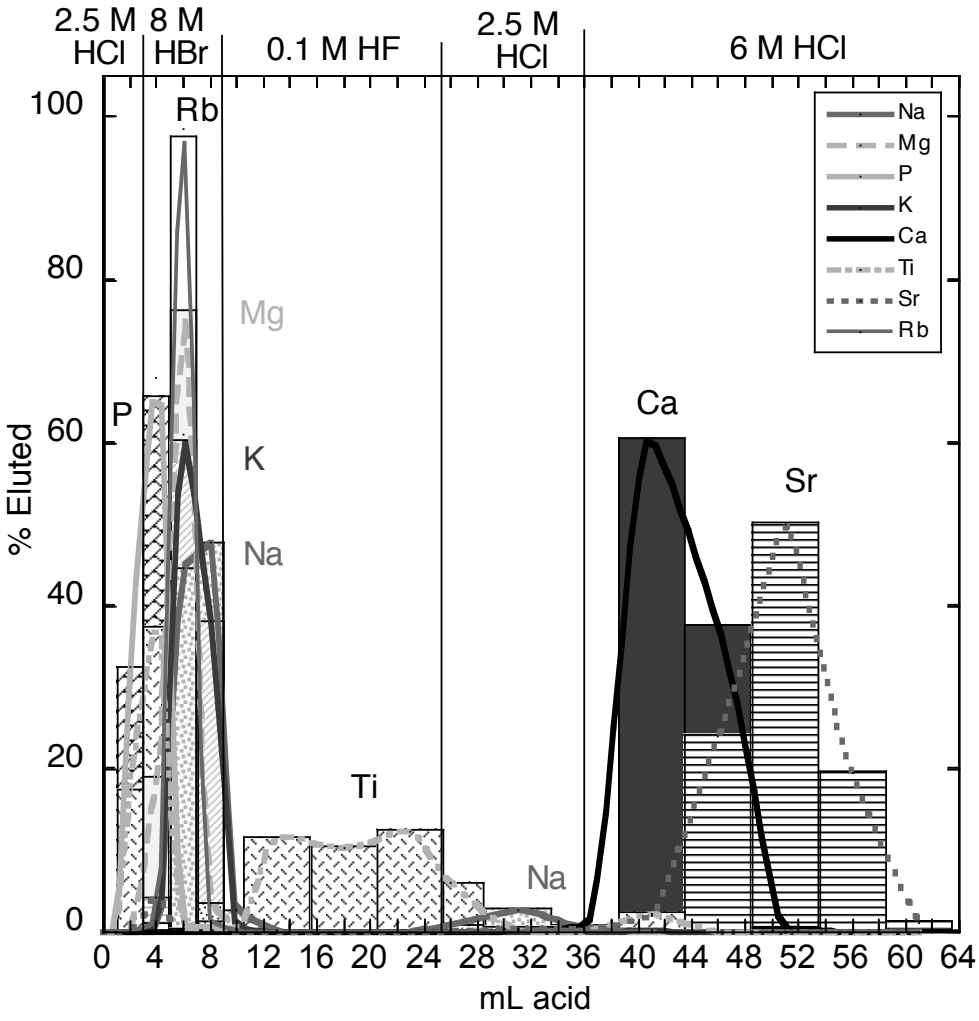

Figure 4-2 Elution curve of new HBr Ca elution chemistry.
Element concentrations were measured by Q-ICP-MS in aliquots that eluted off the column. Vertical lines represent acid changes listed along the top. Percent eluted was determined by adding up all aliquots and dividing that value by the value in a single aliquot. Yields were verified by measuring the elemental composition of the sample before and after chemistry. All samples and elements had at least 85% yield.

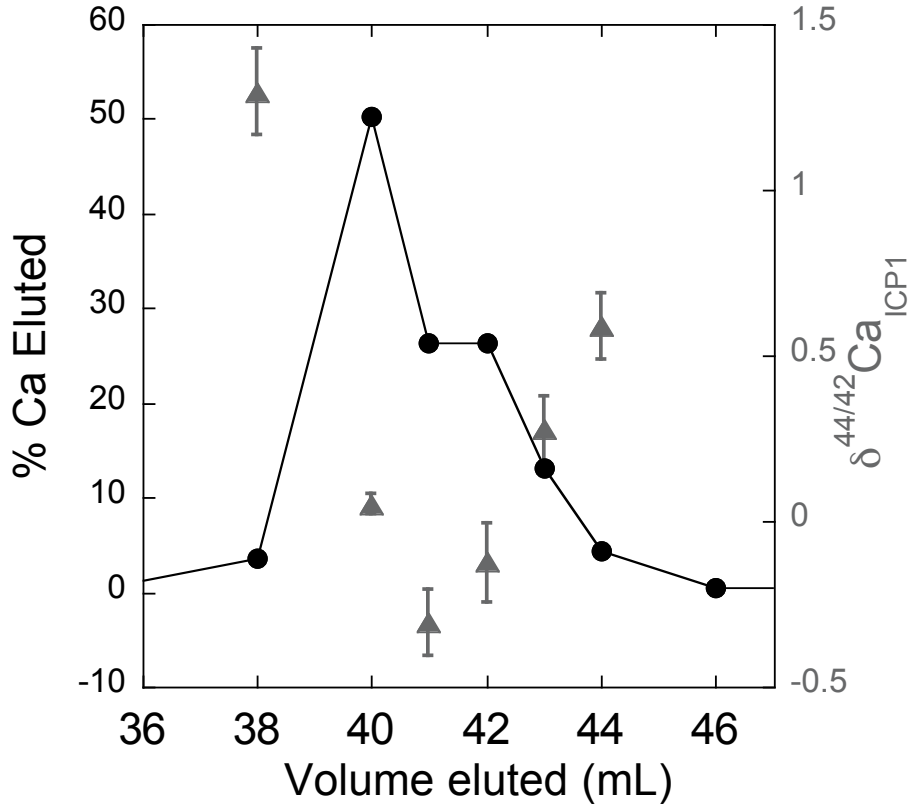

Figure 4-3 Ca isotope composition and % Ca eluted of aliquots of Ca from the HBr column purification chemistry.
Error is ±2σ on triplicate measurements for the isotope values and ± 10 % on the concentration of Ca eluted. The isotope value when integrated over all fractions was $\delta^{44/42}Ca = 0$, as required by mass balance.

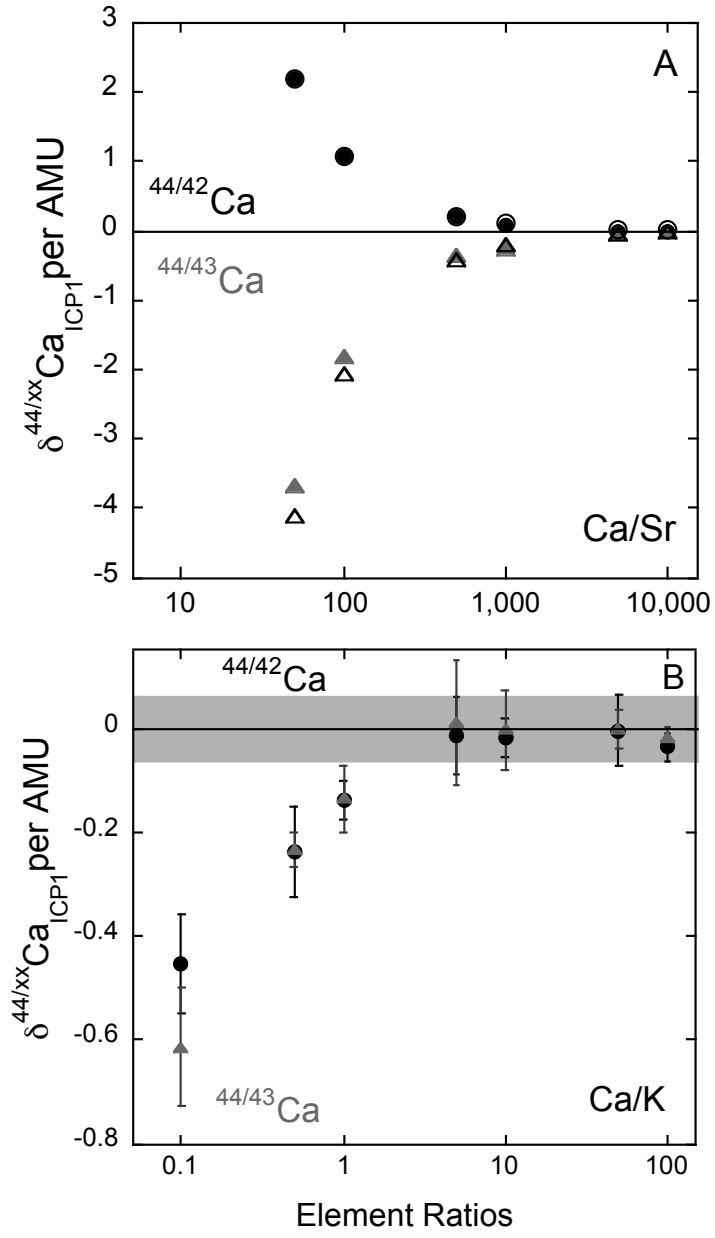

Figure 4-4 Effect of Sr and K on Ca isotope ratios.
A: $\delta^{44/4x}$Ca per AMU as a function of decreasing amount of Sr in the Ca standard (NIST X-10-39Ca, ICP1) measured relative to ICP1 without Sr added. Error bars are smaller than symbols. Open symbols represent calculated offset, closed symbols represent measured offset. B: $\delta^{44/4x}$Ca per AMU as a function of decreasing amount of K in the Ca standard (NIST X-10-39Ca, ICP1) measured relative to ICP1 without K added. Error is 2σ on triplicate measurements.

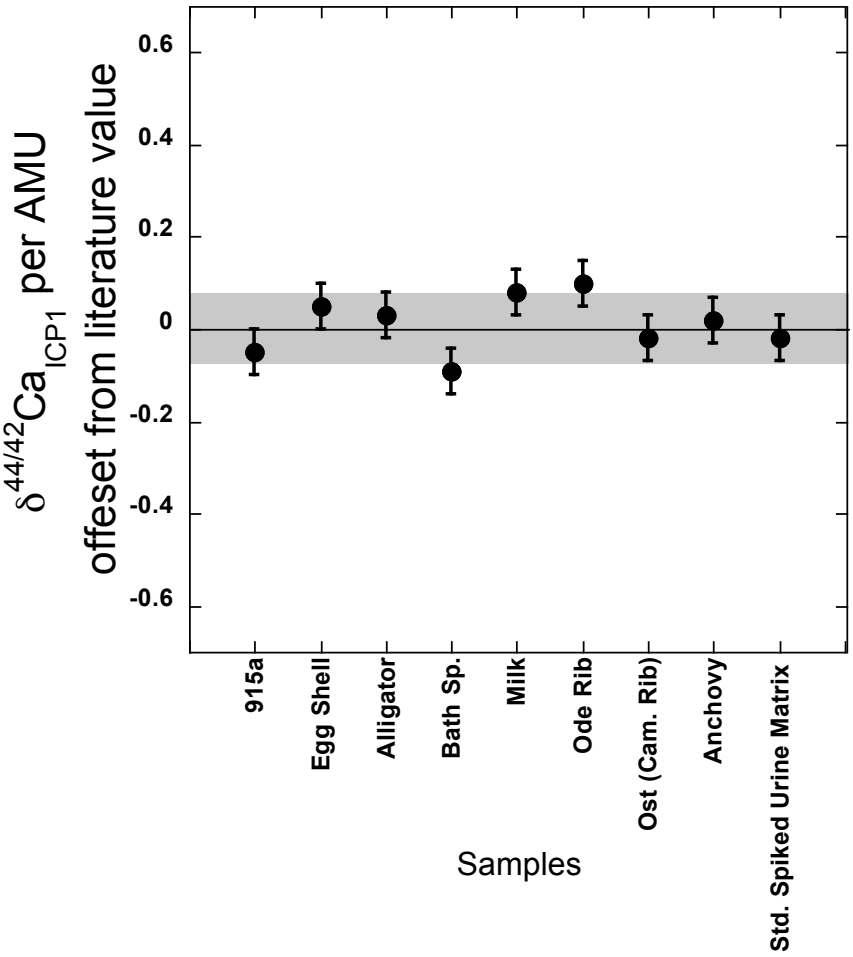

Figure 4-5 Offset of measured values for standards and samples relative to TIMS literature values.
(Chu et al., 2006; Skulan et al., 1997)

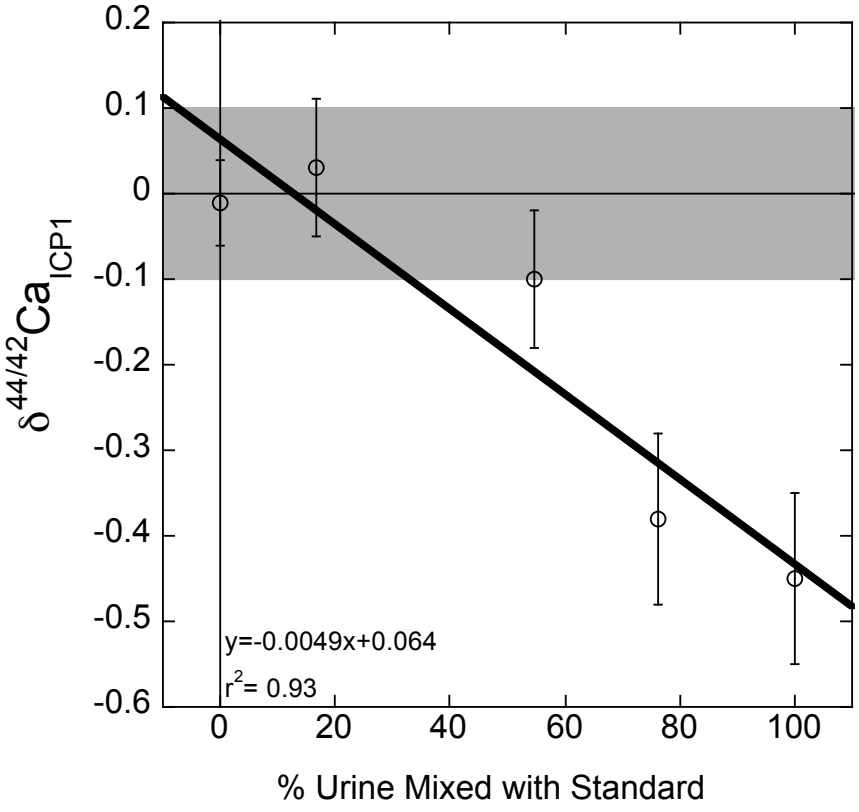

Figure 4-6 Standard/Urine mixing line.
Used to determine urine measurement accuracy. A best fit line y=-.0049x+0.063, R^2=0.936 cross the y-intercept and 100% urine sample within error of the measured value.

4.6 References

Albrecht-Gary, A. M., and Crumbliss, A. L. (1998). Coordination chemistry of siderophores: Thermodynamics and kinetics of iron chelation and release, In Metal ions in biological systems, A. Sigel, and H. Sigel, eds. (CRC Press), pp. 239-316.

Anbar, A., and Rouxel, O. (2007). Metal stable isotopes in paleoceanography. Annu Rev Earth Pl Sci *35*, 717-746.

Anbar, A. D. (2004). Iron stable isotopes: beyond biosignatures. Earth Planet Sci Lett *217*, 223-236.

Anbar, A. D., Roe, J. E., Barling, J., and Nealson, K. H. (2000). Nonbiological Fractionation of Iron Isotopes. Science *288*, 126-128.

Andren, H., Rodushkin, I., Stenberg, A., Malinovsky, D., and Baxter, D. C. (2004). Source of mass bias and isotope ratio variation in multi-collector ICP-MS: optimization of instrumental parameters based on experimental observations. J Anal At Spectrom *19*, 1217-1224.

Arnold, G., Weyer, S., and Anbar, A. D. (2004). Fe isotope variations in natural materials measured using high mass resolution multiple collector ICPMS. Anal Chem *76*, 322-327.

Beard, B. L., Johnson, C. M., Cox, L., Sun, H., Nealson, K. H., and Aguilar, C. (1999). Iron isotope biosignatures. Science *285*, 1889-1892.

Beard, B. L., Johnson, C. M., Skulan, J. L., Nealson, K. H., Cox, L., and Sun, H. (2003). Application of Fe isotopes to tracing the geochemical and biological cycling of Fe. Chem Geol *195*, 87-117.

Becker, J. S., Fullner, K., Seeling, U. D., Fornalczyk, G., and Kuhn, A. J. (2008). Measuing magnesium calcium and potassium isotope ratios using ICP-QMS with octopole collision cell in tracer studies of nutrient uptake and translocation in plants. Anal Bioanal Chem *390*, 571-578.

Bergquist, B. A., and Boyle, E. A. (2006). Iron isotopes in the Amazon River system: Weathering and transport signatures. Earth Planet Sci Lett *248*, 54-68.

Bigeleisen, J., and Mayer, M. G. (1947). Calculation of equilibrium constants for isotopic exchange reactions. J Chem Phys *15*, 261-267.

Brantley, S. L., Liermann, L., and Bullen, T. D. (2001). Fractionation of Fe isotopes by soil microbes and organic acids. Geology *29*, 535-538.

Brantley, S. L., Liermann, L. J., Guynn, R. L., Anbar, A., Icopini, G. A., and Barling, J. (2004). Fe isotopic fractionation during mineral dissolution with and without bacteria. Geochimica et Cosmochimica Acta *68*, 3189-3204.

Bullen, T. D., White, A. F., Childs, C. W., Vivit, D. V., and Schulz, M. S. (2001). Demonstration of significant abiotic iron isotpe fractioant in nature. Geology *29*, 899-702.

Chen, J., Zhang, H., Tomuv, I., Ding, X., and Rentzepis, P. M. (2007). Electron transfer and dissocaition mechanism of ferrioxalate: A time resolved optical and EXAFS study. Chemical Physics Letters *437*, 50-55.

Chu, N.-C., Henderon, G. M., Belshaw, N. S., and Hedges, R. E. M. (2006). Establishing the potential of Ca isotopes as poxy for consumption of dairy products. Applied Geochemistry *21*, 1656-1667.

Damilakis, J., Adams, J. E., Guglielmi, G., and Link, T. M. (2010). Radiation exposure in X-ray-based imaging techniques used in osteoporosis. Eur Radiol *20*, 2707-2714.

DePaolo, D. J. (2004). Calcium Isotopic Variations Produced by Biological, Kinetic, Radiogenic and Nucleosynthetic Processes, In Geochemistry of non-traditional stable isotopes, C. Johnson, B. Beard, and F. Albarede, eds. (Mineralogical Society of America), pp. 255-288.

Dideriksen, K., Baker, J. A., and Stipp, S. L. S. (2008). Equilibrium Fe isotope fractionation between inorganic aqueous Fe(III) and the siderophore complex, Fe(III)-desferrioxamine B. Earth and Planetary Science Letters *269*, 280-290.

Domagal-Goldman, S. D., and Kubicki, J. D. (2008). Density functional theory predictions of equilibrium isotope fractionation of iron due to redox changes and organic complexation. Geochimica Et Cosmochimica Acta *72*, 5201-5216.

Domagal-Goldman, S. D., Paul, K. W., Sparks, D. L., and Kubicki, J. D. (2009). Quantum chemical study of the Fe(III)-desferrioxamine B siderophore complex-Electronic structure, vibrational frequencies, and equilibrium Fe-isotope fractionation. Geochimica Et Cosmochimica Acta *73*, 1-12.

Duan, Y., Anbar, A. D., Arnold, G. L., Lyons, T. W., Gordon, G. W., and Kendall, B. (2010). Molybdenum isotope evidence for mild environmental oxidation before the Great Oxidation Event. Geochimica et Cosmochimica Acta *74*, 6655-6668.

Fantle, M. S., and DePaolo, D. J. (2004). Iron isotopic fractionation during continental weathering. Earth Planet Sci Lett *228*, 547-562.

Fehr, M. A., Andersson, P. S., Halenius, U., and Morth, C. (2008). Iron isotope variations in Holocene sediments of the Gotland Deep, Baltic Sea. Geochimica et Cosmochimica Acta *72*, 807-826.

Fietzke, J., Eisenhauer, A., Gussone, N., Bock, B., Liebetrau, V., Nagler, T. F., Spero, H. J., Bijma, J., and Dullo, C. (2004). Direct measurement of 44Ca/40Ca ratios by MC-ICP-MS using cool plasma technique. Chemical Geology *206*.

Flament, P., Mattielli, N., Aimoz, L., Choel, M., Deboudt, K., de Jong, J., Rimetz-Planchon, J., and Weis, D. (2008). Iron isotopic fractionation in industrial emissions and urban aerosols. Chemosphere *73*, 1793-1798.

Halicz, L., Galy, A., Belshaw, N. S., and O'Nions, R. K. (1999). High-precision measurement of calcium isotopes in carbonates and related materials by multiple collector inductively coupled plasma mass spectrometry (MC-ICP-MS). J Anal At Spectrom *14*, 1835-1838.

Hernlem, B., Vane, L., and Sayles, G. (1996). Stability constants for complexes of the siderophore desferrioxamine B with selected heavy metal cations. Inorganica chimica acta *244*, 179-184.

Heuser, A., and Eisenhauer, A. (2010). A pilot study on the use of natural calcium isotopes (44Ca/40Ca) fractionation in urine as a proxy for the human body calcium balance. Bone *46*, 889-896.

Hirata, T., Tanoshima, M., Suga, A., Tanaka, Y.-k., Nagata, Y., Shinohara, A., and Chiba, M. (2008). Isotopic Analysis of Calcium in Blood Plasma and Bone from Mouse Samples by Multiple Collector-ICP-Mass Spectrometry. Analytical Science *24*, 1501-1507.

Hutchins, D., Witter, A., Butler, A., and Luther III, G. (1999). Competition among marine phytoplankton for different chelated iron species. Nature *400*, 858-861.

Johnson, C. M., Beard, B. L., and Roden, E. E. (2008). The iron isotope fingerprints of redox and biogeochemical cycling in modern and ancient Earth. Annu Rev Earth Pl Sc *36*, 457-493.

Johnson, C. M., Skulan, J. L., Beard, B. L., Sun, H., Nealson, K. H., and Braterman, P. S. (2002). Isotopic fractionation between Fe(III) and Fe(II) in aqueous solutions. Earth Planet Sci Lett *195*, 141-153.

Jouvin, D., Louvat, P., Juillot, F., Marechal, C. N., and Benedetti, M. F. (2009). Zinc isotopic fractionation: why organic matters. Environ Sci Technol *43*, 5747-5754.

Kanis, J. A., McCloskey, E. V., Johansson, H., Oden, A., III, L. J. M., and Khaltaev, N. (2008). A reference standard for the description of osteoporosis. Bone *42*, 467-475.

Leeming, D. J., Alexandersen, P., Karsdal, M. A., Qvist, P., Schaller, S., and Tanko, L. B. (2006). An update on biomarkers of bone turnover and their utility in biomedical research and clinical practice. Eur J Clin Pharmacol *62*, 781-792.

Ludwig, K. R. (2008). Isoplot 3.6 (Berkeley Geochronology Center Spec. Pub).

Majestic, B. J., Anbar, A. D., and Herckes, P. (2009). Stable Isotopes as a Tool to Apportion Atmospheric Iron. Environ Sci Technol *43*, 4327-4333.

Martell, A., and Smith, R. (1989). Critical Stability Constants, Vol 1-6 (New York: Plenum).

Oi, T., Morioka, M., Ogino, H., and Kakihana, H. (1993). Fractionation of Calcium isotopes in Cation-Exchange Chromatography. Separation Science and Technology *28*, 1971-1983.

Ottonello, G., and Zuccolini, M. V. (2008). The iron-isotope fractionation dictated by the carboxylic functional: An ab-initio investigation. Geochimica Et Cosmochimica Acta *72*, 5920-5934.

Raymond, K. N., and Carrano, C. J. (1979). Coordination chemistry and microbial iron transport. Accounts Chem Res *12*, 183-190.

Roe, J. E., Anbar, A. D., and Barling, J. (2003). Nonbiological fractionation of Fe isotopes: evidence of an equilibrium isotope effect. Chem Geol *195*, 69-85.

Russell, W. A., Papanastassiou, D. A., and Tombrello, T. A. (1978). Ca isotope fractionation on the Earth and other solar system materials. Geochimica et Cosmochimica Acta *42*, 1075-1090.

Schmitt, A.-D., Gangloff, S., Cobert, F., Lemarchand, D., Stille, P., and Chabaux, F. (2009). High performance automated ion chromatography separation for Ca isotope measurements in geological and biological samples. J Anal At Spectrom *24*, 1089-1097.

Simpson, L., Hearn, R., Merson, S., and Catterick, T. (2005). A comparison of double-focusing sector field ICP-MS, ICP-OES and octopole collision cell ICP-MS for the high-accuracy determination of calcium in human serum. Talanta *65*, 900-906.

Skulan, J., Bullen, T., Anbar, A. D., Puzas, J. E., Shackelford, L., LeBlanc, A., and Smith, S. M. (2007). Natural Calcium Isotopic Composition of Urine as a Marker of Bone Mineral Balance. Clinical Chemistry *53*, 1155-1158.

Skulan, J., and Depaolo, D. J. (1999). Calcium Isotope Fractionation between Soft and Mineralized Tissue as a Monitor of Calcium Use in Vertebrates. Proceedings of the National Academy of Science *96*, 13709-13713.

Skulan, J., DePaolo, D. J., and Owens, T. L. (1997). Bilogical control of calcium isotopic abondances in the global calcium cycle. Geochimica et Cosmochimica Acta *61*, 2505-2510.

Sorensen, M. G., Henriksen, K., Schaller, S., and Karsdal, M. A. (2007). Biochemical markers in preclinical models of osteoporosis. Biomarkers *12*, 266-286.

Stookey, L. (1970). Ferrozine-a new spectrophotometric reagent for iron. Anal Chem *42*, 779–781.

Sturup, S., Hansen, M., and Molgaard, C. (1997). Measurements of 44Ca: 43Ca and 42Ca: 43Ca Isotopic Ratios in Urine using High Resolution Inductively Coupled Plasma Mass Spectrometry. Journal of Analytical Atomic Spectrometry *12*, 919-923.

Sverjensky, D. A., Shock, E. L., and Helgeson, H. C. (1997). Prediction of thermodynamic properties in aqueous metal complexes to 1000°C and 5 kb. Geochimica et Cosmochimica Acta *61*, 1359-1412.

Tipper, E. T., Louvat, P., Capmas, F., Galy, A., and Gaillardet, J. (2008). Accuracy of stable Mg and Ca isotope data obtained by MC-ICP-MS using the standard addition method. Chem Geol *257*, 65-75.

Urey, H. C. (1947). The thermodynamic properties of isotopic substances. J Chem Soc, 562-581.

Walczyk, T., and von Blanckenburg, F. (2005). Deciphering the iron isotope message of the human body. Int J Mass Spectrom *242*, 117-134.

Welch, S. A., Beard, B. L., Johnson, C. M., and Braterman, P. S. (2003). Kinetic and equilibrium Fe isotope fractionation between aqueous Fe(II) and Fe(III). Geochimica et Cosmochimica Acta *67*, 4231-4250.

Weyer, S., and Schwieters, J. (2003). High precision Fe isotope measurements with high mass resolution MC-ICPMS. Int J Mass Spectrom *226*, 355-368.

Wiederhold, J., Kraemer, S. M., Teutsch, N., Borer, P., Halliday, A., and Kretzschmar, R. (2006). Iron isotope fractionation during proton-

promoted, ligand-controlled, and reductive dissolution of goethite. Environ Sci Technol *40*, 3787-3793.

Wieser, M. E., Buhl, D., Bouman, C., and Schwieters, J. (2004). High precision calcium isotope ratio measurements using a magnetic sector multiple collector inductively coupled plasma mass spectrometer. J Anal At Spectrom *19*, 844-851.

Yeh, H. S., and Berenson, J. R. (2006). Treatment for myeloma bone disease. Clin Cancer Res *12*, 6279s-6284s.

Chapter 5

RAPID CHANGES IN BONE MINERAL BALANCE IN RESPONSE TO ESTROGEN DEPLETION IN RHESUS MONKEYS DETECTED USING TRACER-LESS CALCIUM STABLE ISOTOPE TECHNIQUE

Jennifer L. L. Morgan[1], David H. Abbott[2,3], Ariel D. Anbar[1,4], Gwyneth W. Gordon[4], Joseph L. Skulan[5], and Ricki J. Colman[2]

[1]Department of Chemistry and Biochemistry, Arizona State University, Tempe AZ 85287

[2]Wisconsin National Primate Research Center, University of Wisconsin, Madison, WI 53715

[3]Department of Obstetrics and Gynecology, University of Wisconsin, Madison, WI 53792

[4]School of Earth and Space Exploration, Arizona State University, Tempe, AZ 85287

[5]Geology Museum, University of Wisconsin, Madison, WI 53706

5.1 Abstract

Understanding bone metabolism and the therapeutic development of countermeasures are hampered by an inability to detect rapid changes in bone mineral balance (BMB) or bone mineral density (BMD). Conventional biochemical markers provide information on relatively short-term changes (2-4 weeks) in bone turnover rates, but not quantified changes in BMB. By contrast, the natural Ca isotopic composition of soft tissues such as serum and urine directly reflects

BMB. We tested the utility of using Ca isotope to monitor changes in BMB due to estrogen-depletion bone loss in adult female rhesus monkeys. Female rhesus monkeys (12-16 years) received 150 mg of medroxyprogesterone acetate (MPA, a known suppressor of ovarian estrogen lasting 30 days/dose, intramuscularly [IM]) on day 0 (MPA, n=3). At the same time, control animals were given volume-matched saline IM (Control, n=3). Ca isotopes were measured in urine samples by multiple collector inductively coupled plasma mass spectrometry (MC-ICP-MS). Ca isotope variations revealed a more negative BMB in the MPA group compared to the Control group ($p<0.028$) by day 7. On the same day, estrogen was decreased ($p<0.045$), NTx (bone resorption marker) levels) and osteocalcin (bone formation marker) were unchanged in MPA-injected females. On day 28, the Ca isotope variations for the MPA group and for the Control group both indicate further bone loss. After 84 days, the DXA showed a significant decrease in BMD for both the MPA and Control groups ($p<0.012$). The reason for decrease in BMD in the Control group is unknown, but the bone density scans verified that both groups lost bone during the study. These findings indicate that stable Ca isotope measurements are a tool to assess rapid variations in BMB.

5.2 Introduction

Bone loss, or negative bone mineral balance (BMB), is a symptom of multiple disease states, including osteoporosis and multiple myeloma (Kanis et al., 2008; Yeh and Berenson, 2006). A rapid measure of BMB is essential in diagnosing disease, monitoring disease progression and assessing the effectiveness of countermeasures. Currently, the two main diagnostic techniques for monitoring bone health are dual-energy x-ray absorptiometry (DXA) and

biochemical bone formation and resorption markers (Leeming et al., 2006). DXA can detect bone loss over relatively long (6-12 months) time intervals, but is unable to assess rapid changes of BMB (Damilakis et al., 2010b). Bone formation and resorption markers can be effective measures of bone turnover but do not quantitatively assess BMB (Leeming et al., 2006; Sorensen et al., 2007). The measurement of natural stable Ca isotope variations in urine and soft tissue is emerging as a new tool to rapidly asses BMB (Heuser and Eisenhauer, 2010; Skulan et al., 2007).

Measuring natural stable Ca isotopes to assess BMB does not require administration of any radioactive or stable Ca isotope. The variations measured occur naturally during bone formation and bone resorption (Heuser and Eisenhauer, 2010; Skulan et al., 2007; Skulan and Depaolo, 1999). The formation of bone mineral in vertebrates is known to favor light isotopes of Ca over heavy isotopes (Skulan and Depaolo, 1999). This systematic enrichment of light Ca isotopes in bone leaves the soft tissue with an abundance of heavy Ca isotopes relative to food. During bone resorption, this light Ca pool is released back into serum and excreted in the urine, causing these reservoirs to be enriched in light Ca isotopes compared to food. These natural isotope variations in soft tissue can be resolved with high precision mass spectrometry (Chu et al., 2006; Heuser and Eisenhauer, 2010; Hirata et al., 2008; Russell et al., 1978; Skulan et al., 2007; Skulan and Depaolo, 1999; Wieser et al., 2004). Unlike Ca tracer experiments that require the administration of expensive stable or radioactive Ca isotopes (Abrams, 1999; Beck et al., 2003; Sturup et al., 1997), measuring natural stable Ca isotope variation is less expensive, patients are not

exposed to radiation from radioactive Ca isotopes, and this technique can be performed on archived samples.

Ca isotopes have three advantages over biochemical markers in assessing changes in BMB. First, Ca isotope abundances can be measured with extremely high precision and accuracy. As a result, unlike biochemical markers, inter-laboratory variation in Ca isotopic measurements is miniscule (Skulan et al., 2007). Second, the isotopic composition of soft tissue Ca directly reflects net bone mineral balance. In contrast, biochemical markers measure formation and resorption separately; combining these into a single quantitative metric is challenging (Skulan et al., 2007; Skulan and Depaolo, 1999). Third, the residence time of Ca in soft tissue is very short, on the order of a few days. Hence changes in bone mineral balance, quantifiable in urine, are reflected by changes in soft tissue Ca isotope concentrations within a week and, for large changes, probably within a day (Smith et al., 1996; Smith et al., 2005). By contrast, biochemical markers typically require much longer to respond to changes in bone turnover rate (Shackelford et al., 2004). Of importance, Ca isotope fractionation occurs during bone mineralization, and not during transfer of Ca between non-mineralized compartments. Therefore, release of Ca from non-mineralized pools will not effect the isotope composition of urine (DePaolo, 2004; Skulan et al., 2007; Skulan and Depaolo, 1999; Skulan et al., 1997).

In humans, it has been shown that measurements of the natural Ca isotopic composition of urine reflect changes in BMB after four weeks (Skulan et al., 2007). Here we test the ability of Ca isotope analysis to detect changes in BMD within two weeks of estrogen-depletion bone loss using a well-developed

nonhuman primate model, the female rhesus monkey (Macaca mulatta). Rhesus monkeys are similar to humans in menstrual cycles, natural menopause and bone remodeling processes (Colman et al., 1999), and are good models of pathogenesis and treatment of estrogen-depletion bone loss in humans (Black et al., 2001b; Jerome and Peterson, 2001; Pope et al., 1989). In our experience, 6 consecutive months of monthly medroxyprogesterone acetate (MPA) administration to rhesus monkeys led to a significant change in DXA-measured BMD. These results indicate that bone is lost as a result of MPA injection in the rhesus model.

5.3 Materials and Methods

Animals

All monkeys were housed at the Wisconsin National Primate Research Center and had known birth dates and complete medical histories. No animal had any clinical or experimental history known to affect skeletal parameters. All animals had *ad libitum* access to food and water. Temperature in the animal rooms was maintained at approximately 21°C with average relative humidity of 50-60%. Room lighting was automatically controlled to provide alternating periods of 12 hours light and dark. All monkeys had extensive visual and auditory contact with other animals in the room and were supplied with objects to enrich their environment. Experiments were done with approval of the University of Wisconsin-Madison Graduate School institutional animal care and use committee. Six adult (12-16 years) female rhesus monkeys were evenly randomized into control (Control, n=3) or treatment (MPA, n=3) groups (Table 5-1). Animals in the MPA group received an intramuscular (IM) injection of 150 mg

of medroxyprogesterone acetate, an estrogen inhibitor lasting 30 days/dose on days 0, 28 and 56. Animals in the Control group were given a volume-matched saline injection (IM) on day 0, 28 and 56. From day -14 to week 12 animals were fed a customized diet (Teklad, Madison WI) that contained a small amount of natural Sr in order to alter its Sr isotope composition. This increased the Sr concentration in the food of all animals from 10 to 12 ppm, far too little Sr to affect bone metabolism (Meunier et al., 2004). Ca concentration and isotope composition were not altered in the diet. All other nutritional qualities of the diet were constant.

Bone densitometry

Bone mass and density of the total body, posterior-anterior lumbar spine (lumbar vertebrae 2-4), and radius were measured by DXA (DPX-L, GE/Lunar Corp., Madison WI) on either day 1 (n=3) or day 2 (n=3) and then again on either day 82 (n=3) or day 83 (n=3). After an overnight fast, animals were sedated with a combination of ketamine HCl (10 mg/kg, IM) and xylazine (0.6 mg/kg, IM) and weighed. One operator performed both scans of the total body, radius and posterior-anterior (PA) lumbar spine. BMD coefficient of variation were less than 2.5 % for all sites. Total body and spine scans were acquired with Lunar pediatric software (version 1.5e) and analyzed with Lunar pediatric software version 4.0a. Radius scans were acquired and analyzed with Lunar small animal software version 1.0d.

Biochemical parameters

Fasted morning blood samples were drawn by vacutainer from the saphenous vein on day 0, 1, 2, 8, 14, 28, 56, and 84 while animals were under

manual restraint. Samples were allowed to clot for 30 mins, and then were centrifuged, and serum was aliquoted into separate vials for each analyte. Aliquots were frozen at -80° C until analysis. The following serum analytes were measured: osteocalcin (RIA, Diagnostic Systems Laboratories, Inc., Webster, TX; 8.28%, 4.90%, inter- and intra-assay coefficients of variation respectively), Osteomark® NTx (EIA, Wampole Laboratories, Inc., Dist., Princeton, NJ; 6.9%, 4.6%), and estradiol (RIA, WNPRC in house; 11.09%, 4.7%). All assays validated for use in rhesus monkeys by parallelism and spike recovery experiments.

Sample Preparation and Purification for Ca Isotope analysis

First morning void urine samples were collected from animals in their home cages on days -14, -13, -12, -11, -10, -7, -1, 0, 1, 2, 4, 6, 7, 8, 14, 28, 56, 84, and 133. Samples were centrifuged, after which aliquots were taken and frozen at -80°C. Frozen urine samples were shipped to Arizona State University for Ca isotope analysis. The samples were processed and dissolved using the technique described in CHAPTER 4. Briefly, samples were placed in Teflon microwave digestion vessels with concentrated nitric acid (2 mL) and ultra pure 30% hydrogen peroxide (2 mL). The MARS microwave system was set to ramp to 150°C over 15 min then hold at 150°C for 15 min. The samples were transferred to Teflon reaction vessels, and dried on a hotplate in a metal-free laminar airflow exhaust hood. Alternating rounds of modified aqua regia (1:1 concentrated distilled trace metal grade nitric acid and concentrated distilled trace metal grade hydrochloric acid) and nitric acid plus peroxide digestions were performed until low aqueous surface tension indicated the samples were free of

organic material. All samples and standards were processed in a biosafety level 2, class 100, trace-metal-free clean lab with class 10 laminar airflow exhaust hoods. Acids used for chemical reagents were trace metal grade.

After digestion, samples and standards were run through cation exchange resin (Biorad AG50-WX-12 200-400 mesh) following the method of Wieser, et al. (Wieser et al., 2004). The sample was loaded on to the column in 2 mL of 2.5 M HCl. Volumetric elution of Ca occurred between 25 mL- 45 mL of 2.5 M HCl. Eichrom Sr specific resin was used to separate Sr from Ca. Some of the samples required a second Ca column and Sr column purification because they did not meet the purity criteria described in CHAPTER 4. Yields were checked and were > 90% recovery.

Mass Spectrometry Measurement

Ca isotopes were measured using a multiple collector ICP-MS (MC-ICP-MS, Thermo Scientific Neptune) using an argon plasma, following the method of Wieser et al. (Wieser et al., 2004) and CHAPTER 4. Standard-sample-standard is used to correct for instrumental mass bias. The standard used was NIST X-10-39Ca ("ICP1"), our in house Ca standard. All Ca isotope measurements are reported relative to ICP1 when the $\delta^{44/42}$Ca are given. Six masses were measured: ^{42}Ca, ^{43}Ca, ^{44}Ca, ^{46}Ca, ^{47}Ti and ^{48}Ca; ^{46}Ca (0.004%) was too low intensity to produce reliable data. Values are reported as:

$$\varepsilon^{44/4x}\mathrm{Ca} = \left[\frac{\left(\frac{^{44}\mathrm{Ca}}{^{4x}\mathrm{Ca}}\right)_{\mathrm{Sample}} - \left(\frac{^{44}\mathrm{Ca}}{^{4x}\mathrm{Ca}}\right)_{\mathrm{Standard}}}{\left(\frac{^{44}\mathrm{Ca}}{^{4x}\mathrm{Ca}}\right)_{\mathrm{Standard}}} \right] \times 10{,}000 \qquad (1)$$

For each analysis, 30 measurement cycles with 4.194 second integration times were averaged into a single measured value after exclusion of ratios >2 sigma from the average. Medium resolution modes were used to partially resolve the polyatomic interferences such as ArH_2^+, CO_2^+, N_2O^+ and N_3^+. The isotope ratios that used ^{48}Ca were rejected because of ^{48}Ti at the same mass. We obtain two ratios reliably, $^{44}Ca/^{42}Ca$ and $^{44}Ca/^{42}Ca$. The agreement between $\delta^{44/42}Ca$ and $\delta^{44/43}Ca$ per AMU was used to monitor mass dependence. If the two values differed by more than 0.1 ‰ per AMU, the value was excluded. Ca concentrations in samples and standards in medium-resolution mode were 2.5 ± 0.1 ppm.

Throughout the run, secondary standards including SRM 915a, SRM 915b, IAPSO, and the house standard NIST X-10-39Ca (ICP1) that were passed through the same chemical purification procedures as samples were analyzed and monitored for instrumental performance and accuracy following chemical purification. Based on replicate measurements of each sample, the external precision was no worse than 2 ε ($\varepsilon^{44/42}Ca$, 2σ).

Statistical analysis

Log-transformation of the NTx data were performed to achieve homogeneity of variance and to increase linearity (Sokal and Rohlf, 1995). Regression models with estimation by generalized estimating equations (GEE) were used. A backward elimination procedure was used to select the final GEE models. Two-way analysis of variance (ANOVA) was used to examine the Ca isotopes, osteocalcin, DXA, weight, and estradiol to determine the independent effects of these variables and their possible interaction. One-way ANOVA was used to

compare MPA and Control. Kruskal – Wallis one-way ANOVA was performed when data were not normally distributed. All data are expressed as mean + SE, or back-transformed log10 mean (95% confidence intervals) as appropriate. Significance was determined as $P< 0.05$.

5.4 Results and Discussions

Animal Status

Animals were healthy throughout the study. Animal physical characteristics are presented in Table 5-1. There was no significant difference in average age or weight between groups. Both groups experienced an approximately 4% weight loss on day 7 ($p<0.023$) and day 14 ($p<0.037$) with no significant difference between groups throughout the study.

Traditional BMD Techniques

The concentrations of biomarkers (estradiol, NTx, and Osteocalcin) in all the blood samples collected are presented in Table 5-2. Figure 5-1A, B, and C compares the percent change for the biomarkers, on 5 days post injection (Day 7, 14, 28, 56, 84).

Estradiol

MPA is an estrogen suppressing drug; by measuring the amount of estradiol in the blood of the monkeys, we can evaluate the effectiveness of the MPA treatment. There is a decline in estradiol in the MPA group post injection ($p<0.05$). The difference in estradiol between the MPA and Control groups is significant on day 7, 28, and 84 ($p<0.046$, $p<0.018$, and $p<0.038$, respectively Table 5-2, Figure 5-1A). There is no difference between the MPA and Control groups on day 14 or 56 ($p>0.05$). The high variations in the Control group are

due to normal estrogen cycle during menstruation. There is decrease in estrogen and low variability in estrogen concentration for the MPA group. This is verification that MPA has prevented the formation of estrogen and that the animals in the MPA group are estrogen deprived.

NTx

NTx (amino-terminal cross-linked telopeptide of type I collagen) is a bone resorption biomarker. The NTx data was not normally distributed around the mean therefore the data needed to be log transformed to normalize the data. The log-transformed data was tested for significance. There was no time dependant variation in NTx for either group ($p>0.05$). There is no significant difference between groups during the study ($p>0.05$) (Table 5-2 and Figure 5-1C). On day 14 there was a greater percent change from baseline for the MPA group compared to the Control group ($p<0.033$). This may indicate a treatment effect but since there is no subsequent measurements of NTx matching the 14-day time point it is difficult to make broad conclusions. Since the MPA injection is given every 28 days the effect may be transient. All subsequent measurements were taken 28 days post injection. Therefore days 28, 56 and 84 represent time points where MPA is least potent and could have the least effect on BMB.

Osteocalcin

Osteocalcin, a bone formation biomarker, did not change between MPA and Control groups or between baseline and any day post injection ($p>0.05$). The biological processes that form bone require several weeks to begin to produce new bone. Osteoblasts need to differentiate which can take several weeks once the body signals the need for new osteoblast formation (Manolagas, 2000).

There is no significant change in osteocalcin over the course of the study, indicating no change in bone formation rate.

DXA

Bone densitometry measurements of total skeleton are presented in Table 5-3 as measured on day 0, and day 84. There was no significant difference between MPA and Control groups ($p>0.05$). However, there is a decrease in bone density from day 0 to day 84 in both groups of -2.18 % ($p<0.012$). These results indicate that there is no effect from treatment on bone density but that both groups experience significant bone loss as measured by DXA. The cause of the bone loss in the Control group is unknown.

Ca Isotope Technique

The resolution of sampling for the Ca method was much higher than the biomarker samples because we wanted to capture exactly when the Ca isotopes changed from baseline. The Ca isotopes begin to decrease on the first sample post injection (day 1), but the variability between the three monkeys is very high. The Ca isotope composition shifted lightward and stabilized by day 6. We decided not to include day 1 and day 2 in the average post injection time point because this is a period of transition during which the Ca isotope ratios decline sharply before settling at a stable value for all three monkeys. The Ca isotope composition of food was 1.5 ± 1.5 ε prior to and during the study. Therefore, the variations observed in urine Ca during the study are a result of changes in BMB, not dietary changes.

The trend for Ca isotopes indicates that both groups enter negative bone mineral balance during the study. The difference between MPA and Control

groups is significant on days 7 and 14 ($p<0.022$ and $p<0.004$). The negative Ca isotope deviation on days 7 and 14 indicates the monkeys in MPA group were loosing bone. There is a significant difference between baseline and days 7, 14, 28 and 56 for the MPA group. There is also a significant difference between baseline and days 28 and 56 for the Control group. Hence, the variations in the MPA and Control groups within error of each other (Figure 5-1D).

The Ca isotope signal for the MPA group on day 84 shows no significant difference between the Control group or baseline. By day 84, the Ca isotope signal for the MPA group had returned to baseline, and the Control group had also increased to near baseline. The return to baseline indicates that the animals were close to zero net BMB on day 84. However, bone that was lost during day 7 - 54 apparently was not recovered, as there is no sign that the animals went into positive BMB.

Comparison of Ca isotope to Traditional Markers and Measures

The purpose of this study was to examine the effectiveness of using Ca isotope measurements as an indicator of BMB. Ca isotope values suggest that bone loss in the MPA group occurred rapidly as a result of MPA injection. This dramatic shift in Ca isotopes may occur when MPA is the most potent and wear off as MPA is metabolized. All samples post day 28 were taken when MPA was the least potent (day 56 and 84). Therefore, the effect of later MPA injections was not fully captured.

In addition to the rapid change seen in the MPA group, the Control group's Ca isotope composition also seems to indicate that they are in negative BMB. This result is confirmed by the DXA scan which shows that there was a

significant decrease in BMD for both groups by day 84. This loss of bone was not detected using NTx, a traditional biomarker of bone resorption. Therefore, it appears that Ca isotopes are able to detect smaller changes in BMB than NTx.

The amount of bone lost can be quantified using the Ca isotope technique. Using the Ca isotope bone models presented in Skulan et al. (2007) and Heuser et al. (2010), we can calculate the percent bone loss using Ca isotopes (Heuser and Eisenhauer, 2010; Skulan et al., 2007; Skulan and Depaolo, 1999). For example, if we assume that the total bone mineral content of a female Rhesus Monkey is 400 g (Black et al., 2001a), that the amount of Ca absorbed from the diet is 0.135 g (Black et al., 2001a), and that the isotope composition of the diet can be neglected because all the isotope values are normalized to baseline, then the measured Ca isotope variation (3.0 ε) indicates that the monkeys in this study lost approximately 2.48 ± 0.62 % of bone mass over the 84-day study. This estimate matches the value give by DXA (2.18 ± 1.0 %). DXA scans typically have an accuracy of 3 % and a precision of 1 % (Larkin et al., 2008). The Ca isotope technique is more precise and can more rapidly detect changes in BMB and quantify changes in BMD.

5.5 Conclusion

Mass spectrometric measurements of urinary Ca isotope compositions reveal loss of bone Ca within a week of onset of estrogen depletion in adult female rhesus monkeys. In addition the Ca isotopes indicate that the Control is also losing bone due to an unknown cause. These inferences from Ca isotopes are fully consistent with results from DXA at the end of the study which also

indicated that both groups lost bone mass. The magnitude of bone loss quantified from the Ca isotope data agrees with determinations from the DXA results. However, Ca isotope variation was detectable long before DXA could have indicated significant bone loss. Because Ca isotopes reflect net BMB, they also give more direct information about short-term changes in BMD than can be provided by separate markers of bone formation and resorption. By providing sensitive and rapid measurement of BMB Ca isotopes promise new insight into understanding short-term dynamics in bone metabolism.

Table 5-1: Average physical statistics ± SE		
	MPA	Control
N	3	3
Age (years, day 0)	14.07 ± 1.02	14.02 ± 0.55
Body Wt (kg, day 0)	9.51 ± 1.51	9.17 ± 1.51
Body Wt (kg, day 14)	9.30 ± 1.36	8.55 ± 1.36
Body Wt (kg, day 84)	10.21 ± 1.16	9.00 ± 1.16

Table 5-2: Average concentration of biomarker in serum ± SE (n=3 per treatment) or (Upper 95% Confidence limit, Lower 95% Confidence limit)						
	Estradiol (pg/mL)		NTx (nMBCE)		Osteocalcin (ng/mL)	
Day	MPA	Control	MPA	Control	MPA	Control
0	79.3 ± 9.4	84.0 ± 9.4	14.6 (28.1, 7.6)	15.1 (29.0, 7.8)	21.2 ± 9.3	18.3 ± 9.3
7	47.3 ± 23.1	140.7 ± 23.1	18.1 (37.0, 8.9)	11.7 (23.9, 5.7)	22.6 ± 7.6	18.5 ± 7.6
14	37.7 ± 14.7	86.0 ± 14.7	21.1 (35.2, 12.7)	11.4 (19.0, 6.8)	27.1 ± 8.1	19.7 ± 8.1
28	43.3 ± 6.8	80.7 ± 6.8	18.8 (33.6, 10.5)	18.9 (33.8, 10.5)	31.0 ± 9.2	28.5 ± 9.2
56	47.3 ± 7.2	72.3 ± 7.2	17.7 (30.1, 10.5)	22.9 (38.8, 13.5)	29.9 ± 9.3	38.2 ± 9.3
84	38.7 ± 13.2	95.7 ± 13.2	18.8 (29.5, 12.1)	20.0 (31.3, 13.5)	26.2 ± 9.1	33.5 ± 9.1

Table 5-3: Average BMD (g/cm^2) of total skeleton		
Day	MPA	Control
0	0.893 ± 0.028	0.937 ± 0.027
84	0.873 ± 0.021	0.917 ± 0.021

Table 5-4: Average $\varepsilon^{44/42}$Ca in urine (‰) ± SE		
Days	MPA	Control
-14, -13, -12, -11, -10, -7, -1, 0	2.11 ± 1.11	4.26 ± 1.11
1	-1.55 ± 1.35	1.41 ± 1.35
2	-0.89 ± 1.43	2.46 ± 1.43
4	-0.69 ± 1.79	1.15 ± 1.79
6, 7, 8	-2.93 ± 1.09	2.67 ± 1.09
14	-3.01 ± 0.71	3.05 ± 0.71
28	-2.83 ± 0.65	-1.73 ± 0.65
56	-1.50 ± 0.56	-0.97 ± 0.56
84	2.33 ± 0.58	1.89 ± 0.58

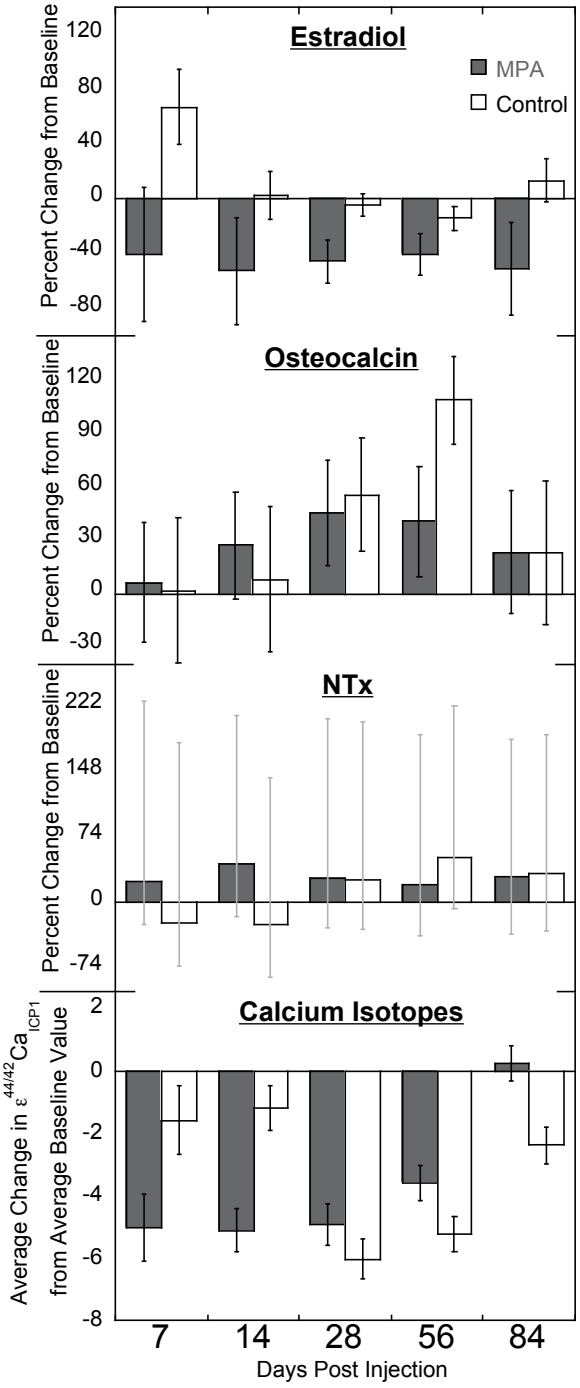

Figure 5-1 Change in Biomarker and Ca isotope values from baseline. Black error bars are SE around the mean. Gray error bars are 95% confidence intervals around the log transformed mean.

5.6 References

Abrams, S. A. (1999). Using stable isotopes to assess mineral absorption and utilization by children. Am J Clin Nutr *70*, 995-965.

Beck, A. B., Bugel, S., Sturup, S., Jensen, M., Molgaard, C., Hansen, M., Krogsgaard, O. W., and Sandstrom, B. (2003). A novel dual radio- and stable-isotope method for measuring calcium absorption in humans: comparison with the whole-body radioisotope retention method. Am J Clin Nutr *77*, 399-405.

Black, A., Talmont, E. M., Baer, D. J., Rumpler, W. V., Roth, G. S., and Lane, M. A. (2001a). Accuracy and precision od duel-energy X-ray absorptiometry for body composition measurments in rhesus monkeys. Journal of Medical Primatology *30*, 94-99.

Black, A., Talmont, E. M., Handy, A. M., Scott, W. W., Shapses, S. A., Ingram, D. K., Roth, G. S., and Lane, M. A. (2001b). A nonhuman primate Model of Age-Related Bone Loss: A Longitudinal Study in Male and Premenopausal Female Rhesus Monkeys. Bone *28*, 295-302.

Chu, N.-C., Henderon, G. M., Belshaw, N. S., and Hedges, R. E. M. (2006). Establishing the potential of Ca isotopes as poxy for consumption of dairy products. Applied Geochemistry *21*, 1656-1667.

Colman, R. J., Kemnitz, J. W., Lane, M. A., Abbott, D. H., and binkley, N. (1999). Skeletal effects of aging and menopausal status in female rhesus macaques. J Clin Endocrinol Metab *84*, 4144-4148.

Damilakis, J., Adams, J. E., Guglielmi, G., and Link, T. M. (2010). Radiation exposure in X-ray-based imaging techniques used in osteoporosis. Eur Radiol *20*, 2707-2714.

DePaolo, D. J. (2004). Calcium Isotopic Variations Produced by Biological, Kinetic, Radiogenic and Nucleosynthetic Processes, In Geochemistry of non-traditional stable isotopes, C. Johnson, B. Beard, and F. Albarede, eds. (Mineralogical Society of America), pp. 255-288.

Heuser, A., and Eisenhauer, A. (2010). A pilot study on the use of natural calcium isotopes (44Ca/40Ca) fractionation in urine as a proxy for the human body calcium balance. Bone *46*, 889-896.

Hirata, T., Tanoshima, M., Suga, A., Tanaka, Y.-k., Nagata, Y., Shinohara, A., and Chiba, M. (2008). Isotopic Analysis of Calcium in Blood Plasma and Bone from Mouse Samples by Multiple Collector-ICP-Mass Spectrometry. Analytical Science *24*, 1501-1507.

Jerome, C. P., and Peterson, P. E. (2001). Nonhuman primate models in skeletal research. Bone *29*, 1-6.

Kanis, J. A., McCloskey, E. V., Johansson, H., Oden, A., III, L. J. M., and Khaltaev, N. (2008). A reference standard for the description of osteoporosis. Bone *42*, 467-475.

Larkin, A., Sheahan, N., O'Connor, U., Gray, L., Dowling, A., Vano, E., Torbica, P., Salat, D., Schreiner, A., Neofotistou, V., and Malone, J. F. (2008). QA/ acceptance testing of DEXA X-ray systems used in bone mineral densitometry. Radiation Protection Dosimetry *129*, 279-283.

Leeming, D. J., Alexandersen, P., Karsdal, M. A., Qvist, P., Schaller, S., and Tanko, L. B. (2006). An update on biomarkers of bone turnover and their utility in biomedical research and clinical practice. Eur J Clin Pharmacol *62*, 781-792.

Manolagas, S. C. (2000). Birth and Death of Bone Cells: Basic Regulatory Mechanisms and Implications for the Pathogenesis and Treatment of Osteoporosis. Endocrine Reviews *21*, 115-137.

Meunier, P. J., Roux, C., Seeman, E., Ortolani, S., Badurski, J., Spector, T. D., Cannata, J., Balogh, A., Lemmel, E.-M., Pors-Nielsen, S.*, et al.* (2004). The effects of Strontium Ranelate on the Risk of Vertebral Fracture in Women with Postmenopausal Osteoporosis. The New England Journal of Medicine *350*, 459-468.

Pope, N. S., Gould, K. G., Anderson, D. C., and Mann, D. R. (1989). Effects of Age and Sex on Bone Density in the Rhesus Monkey. Bone *10*, 109-112.

Russell, W. A., Papanastassiou, D. A., and Tombrello, T. A. (1978). Ca isotope fractionation on the Earth and other solar system materials. Geochimica et Cosmochimica Acta *42*, 1075-1090.

Shackelford, L., LeBlanc, A., Driscoll, T. B., Evans, H. J., Rianon, N. J., Smith, S. M., Feeback, D. L., and Lai, D. (2004). Resistance exercise as a countermeasure to disues-induced bone loss. J Appl Physiol *97*, 119-129.

Skulan, J., Bullen, T., Anbar, A. D., Puzas, J. E., Shackelford, L., LeBlanc, A., and Smith, S. M. (2007). Natural Calcium Isotopic Composition of Urine as a Marker of Bone Mineral Balance. Clinical Chemistry *53*, 1155-1158.

Skulan, J., and Depaolo, D. J. (1999). Calcium Isotope Fractionation between Soft and Mineralized Tissue as a Monitor of Calcium Use in Vertebrates. Proceedings of the National Academy of Science *96*, 13709-13713.

Skulan, J., DePaolo, D. J., and Owens, T. L. (1997). Bilogical control of calcium isotopic abondances in the global calcium cycle. Geochimica et Cosmochimica Acta *61*, 2505-2510.

Smith, S. M., E., W. M., E., N. L., Shih, C. Y., Wiesmann, H., Nillen, J. L., and Lane, H. W. (1996). Calcium kinetics with microgram stable isotope dose and saliva sampling. J Mass Spectrom *31*, 1265-1270.

Smith, S. M., Wastney, M. E., O'Brien, K. O., Morunkov, B. V., Larina, I. M., Abrams, S. A., Davis-Street, J. E., Oganov, V., and Shackelford, L. (2005). Bone markers, calcium metabolism, and calcium kinetics during extended-duration space flight on Mir space station. J Bone Miner Res *20*, 208-218.

Sokal, R. R., and Rohlf, F. J. (1995). The Principles and Practice of Statistics in Biological Research, 3rd edn (New York: WH Freeman and Co).

Sorensen, M. G., Henriksen, K., Schaller, S., and Karsdal, M. A. (2007). Biochemical Markers in preclinical models of osteoporosis. Biomarkers *12*, 266-286.

Sturup, S., Hansen, M., and Molgaard, C. (1997). Measurements of 44Ca: 43Ca and 42Ca: 43Ca Isotopic Ratios in Urine using High Resolution

Inductively Coupled Plasma Mass Spectrometry. Journal of Analytical Atomic Spectrometry *12*, 919-923.

Wieser, M. E., Buhl, D., Bouman, C., and Schwieters, J. (2004). High precision calcium isotope ratio measurements using a magnetic sector multiple collector inductively coupled plasma mass spectrometer. J Anal At Spectrom *19*, 844-851.

Yeh, H. S., and Berenson, J. R. (2006). Treatment for myeloma bone disease. Clin Cancer Res *12*, 6279s-6284s.

Chapter 6

RAPIDLY ASSESSING CHANGES IN BONE MINERAL BALANCE USING NATURAL STABLE CALCIUM ISOTOPES

Jennifer L. L. Morgan[1]; Gwyneth W. Gordon[2]; Stephen J. Romaniello[2]; Joseph L. Skulan[3]; Scott M. Smith[4]; Ariel D. Anbar[1,2]

[1]Arizona State University, Department of Chemistry and Biochemistry, PO Box 871604, Tempe, AZ 85287

[2]Arizona State University, School of Earth and Space Exploration, PO Box 871404, Tempe, AZ 85287

[3]University of Wisconsin, Geology Museum, 1215 W. Dayton St. Madison, WI 53706

[4]Human Adaptation and Countermeasures Division, National Aeronautics and Space Administration Johnson Space Center, Houston, TX 77058

6.1 Introduction

Direct, quantitative measurement of short-term changes in bone mineral balance (BMB) would be of great utility in diagnosing and treating diseases such as osteoporosis, multiple myeloma and Paget's disease that lead to loss of bone mineral density (BMD)(Kanis et al., 2008; Yeh and Berenson, 2006). Currently, X-ray bone scans or histological biopsies are the only methods of measuring BMD in widespread clinical use. X-ray densitometry measurements expose patients to radiological hazards and histological biopsies are invasive (Damilakis

et al., 2010a). Both techniques can detect bone loss over long (3-12 months) time intervals when progressive bone loss is occurring, but are unable to rapidly assess small changes of BMB or BMD (Damilakis et al., 2010a). We hypothesize that natural variations in Ca isotopes provide a more rapid and safer alternative.[7] Bone formation produces a measurable mass-dependent fractionation in the natural isotopes of calcium (Ca), with bone being isotopically lighter than diet (Reynard et al., 2010; Skulan and Depaolo, 1999). Bone is resorbed in bulk, and the isotopically light reservoir of Ca from bone is released back into the blood stream and eventually to urine. Therefore, a shift to larger $^{44}Ca/^{42}Ca$ values in blood or urine should indicate a net positive BMB, while a shift to smaller $^{44}Ca/^{42}Ca$ should indicate net bone loss (Heuser and Eisenhauer, 2010; Skulan et al., 2007). Measurement of these variations does not require administration of an isotopic tracer or other diagnostic agents. In a study of individuals confined to bed rest, a condition known to induce negative BMB, we show that Ca isotope ratios shift in a direction consistent with negative net BMB after just 7 days, long before detectible changes in BMD occur. Consistent with this interpretation, the Ca isotope variations track changes observed in N-teleopeptide (NTx), a bone resorption biomarker,(Leeming et al., 2006; Sorensen et al., 2007) while bone alkaline phosphatase (BSAP), a biomarker of bone formation,(Leeming et al., 2006; Sorensen et al., 2007) is unchanged. Unlike biochemical markers, changes in Ca isotopes directly measure net BMB and can in principle be used to quantify changes in BMD. Ca isotopes indicate an average decrease of 0.62 ± 0.16 % in BMD over the course of this 30-day study. The Ca isotope technique should permit evaluation of countermeasures to bone loss, accelerate the pace of

discovery of new treatments for metabolic bone disease, and provide novel insights into the dynamics of bone metabolism.

Ca isotope variations are a result of the six naturally occurring Ca isotopes (^{40}Ca, ^{42}Ca, ^{43}Ca, ^{44}Ca, ^{46}Ca and ^{48}Ca) reacting at different rates depending on atomic mass. In soft tissue, these variations exist because bone formation depletes soft tissue of light Ca isotopes. Bone resorption releases that isotopically light Ca back into soft tissue. As a result, the Ca isotope composition of soft tissue should shift toward lighter values when bone is resorbed, and toward heavier values when bone is formed.

An earlier study observed variations in Ca isotope abundances correlated with bone density measurements and consistent with net bone resorption after 4 weeks in a 90-day bed rest study (data collected at 0, 4, 8 and 12 weeks)(Skulan et al., 2007). To assess how rapidly this signal appears, the present study centers on a 30-day bed rest study involving 12 patients on a controlled diet, monitored for 12 days prior to bed rest and 7 days post bed rest. Samples of urine were collected frequently throughout the study to examine short-term variations in Ca isotope abundances.

6.2 Results and Discussion

After 7 days of bed rest, the mean value of $\varepsilon^{44/42}$Ca decreases by approximately 3.0 ε* for all 12 patients (Figure 6-1C); $\varepsilon^{44/42}$Ca remains low during the remainder of bed rest and into the post bed rest period. This decrease is explained most simply as reflecting the onset of negative BMB. Since the patients entered the bed rest study at different times, systematic changes in the environment cannot explain the similar drop in $\varepsilon^{44/42}$Ca among all patients. The

patients' meals were on a 10-day diet rotation and study days did not correlate with the meal cycle. For the 12 days pre bed rest, the average $\varepsilon^{44/42}$Ca did not change systematically, but varied by approximately 1.5 ε. This intra-individual variability may result from differences in diet, metabolism or intestinal absorption. However, since each patient's $\varepsilon^{44/42}$Ca is compared to their pre-bed rest baseline, this intra-individual variation does not factor into assessment of bone loss.

Ca isotopes in urine and organic biomarkers in serum both indicate bone is being resorbed. NTx increases by day 9 of bed rest ($P<0.05$), the first sample measured after initiation of bed rest (Figure 6-1B). The NTx signal remains significantly elevated throughout bed rest and into the post bed rest period, consistent with the resorption of bone. BSAP, however, does not change during bed rest ($p>0.05$; Figure 6-1A). Bone formation includes a lag time for osteoblast cells to differentiate, which can take up to 30 days (Manolagas, 2000). Hence, a significant increase in bone formation rates is not expected on the time scale of this study. Bone resorption via osteoclastogenesis occurs much more rapidly than bone formation, with onset after just four days(Brage et al., 2004) . When taken together, $\varepsilon^{44/42}$Ca, NTx and BSAP give a complete view of the bone status of these patients undergoing bed rest.

NTx and BSAP are independent qualitative biomarkers of bone resorption and formation, respectively. They each measure a single process – bone formation or resorption – and so relating these markers to net BMB is only possible to the extent that the measurements of these markers in serum can be quantitatively correlated to the rates of each process. The quantitative correlation

of biomarkers to BMB is not possible at this time for several reasons. First, inter- and intra-personal variation in the response of each biomarker is high(Leeming et al., 2006; Sorensen et al., 2007). Second, the biomarkers of bone resorption and bone formation have different residence times in the body(Leeming et al., 2006; Sorensen et al., 2007). Third, the inter-laboratory variation is high(Leeming et al., 2006; Sorensen et al., 2007). In contrast: $\varepsilon^{44/42}$Ca directly reflects the net effect of bone resorption and formation; Ca has a 2-3 day residence time in the body,(Smith et al., 1996; Smith et al., 2005) so Ca isotopes can be used as a rapid measure of BMB; and the inter-laboratory variation of $\varepsilon^{44/42}$Ca is within the analytical uncertainty for a single lab.[†]

A major benefit of the Ca isotope method is the potential to use Ca isotopes to quantitatively assess bone loss. We have quantified the amount of bone lost during the 30-day bed rest study using the model of Skulan et al. and Heuser et al. (Heuser and Eisenhauer, 2010; Skulan and Depaolo, 1999) depicted in Figure 6-2A and detailed in Appendix B. In addition to measurements of $\varepsilon^{44/42}$Ca, the model requires that we estimate values for the fractionation of Ca isotopes between soft tissue and bone, the mass of skeletal Ca, and the rate of Ca intestinal absorption. We estimate the difference of $\varepsilon^{44/42}$Ca between soft tissue and bone is 6.5 ε*, which equals the offset of bone to diet in terrestrial vertebrates(Reynard et al., 2010; Skulan and Depaolo, 1999). To estimate the mass of skeletal Ca we use data from a modern skeletal population, and estimate ~1300 g of Ca is stored in the skeleton. The 1300 g Ca is calculated by assuming that the skeletal populations weight 3323.8 ± 779.6 g as measured in Silva et al.(Silva et al., 2009) are composed of hydroxyapatite. We neglect the

contribution of organics in the bone matrix. The amount of Ca absorbed in the diet can be estimated by assuming that 1 g of Ca is consumed everyday and, accounting for the bioavailability of different foods in the typical diet, we estimate that 275 mg is absorbed every day (Weaver et al., 1999; Weaver et al., 2006). Heuser et al. expanded the model of Skulan et al. to include Ca fractionation between serum and soft tissue, renal fractionation, and long-term variations in diet. Here, we avoid these complications by normalizing to each individual patient's baseline $\varepsilon^{44/42}$Ca. By performing this normalization, long-term variations in diet and insufficiently understood fractionations during Ca uptake and excretion can be safely ignored because the dietary Ca is tightly controlled during the study window for all patients and because the mechanism of renal excretion is not expected to change with bed rest(Whedon and Rambaut, 2006). The result is a simple and elegant mixing model that uses changes in urinary Ca isotopes to predict percent bone loss (Figure 6-2B).

Using this model, we estimate that patients lost on average 0.62 ± 0.16 % of bone mass between days 7 - 30 of bed rest. This rate of bone loss extrapolates to a loss of ~ 2.0 ± 0.50 % of skeletal mass over ~ 90 days. Such changes have been detected using DXA scans in long-term bed rest studies(Smith et al., 2002; Smith et al., 2005; Whedon and Rambaut, 2006). Therefore, the Ca isotope method yields quantitative results that are fully consistent with the best existing measures of changes in BMD.

Our demonstration that natural changes in Ca isotopes indicative of bone loss can be detected within a few days demonstrates the potential to dramatically shorten the experiment duration required for studies of bone metabolism by 60%

or more. Our ability to rapidly assess changes in BMB will provide insights into the dynamics of bone metabolism, accelerate the pace of discovery of new treatments for metabolic bone disease, and may be the basis for future techniques to assess changes in bone density in clinical settings.

6.3 Methods Summary

Bed rest was conducted in the General Clinical Research Center (GCRC) at the University of Texas Medical Branch. Bed rest conditions were rigorously controlled including room temperature, patient sleep and wake cycles, patient diet, and patient weight. During bed rest, subjects were confined to a strict 6° head down tilt bed rest. Subjects were monitored to ensure round-the-clock compliance. For this study, 12 patients with an average age of 36 ± 4 yrs were enrolled at different times throughout a 6-month period. Johnson Space Center Committee for the Protection of Human Subjects and the University of Texas Medical Branch Institutional Review Board approved the study protocol. All subjects provided written, informed consent prior to enrollment.

Urine, blood and food samples were collected from all patients. The urine was acidified with trace metal grade 20% HNO_3 and shipped to Arizona State University. Digestion, purification and measurement of selected samples followed the method of CHAPTER 4. Isotope compositions were measured by multiple collector inductively couple plasma mass spectrometry (MC-ICP-MS; ThermoScientific Neptune)(Wieser et al., 2004). The abundance ratio of $^{44}Ca/^{42}Ca$ can be measured using < 25 mg of Ca with a typical precision of ± 1.5 (± 2s) parts per ten thousand compared to a standard (epsilon, ε). Measurement

accuracy is based on comparison with published Ca isotope data obtained by other methods (TIMS).

Table 6-1 Summary of data for 12 patients in bed rest. Mean ± SE; number of samples			
Biomarker	unit	Average Pre-bed rest value Day -14 to 0	Average Value Day 7-30
BSPA	U/L	25.73 ± 1.66; 24	24.85 ± 1.66; 48
NTx	nmol/d	539.31 ± 31.15; 49	742.31 ± 33.97; 91
Ca isotopes	ε	2.4 ± 0.33; 47	0.9 ± 0.21; 116

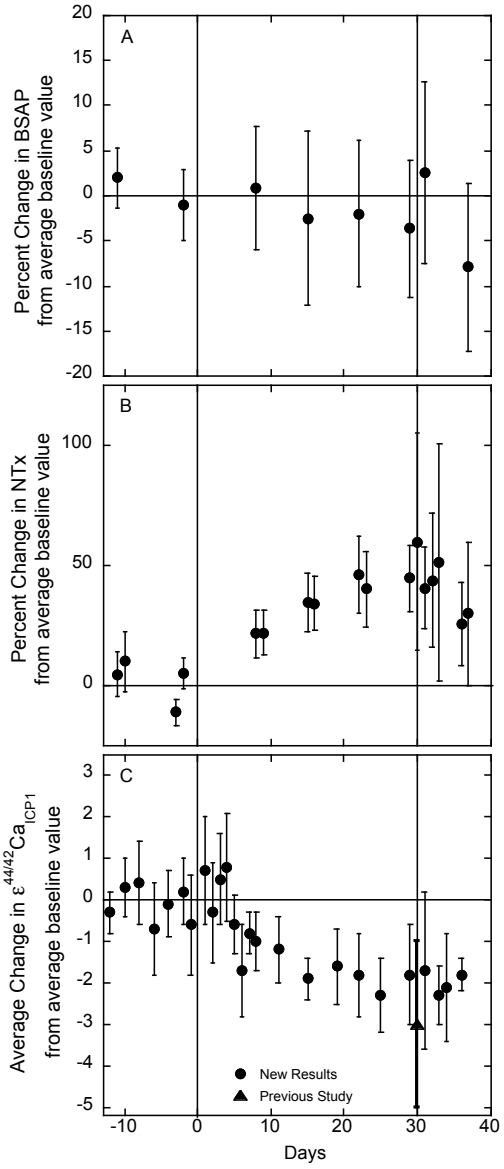

Figure 6-1 Change in Biomarker and Ca isotopes over bed rest.
A) Percent change from baseline in concentration of bone alkaline phosphatase (BSAP), a bone formation biomarker, (±2se, n=12). B) Percent change from baseline in concentration of NTx, a bone resorption biomarker, concentration from average baseline value (±2se, n=12). C) Urinary Ca isotope changes from baseline in bed rest urine samples (±2se, n=12). Changes were determined by calculating the difference between the measured value at each time point and the average of the pre-bed rest values for that individual. This difference determination was necessary because initial $\varepsilon^{44/42}$Ca varied among patients and is the same presentation method as traditional biomarkers. Decrease in $\varepsilon^{44/42}$Ca on about day 7 of bed rest reflects the onset of negative bone mineral balance. The 12 patients are averaged such that the values reported at each time point represent the mean (±2se) of all difference determinations from that time.

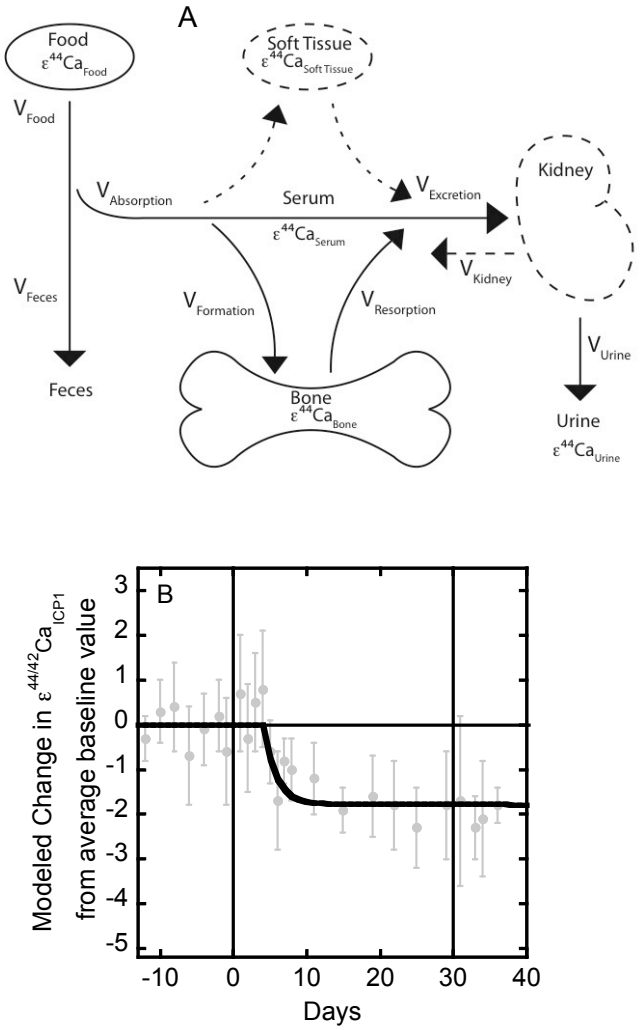

Figure 6-2 Model of Ca isotope fluxes.
A) Model of Ca isotope fluxes through the organism. B) Model fit for data.

6.4 References

† For comparison to literature values, the $\varepsilon^{44/42}Ca_{ICP1}$ value for IAPSO measured relative to ICP1 is 7.6 ± 1.5 ε and for SRM 915a is -1.5 ± 1.3 ε; all Ca isotope measurements are reported relative to ICP1.

* Ca data are reported as:

$$\varepsilon^{44/42}\mathrm{Ca} = \left[\frac{\left(\frac{^{44}\mathrm{Ca}}{^{42}\mathrm{Ca}}\right)_{\mathrm{Sample}} - \left(\frac{^{44}\mathrm{Ca}}{^{42}\mathrm{Ca}}\right)_{\mathrm{Standard}}}{\left(\frac{^{44}\mathrm{Ca}}{^{42}\mathrm{Ca}}\right)_{\mathrm{Standard}}} \right] \times 10{,}000$$

Brage, M., Lie, A., Ransjo, M., kasprzykowski, F., Kasprzykowska, R., Abrahamson, M., Grubb, A., and Lerner, U. H. (2004). Osteoclastogenesis is decreased by cystein proteinase inhibitors. Bone *34*, 412-424.

Damilakis, J., Adams, J. E., Guglielmi, G., and Link, T. M. (2010). Radiation exposure in X-ray-based imaging techniques used in osteoporosis. Eur Radiol *20*, 2707-2714.

Heuser, A., and Eisenhauer, A. (2010). A pilot study on the use of natural calcium isotopes (44Ca/40Ca) fractionation in urine as a proxy for the human body calcium balance. Bone *46*, 889-896.

Kanis, J. A., McCloskey, E. V., Johansson, H., Oden, A., III, L. J. M., and Khaltaev, N. (2008). A reference standard for the description of osteoporosis. Bone *42*, 467-475.

Leeming, D. J., Alexandersen, P., Karsdal, M. A., Qvist, P., Schaller, S., and Tanko, L. B. (2006). An update on biomarkers of bone turnover and their utility in biomedical research and clinical practice. Eur J Clin Pharmacol *62*, 781-792.

Manolagas, S. C. (2000). Birth and Death of Bone Cells: Basic Regulatory Mechanisms and Implications for the Pathogenesis and Treatment of Osteoporosis. Endocrine Reviews *21*, 115-137.

Reynard, L. M., Henderson, G. M., and Hedges, R. E. M. (2010). Calcium isotope ratios in animal and human bone. Geochimica et Cosmochimica Acta *74*, 3735-3750.

Silva, A. M., Crubezy, E., and Cunha, E. (2009). Bone Weith: new reference values based on a modern Portuguese identified skeletal collection. Int J Osteoarchaeol *19*, 628-641.

Skulan, J., Bullen, T., Anbar, A. D., Puzas, J. E., Shackelford, L., LeBlanc, A., and Smith, S. M. (2007). Natural Calcium Isotopic Composition of Urine as a Marker of Bone Mineral Balance. Clinical Chemistry *53*, 1155-1158.

Skulan, J., and Depaolo, D. J. (1999). Calcium Isotope Fractionation between Soft and Mineralized Tissue as a Monitor of Calcium Use in Vertebrates. Proceedings of the National Academy of Science *96*, 13709-13713.

Smith, S. M., E., W. M., E., N. L., Shih, C. Y., Wiesmann, H., Nillen, J. L., and Lane, H. W. (1996). Calcium kinetics with microgram stable isotope dose and saliva sampling. J Mass Spectrom *31*, 1265-1270.

Smith, S. M., Uchakin, P. N., and Torbin, B. W. (2002). Space flight nutrition research: platforms and analogs. Nutrition *18*, 926-929.

Smith, S. M., Wastney, M. E., O'Brien, K. O., Morunkov, B. V., Larina, I. M., Abrams, S. A., Davis-Street, J. E., Oganov, V., and Shackelford, L. (2005). Bone markers, calcium metabolism, and calcium kinetics during extended-duration space flight on Mir space station. J Bone Miner Res *20*, 208-218.

Sorensen, M. G., Henriksen, K., Schaller, S., and Karsdal, M. A. (2007). Biochemical markers in preclinical models of osteoporosis. Biomarkers *12*, 266-286.

Weaver, C. M., Proulx, W. R., and Heaney, R. (1999). Choices for achieving adequate dietary calcium with a vegiterian diet. Am J Clin Nutr *70*, 543-548.

Weaver, C. M., Rothwell, A. P., and Wood, K. V. (2006). Measuring calcium absorption and utilization in humans. Current Opinion in Clincal Nutrition and Metabolic Care *9*, 568-574.

Whedon, G. D., and Rambaut, P. C. (2006). Effects of long-duration space flight on calcium metabolism: Review of human studies from Skylab to the present. Acta Astronautica *58*, 59-81.

Wieser, M. E., Buhl, D., Bouman, C., and Schwieters, J. (2004). High precision calcium isotope ratio measurements using a magnetic sector multiple collector inductively coupled plasma mass spectrometer. J Anal At Spectrom *19*, 844-851.

Yeh, H. S., and Berenson, J. R. (2006). Treatment for myeloma bone disease. Clin Cancer Res *12*, 6279s-6284s.

BIBLIOGRAPHY

Abrams, S. A. (1999). Using stable isotopes to assess mineral absorption and utilization by children. Am J Clin Nutr *70*, 995-965.

Albrecht-Gary, A. M., and Crumbliss, A. L. (1998). Coordination chemistry of siderophores: Thermodynamics and kinetics of iron chelation and release, In Metal ions in biological systems, A. Sigel, and H. Sigel, eds. (CRC Press), pp. 239-316.

Anbar, A., Jarzecki, A. A., and Spiro, T. G. (2005). Theoretical investigation of iron isotope fractionation between (H2O)63+ and Fe(H2O)62+: implications for iron stable isotope geochemistry. Geochimica et Cosmochimica Acta *69*, 825-837.

Anbar, A., and Rouxel, O. (2007a). Metal stable isotopes in paleoceanography. Annu Rev Earth Pl Sci *35*, 717-746.

Anbar, A. D. (2004). Iron stable isotopes: beyond biosignatures. Earth Planet Sci Lett *217*, 223-236.

Anbar, A. D., Roe, J. E., Barling, J., and Nealson, K. H. (2000). Nonbiological Fractionation of Iron Isotopes. Science *288*, 126-128.

Anbar, A. D., and Rouxel, O. (2007b). Metal Stable Isotopes in paleoceanography. Annu Rev Earth Planet Sci *35*, 717-746.

Andren, H., Rodushkin, I., Stenberg, A., Malinovsky, D., and Baxter, D. C. (2004). Source of mass bias and isotope ratio variation in multi-collector ICP-MS: optimization of instrumental parameters based on experimental observations. J Anal At Spectrom *19*, 1217-1224.

Andrews, N. C. (2008). Forging a field: the golden age of iron biolgy. Blood *112*, 219-230.

Andrews, N. C., and Schmidt, P. J. (2007). Iron Homeostasis. Annu Rev Physiol *69*.

Arnold, G., Weyer, S., and Anbar, A. D. (2004a). Fe isotope variations in natural materials measured using high mass resolution multiple collector ICPMS. Anal Chem *76*, 322-327.

Arnold, G. L., Weyer, S., and Anbar, A. D. (2004b). Fe isotope variations in natural materials measured using high mass resolution multiple collector ICPMS. Anal Chem *76*, 322-327.

Barling, J., Arnold, G., and Anbar, A. D. (2001). Natural mass-dependent variations in the isotopic composition of molybdenum. Earth and Planetary Science Letters *193*, 447-457.

Beard, B. L., Johnson, C. M., Cox, L., Sun, H., Nealson, K. H., and Aguilar, C. (1999). Iron isotope biosignatures. Science *285*, 1889-1892.

Beard, B. L., Johnson, C. M., Skulan, J. L., Nealson, K. H., Cox, L., and Sun, H. (2003). Application of Fe isotopes to tracing the geochemical and biological cycling of Fe. Chem Geol *195*, 87-117.

Beck, A. B., Bugel, S., Sturup, S., Jensen, M., Molgaard, C., Hansen, M., Krogsgaard, O. W., and Sandstrom, B. (2003). A novel dual radio- and stable-isotope method for measuring calcium absorption in humans: comparison with the whole-body radioisotope retention method. Am J Clin Nutr *77*, 399-405.

Becker, J. S., Fullner, K., Seeling, U. D., Fornalczyk, G., and Kuhn, A. J. (2008). Measuing magnesium calcium and potassium isotope ratios using ICP-QMS with octopole collision cell in tracer studies of nutrient uptake and translocation in plants. Anal Bioanal Chem *390*, 571-578.

Bergquist, B. A., and Boyle, E. A. (2006). Iron isotopes in the Amazon River system: Weathering and transport signatures. Earth Planet Sci Lett *248*, 54-68.

Bigeleisen, J., and Mayer, M. G. (1947). Calculation of equilibrium constants for isotopic exchange reactions. J Chem Phys *15*, 261-267.

Black, A., Talmont, E. M., Baer, D. J., Rumpler, W. V., Roth, G. S., and Lane, M. A. (2001a). Accuracy and precision od duel-energy X-ray absorptiometry

for body composition measurments in rhesus monkeys. Journal of Medical Primatology *30*, 94-99.

Black, A., Talmont, E. M., Handy, A. M., Scott, W. W., Shapses, S. A., Ingram, D. K., Roth, G. S., and Lane, M. A. (2001b). A nonhuman primate Model of Age-Related Bone Loss: A Longitudinal Study in Male and Premenopausal Female Rhesus Monkeys. Bone *28*, 295-302.

Bothwell, T. H., Charlton, R. W., Cook, J. D., and Finch, C. A. (1979). Iron metabolism in man (Oxford: Blackwell Scientific).

Brage, M., Lie, A., Ransjo, M., kasprzykowski, F., Kasprzykowska, R., Abrahamson, M., Grubb, A., and Lerner, U. H. (2004). Osteoclastogenesis is decreased by cystein proteinase inhibitors. Bone *34*, 412-424.

Brantley, S. L., Liermann, L., and Bullen, T. D. (2001). Fractionation of Fe isotopes by soil microbes and organic acids. Geology *29*, 535-538.

Brantley, S. L., Liermann, L. J., Guynn, R. L., Anbar, A., Icopini, G. A., and Barling, J. (2004). Fe isotopic fractionation during mineral dissolution with and without bacteria. Geochimica et Cosmochimica Acta *68*, 3189-3204.

Bullen, T. D., White, A. F., Childs, C. W., Vivit, D. V., and Schulz, M. S. (2001). Demonstration of significant abiotic iron isotpe fractioant in nature. Geology *29*, 899-702.

Chen, J., Zhang, H., Tomuv, I., Ding, X., and Rentzepis, P. M. (2007). Electron transfer and dissocaition mechanism of ferrioxalate: A time resolved optical and EXAFS study. Chemical Physics Letters *437*, 50-55.

Chu, N.-C., Henderon, G. M., Belshaw, N. S., and Hedges, R. E. M. (2006). Establishing the potential of Ca isotopes as poxy for consumption of dairy products. Applied Geochemistry *21*, 1656-1667.

Colman, R. J., Kemnitz, J. W., Lane, M. A., Abbott, D. H., and binkley, N. (1999). Skeletal effects of aging and menopausal status in female rhesus macaques. J Clin Endocrinol Metab *84*, 4144-4148.

Criss, R. E. (1999). Principles of Stable Isotope Distribution (New York: Oxford University Press).

Damilakis, J., Adams, J. E., Guglielmi, G., and Link, T. M. (2010a). Radiation exposure in X-ray-based imaging techniques used in osteoporosis. Eur Radiol *20*, 2707-2714.

Damilakis, J., Adams, J. E., Guglielmi, G., and Link, T. M. (2010b). Radiation exposure in X-ray-based imaging techniques used in osteoporosis. Eur Radiol *20*, 2707-2714.

Dauphas, N., and Rouxel, O. (2006). Mass spectrometry and natrual variations of iron isotopes. Mass Spectrom Rev *25*, 515-550.

Dawson, P. H. (1976). Quadrupole Mass Spectrometry and its Application: Elsevier).

DeNiro, M. J., and Epstein, S. (1978a). Carbon isotopic evidence for different feeding patterns in two hyrax species occupying the same habitat. Science *201*, 906-908.

DeNiro, M. J., and Epstein, S. (1978b). Influence of deit on distribution of carbon isotopes in animals. Geochimica et Cosmochimica Acta *42*, 495-506.

DePaolo, D. J. (2004). Calcium Isotopic Variations Produced by Biological, Kinetic, Radiogenic and Nucleosynthetic Processes, In Geochemistry of non-traditional stable isotopes, C. Johnson, B. Beard, and F. Albarede, eds. (Mineralogical Society of America), pp. 255-288.

Dideriksen, K., Baker, J. A., and Stipp, S. L. S. (2006). Iron isotopes in natural minerals determined by MC-ICP-MS with a 58Fe-54Fe double spike. Geochimica et Cosmochimica Acta *70*, 118-132.

Dideriksen, K., Baker, J. A., and Stipp, S. L. S. (2008). Equilibrium Fe isotope fractionation between inorganic aqueous Fe(III) and the siderophore complex, Fe(III)-desferrioxamine B. Earth and Planetary Science Letters *269*, 280-290.

Domagal-Goldman, S. D., and Kubicki, J. D. (2008). Density functional theory predictions of equilibrium isotope fractionation of iron due to redox changes and organic complexation. Geochimica Et Cosmochimica Acta *72*, 5201-5216.

Domagal-Goldman, S. D., Paul, K. W., Sparks, D. L., and Kubicki, J. D. (2009). Quantum chemical study of the Fe(III)-desferrioxamine B siderophore complex-Electronic structure, vibrational frequencies, and equilibrium Fe-isotope fractionation. Geochimica Et Cosmochimica Acta *73*, 1-12.

Donovan, A., Roy, C. N., and Andrews, N. C. (2006). The ins and outs of iron homeostasis. Physiolgy *21*, 115-123.

Duan, Y., Anbar, A. D., Arnold, G. L., Lyons, T. W., Gordon, G. W., and Kendall, B. (2010). Molybdenum isotope evidence for mild environmental oxidation before the Great Oxidation Event. Geochimica et Cosmochimica Acta *74*, 6655-6668.

Fantle, M. S., and DePaolo, D. J. (2004). Iron isotopic fractionation during continental weathering. Earth Planet Sci Lett *228*, 547-562.

Fehr, M. A., Andersson, P. S., Halenius, U., and Morth, C. (2008). Iron isotope variations in Holocene sediments of the Gotland Deep, Baltic Sea. Geochimica et Cosmochimica Acta *72*, 807-826.

Fietzke, J., Eisenhauer, A., Gussone, N., Bock, B., Liebetrau, V., Nagler, T. F., Spero, H. J., Bijma, J., and Dullo, C. (2004). Direct measurement of 44Ca/40Ca ratios by MC-ICP-MS using cool plasma technique. Chemical Geology *206*.

Flament, P., Mattielli, N., Aimoz, L., Choel, M., Deboudt, K., de Jong, J., Rimetz-Planchon, J., and Weis, D. (2008). Iron isotopic fractionation in industrial emissions and urban aerosols. Chemosphere *73*, 1793-1798.

Galvez, N., Fernandez, B., Sanchez, P., Cuesta, R., Ceolin, M., Clemente-Leon, M., Trasobares, S., Lopez-Haro, M., Calvino, J. J., Stephan, O., and Dominguez-Vera, J. M. (2008). Comparative Structural and Chemical Studies of Ferritin Cores with Gradual Removal of their Iron Contents. J Am Chem Soc *130*, 8062-8068.

Green, R., Charlton, R., Seftel, H., and Bothwell, T. (1968). Body Iron Excreation in Man. Am J Med *45*, 336-353.

Halicz, L., Galy, A., Belshaw, N. S., and O'Nions, R. K. (1999). High-precision measurement of calcium isotopes in carbonates and related materials by multiple collector inductively coupled plasma mass spectrometry (MC-ICP-MS). J Anal At Spectrom *14*, 1835-1838.

Harris, D. C. (1978). Iron exchange between ferritin and transferrin in vitro. Biochemistry *17*, 3071-3078.

Hentze, M. W., Muckenthaler, M. U., and Andrews, N. C. (2004). Balancing Acts: Molecular Control of Mammalian Iron Metabolism. `Cell *117*, 285-297.

Hernlem, B., Vane, L., and Sayles, G. (1996). Stability constants for complexes of the siderophore desferrioxamine B with selected heavy metal cations. Inorganica chimica acta *244*, 179-184.

Heuser, A., and Eisenhauer, A. (2010). A pilot study on the use of natural calcium isotopes (44Ca/40Ca) fractionation in urine as a proxy for the human body calcium balance. Bone *46*, 889-896.

Hirata, T., Tanoshima, M., Suga, A., Tanaka, Y.-k., Nagata, Y., Shinohara, A., and Chiba, M. (2008). Isotopic Analysis of Calcium in Blood Plasma and Bone from Mouse Samples by Multiple Collector-ICP-Mass Spectrometry. Analytical Science *24*, 1501-1507.

Hotz, K., Augsburger, H., and Walczyk, T. (2011). Isotopic signatures of iron in body tissue as a potential biomarker for iron metabolism. J Anal At Spectrom.

Hunt, J. R., Zito, C. A., and Hohnson, L. K. (2009). Body iron excretion by healthy men and women. American Journal of Clinical Neutrition *89*, 1792-1798.

Hutchins, D., Witter, A., Butler, A., and Luther III, G. (1999). Competition among marine phytoplankton for different chelated iron species. Nature *400*, 858-861.

Jerome, C. P., and Peterson, P. E. (2001). Nonhuman primate models in skeletal research. Bone *29*, 1-6.

Johnson, C. M., Beard, B. L., and Roden, E. E. (2008). The iron isotope fingerprints of redox and biogeochemical cycling in modern and ancient Earth. Annu Rev Earth Pl Sc *36*, 457-493.

Johnson, C. M., Beard, B. L., Roden, E. E., Newman, D. K., and Nealson, K. H. (2004). Isotopic Constraints on Biogeochemical Cycling of Fe. Reviews in Mineralogy & Geochemistry *55*, 359-408.

Johnson, C. M., Skulan, J. L., Beard, B. L., Sun, H., Nealson, K. H., and Braterman, P. S. (2002). Isotopic fractionation between Fe(III) and Fe(II) in aqueous solutions. Earth Planet Sci Lett *195*, 141-153.

Jouvin, D., Louvat, P., Juillot, F., Marechal, C. N., and Benedetti, M. F. (2009). Zinc isotopic fractionation: why organic matters. Environ Sci Technol *43*, 5747-5754.

Kanis, J. A., McCloskey, E. V., Johansson, H., Oden, A., III, L. J. M., and Khaltaev, N. (2008). A reference standard for the description of osteoporosis. Bone *42*, 467-475.

Krayenbuehl, P.-A., Walczyk, T., Schoenberg, R., von Blanckenburg, F., and Schulthess, G. (2005). Hereditary hemochromatosis is reflected in the iron isotope composition of blood. Blood *105*.

Larkin, A., Sheahan, N., O'Connor, U., Gray, L., Dowling, A., Vano, E., Torbica, P., Salat, D., Schreiner, A., Neofotistou, V., and Malone, J. F. (2008). QA/ acceptance testing of DEXA X-ray systems used in bone mineral densitometry. Radiation Protection Dosimetry *129*, 279-283.

Leeming, D. J., Alexandersen, P., Karsdal, M. A., Qvist, P., Schaller, S., and Tanko, L. B. (2006). An update on biomarkers of bone turnover and their utility in biomedical research and clinical practice. Eur J Clin Pharmacol *62*, 781-792.

Lopes, T. J., Luganskaja, T., Spasie, M. V., Hentze, M. W., Muckenthaler, M. U., Schumann, K., and Reich, J. G. (2010). Systems analysis of iron

metabolism: the network of iron pools and fluxes. BMC System Biology *4*, 1-18.

Ludwig, K. R. (2008). Isoplot 3.6 (Berkeley Geochronology Center Spec. Pub).

Majestic, B. J., Anbar, A. D., and Herckes, P. (2009). Stable Isotopes as a Tool to Apportion Atmospheric Iron. Environ Sci Technol *43*, 4327-4333.

Manolagas, S. C. (2000). Birth and Death of Bone Cells: Basic Regulatory Mechanisms and Implications for the Pathogenesis and Treatment of Osteoporosis. Endocrine Reviews *21*, 115-137.

Marechal, C. N., Telouk, P., and Albarede, F. (1999). Precise analysis of copper and zinc isotopic compositions by plasma-source mass spectrometry. Chem Geol *156*, 251-273.

Martell, A., and Smith, R. (1989). Critical Stability Constants, Vol 1-6 (New York: Plenum).

Meunier, P. J., Roux, C., Seeman, E., Ortolani, S., Badurski, J., Spector, T. D., Cannata, J., Balogh, A., Lemmel, E.-M., Pors-Nielsen, S.*, et al.* (2004). The effects of Strontium Ranelate on the Risk of Vertebral Fracture in Women with Postmenopausal Osteoporosis. The New England Journal of Medicine *350*, 459-468.

Morgan, J. L. L., Wasylenki, L. E., Neuster, J., and Anbar, A. D. (2010). Fe isotope fractionation during equilibration of Fe-organic complexes. Environ Sci Technol *44*, 6095-6101.

Ohno, T., Shinohara, A., Kohge, I., Chiba, M., and Hirata, T. (2004). Isotopic Analysis of Fe in Human Red Blood Cells by Multiple Collector-ICP-Mass Spectrometry. Analytical Science *20*, 617-621.

Oi, T., Morioka, M., Ogino, H., and Kakihana, H. (1993). Fractionation of Calcium isotopes in Cation-Exchange Chromatography. Separation Science and Technology *28*, 1971-1983.

Osmond, C. B., Allaway, W. G., Sutton, B. G., Troughton, J. H., Queiroz, O., Luttge, U., and Winter, K. (1973). Carbon Isotope Discrimination in Photosynthesis of CAM Plants. Nature *246*, 41-42.

Ottonello, G., and Zuccolini, M. V. (2008). The iron-isotope fractionation dictated by the carboxylic functional: An ab-initio investigation. Geochimica Et Cosmochimica Acta *72*, 5920-5934.

Polyakov, V. B. (1997). Equilibrium fractionation of iron isotopes: Estimation from Mossbauer spectroscopy data. Geochimica et Cosmochimica Acta *61*, 4213-4217.

Polyakov, V. B., and Mineev, S. D. (2000). The use of Mossbauer spectroscopy in stable isotope geochemistry. Geochimica et Cosmochimica Acta *64*, 849-865.

Pope, N. S., Gould, K. G., Anderson, D. C., and Mann, D. R. (1989). Effects of Age and Sex on Bone Density in the Rhesus Monkey. Bone *10*, 109-112.

Raymond, K. N., and Carrano, C. J. (1979). Coordination chemistry and microbial iron transport. Accounts Chem Res *12*, 183-190.

Reynard, L. M., Henderson, G. M., and Hedges, R. E. M. (2010). Calcium isotope ratios in animal and human bone. Geochimica et Cosmochimica Acta *74*, 3735-3750.

Ripperger, S., and Rhkamper, M. (2007). Precise determination of cadmium isotope fractionation in seawater by double spike MC-ICPMS. Geochimica et Cosmochimica Acta *71*, 631-642.

Roe, J. E., Anbar, A. D., and Barling, J. (2003). Nonbiological fractionation of Fe isotopes: evidence of an equilibrium isotope effect. Chem Geol *195*, 69-85.

Russell, W. A., Papanastassiou, D. A., and Tombrello, T. A. (1978). Ca isotope fractionation on the Earth and other solar system materials. Geochimica et Cosmochimica Acta *42*, 1075-1090.

Schauble, E. A., Rossman, G. R., and Taylor, H. P. (2001). Theoretical estimates of equilibrium Fe-isotope fractionations from vibrational spectroscopy. Geochimica et Cosmochimica Acta *65*, 2487-2497.

Schmitt, A.-D., Gangloff, S., Cobert, F., Lemarchand, D., Stille, P., and Chabaux, F. (2009). High performance automated ion chromatography separation for Ca isotope measurements in geological and biological samples. J Anal At Spectrom *24*, 1089-1097.

Shackelford, L., LeBlanc, A., Driscoll, T. B., Evans, H. J., Rianon, N. J., Smith, S. M., Feeback, D. L., and Lai, D. (2004). Resistance exercise as a countermeasure to disues-induced bone loss. J Appl Physiol *97*, 119-129.

Shemin, D., and Rittenberg, D. (1946). The lifespan of the human red blood cell. J Biol Chem *166*, 627-626.

Siebert, C., Nagler, T. F., and Kramers, J. D. (2001). Determination of molybdenum isotope fractionation by double-spike multicollector inductively coupled plasma mass spectrometry. Geochemistry Geophysics Geosystems *2*, 1-16.

Silva, A. M., Crubezy, E., and Cunha, E. (2009). Bone Weith: new reference values based on a modern Portuguese identified skeletal collection. Int J Osteoarchaeol *19*, 628-641.

Simpson, L., Hearn, R., Merson, S., and Catterick, T. (2005). A comparison of double-focusing sector field ICP-MS, ICP-OES and octopole collision cell ICP-MS for the high-accuracy determination of calcium in human serum. Talanta *65*, 900-906.

Skulan, J., Bullen, T., Anbar, A. D., Puzas, J. E., Shackelford, L., LeBlanc, A., and Smith, S. M. (2007). Natural Calcium Isotopic Composition of Urine as a Marker of Bone Mineral Balance. Clinical Chemistry *53*, 1155-1158.

Skulan, J., and Depaolo, D. J. (1999). Calcium Isotope Fractionation between Soft and Mineralized Tissue as a Monitor of Calcium Use in Vertebrates. Proceedings of the National Academy of Science *96*, 13709-13713.

Skulan, J., DePaolo, D. J., and Owens, T. L. (1997). Bilogical control of calcium isotopic abondances in the global calcium cycle. Geochimica et Cosmochimica Acta *61*, 2505-2510.

Smith, S. M., E., W. M., E., N. L., Shih, C. Y., Wiesmann, H., Nillen, J. L., and Lane, H. W. (1996). Calcium kinetics with microgram stable isotope dose and saliva sampling. J Mass Spectrom *31*, 1265-1270.

Smith, S. M., Uchakin, P. N., and Torbin, B. W. (2002). Space flight nutrition research: platforms and analogs. Nutrition *18*, 926-929.

Smith, S. M., Wastney, M. E., O'Brien, K. O., Morunkov, B. V., Larina, I. M., Abrams, S. A., Davis-Street, J. E., Oganov, V., and Shackelford, L. (2005). Bone markers, calcium metabolism, and calcium kinetics during extended-duration space flight on Mir space station. J Bone Miner Res *20*, 208-218.

Soddy, F. (1914). Intra-atomic charge. Nature *92*, 399.

Sokal, R. R., and Rohlf, F. J. (1995). The Principles and Practice of Statistics in Biological Research, 3rd edn (New York: WH Freeman and Co).

Sorensen, M. G., Henriksen, K., Schaller, S., and Karsdal, M. A. (2007). Biochemical markers in preclinical models of osteoporosis. Biomarkers *12*, 266-286.

Stookey, L. (1970). Ferrozine-a new spectrophotometric reagent for iron. Anal Chem *42*, 779–781.

Sturup, S., Hansen, M., and Molgaard, C. (1997). Measurements of 44Ca: 43Ca and 42Ca: 43Ca Isotopic Ratios in Urine using High Resolution Inductively Coupled Plasma Mass Spectrometry. Journal of Analytical Atomic Spectrometry *12*, 919-923.

Sverjensky, D. A., Shock, E. L., and Helgeson, H. C. (1997). Prediction of thermodynamic properties in aqueous metal complexes to 1000°C and 5 kb. Geochimica et Cosmochimica Acta *61*, 1359-1412.

Thomson, J. J. (1913). Bakerian Lecture: Rays of Positive Electricity. Proceedings of the Royal Society of London *89*, 1-20.

Tipper, E. T., Louvat, P., Capmas, F., Galy, A., and Gaillardet, J. (2008). Accuracy of stable Mg and Ca isotope data obtained by MC-ICP-MS using the standard addition method. Chem Geol *257*, 65-75.

Urey, H. C. (1947). The thermodynamic properties of isotopic substances. J Chem Soc, 562-581.

Walczyk, T., and von Blanckenburg, F. (2002). Natural iron isotope variations in human blood. Science *295*, 2065-2066.

Walczyk, T., and von Blanckenburg, F. (2005). Deciphering the iron message in the human body. International Journal of Mass Spectrometry *242*, 117-134.

Walczyk, T., and von Blanckenburg, F. (2005). Deciphering the iron isotope message of the human body. Int J Mass Spectrom *242*, 117-134.

Watt, R. K., Hilton, R. J., and Graff, M. (2010). Oxido-reduction is not the only mechanism allowing ions to traverse the ferritin protein shell. Biochemica et Biophysica Acta *1800*, 745-759.

Weaver, C. M., Proulx, W. R., and Heaney, R. (1999). Choices for achieving adequate dietary calcium with a vegiterian diet. Am J Clin Nutr *70*, 543-548.

Weaver, C. M., Rothwell, A. P., and Wood, K. V. (2006). Measuring calcium absorption and utilization in humans. Current Opinion in Clincal Nutrition and Metabolic Care *9*, 568-574.

Welch, S. A., Beard, B. L., Johnson, C. M., and Braterman, P. S. (2003). Kinetic and equilibrium Fe isotope fractionation between aqueous Fe(II) and Fe(III). Geochimica et Cosmochimica Acta *67*, 4231-4250.

Weyer, S., and Schwieters, J. (2003a). High precision Fe isotope measurements with high mass resolution MC-ICPMS. Int J Mass Spectrom *226*, 355-368.

Weyer, S., and Schwieters, J. B. (2003b). High precision Fe isotope measurements with high mass resolution MC-ICPMS. International Journal of Mass Spectrometry *226*, 355-368.

Whedon, G. D., and Rambaut, P. C. (2006). Effects of long-duration space flight on calcium metabolism: Review of human studies from Skylab to the present. Acta Astronautica *58*, 59-81.

Wiederhold, J., Kraemer, S. M., Teutsch, N., Borer, P., Halliday, A., and Kretzschmar, R. (2006). Iron isotope fractionation during proton-promoted, ligand-controlled, and reductive dissolution of goethite. Environ Sci Technol *40*, 3787-3793.

Wieser, M. E., Buhl, D., Bouman, C., and Schwieters, J. (2004). High precision calcium isotope ratio measurements using a magnetic sector multiple collector inductively coupled plasma mass spectrometer. J Anal At Spectrom *19*, 844-851.

Yang, L. (2009). Accurate and Precise Determination of Isotopic Ratios by MC-ICP-MS: A Review. Mass Spectrometry Reviews *28*, 990-1011.

Yeh, H. S., and Berenson, J. R. (2006). Treatment for myeloma bone disease. Clin Cancer Res *12*, 6279s-6284s.

Zhu, X. K., Guo, Y., Williams, R. J. P., O'Nions, R. K., Matthews, A., Belshaw, N. S., Canters, G. W., Waal, E. C. d., Weser, U., Burgess, B. K., and Salvato, B. (2002). Mass fractionation process of transition metal isotopes. Earth Planet Sci Lett *200*, 47-62.

APPENDIX A

SUPPLEMENT TO CHAPTER 3

Calculating the Isotope Composition of Fe Fluxes

The isotope fractionations corresponding to the Fe fluxes shown in Figure 3-2 were calculated using a system of linear equations describing the isotope mass balance between various tissues. Derivation of each equation can be found below but Equation 1 is an example representing the flux of Fe into bone (where it is present primarily in bone marrow) and out of bone via the production of red blood cells (RBC):

$$\delta^{56/54}Fe_{Serum\text{-}Bone}F_{Serum\text{-}Bone} = \delta^{56/54}Fe_{Bone\text{-}RBC}\ F_{Bone\text{-}RBC} \quad (1)$$

The left side of the equation is the flux into bone multiplied by its isotope composition, and the right side of the equation is the flux out of bone multiplied by its isotope composition. The isotopic composition of these fluxes cannot be measured directly. However, we can calculate these values using Equations 2 and 3, which use the measured $\delta^{56/54}Fe_{serum}$, $\delta^{56/54}Fe_{bone}$, and the fractionations that occur during Fe incorporation into bone and RBCs ($\Delta^{56/54}Fe_{SerumtoBone}$, $\Delta^{56/54}Fe_{RBC,\ formation}$).

$$\delta^{56/54}Fe_{Serum\text{-}Bone} = \delta^{56/54}Fe_{Serum} - \Delta^{56/54}Fe_{Serum\text{-}Bone} \quad (2)$$

$$\delta^{56/54}Fe_{Bone\text{-}RBC} = \delta^{56/54}Fe_{Bone} - \Delta^{56/54}Fe_{Bone\text{-}RBC} \quad (3)$$

Equation 4 is the result of substituting Equation 2 and Equation 3 into Eq. 1 and rearranging the variables. Equation 4 is one of the six linear equations used to solve for the fractionation between organs.

$$\begin{aligned}\delta^{56/54}Fe_{serum}F_{Serum\text{-}Bone} - \delta^{56/54}Fe_{Bone}F_{Bone\text{-}RBC} \\ = \Delta^{56/54}Fe_{Serum\text{-}Bone}F_{Serum\text{-}Bone} - \Delta^{56/54}Fe_{Bone\text{-}RBC}F_{Bone\text{-}RBC}\end{aligned} \quad (4)$$

The fluxes are presented in Figure 3-2.

Sensitivity Analysis

The Fe isotope fractionation values and their associated uncertainties are derived from a combination of direct measurements and the isotopic mass balance model. In order to estimate the combined data and model errors, a Monte Carlo approach was used. The measured Fe isotope data were randomly sampled assuming the results were normally distributed with the mean values and standard deviations reported in Table 3-1. The values for a subset of the Fe fluxes used in the mass balance model were also randomly sampled assuming a 25% uncertainty, such that all of the remaining Fe fluxes were uniquely determined by the requirement for overall mass balance. After repeated iteration ($N=10^6$), the standard deviations of the tabulated results were reported as the combined model-data uncertainty (Figure 3-2). To assess the portion of error derived from either the isotope measurements or model uncertainties, the Monte Carlo process was repeated considering each source of error independently. In all cases, the uncertainty in the isotope measurements alone contributed >95% of the combined model-data error, implying that the exact choice of Fe fluxes do not significantly impact the calculated Fe isotope fractionations.

Derivation of the Mass Balance Equations:

Details of the derivation of the isotope mass balance equation for each pool in Figure 3-2 is given below.

Bone

$\delta_{Serum\text{-}Bone}F_{Serum\text{-}Bone}=\delta_{Bone\text{-}RBC}F_{Bone\text{-}RBC}$

$(\delta_{Serum}-\Delta_{Serum\text{-}Bone})F_{Serum\text{-}Bone} = (\delta_{Bone}-\Delta_{Bone\text{-}RBC})F_{Bone\text{-}RBC}$

$\delta_{Serum}F_{Serum\text{-}Bone} -\Delta_{Serum\text{-}Bone} F_{Serum\text{-}Bone} = \delta_{Bone}F_{Bone\text{-}RBC} -\Delta_{Bone\text{-}RBC} F_{Bone\text{-}RBC}$

$\mathbf{\delta_{Serum}F_{Serum\text{-}Bone} -\delta_{Bone}F_{Bone\text{-}RBC} =\Delta_{Serum\text{-}Bone} F_{Serum\text{-}Bone}-\Delta_{Bone\text{-}RBC} F_{Bone\text{-}RBC}}$

RBC

$\delta_{Bone\text{-}RBC}F_{Bone\text{-}RBC} =\delta_{RBC\text{-}Spleen}F_{RBC\text{-}Spleen}+ \delta_{Bleed}F_{Bleed}$

$(\delta_{Bone}-\Delta_{Bone\text{-}RBC})F_{Bone\text{-}RBC} = (\delta_{RBC}-\Delta_{bone})F_{RBC\text{-}Spleen}+(\delta_{RBC}-\Delta_{Bleed})F_{Bleed}$

$\delta_{Bone}F_{Bone\text{-}RBC} - \Delta_{Bone\text{-}RBC}F_{Bone\text{-}RBC} = \delta_{RBC}F_{Spleen} - \Delta_{RBC\ Spleen}F_{RBC\ Spleen} + \delta_{RBC}F_{Bleed} - \Delta_{Bleed}F_{Bleed}$

$(\Delta_{RBC\text{-}Spleen}, \Delta_{Bleed} \equiv 0)$

$\delta_{Bone}F_{Bone\text{-}RBC}-\delta_{RBC}F_{RBC\text{-}Spleen}-\delta_{RBC}F_{Bleed} = \Delta_{Bone\text{-}RBC}F_{Bone\text{-}RBC}$

SPLEEN

$\delta_{RBC\text{-}Spleen}F_{RBC\text{-}Spleen} = \delta_{Spleen\text{-}Serum}F_{Spleen\text{-}Serum}$

$(\delta_{RBC}-\Delta_{RBC\text{-}Spleen})F_{RBC\text{-}Spleen} = (\delta_{Spleen}-\Delta_{Spleen\text{-}Serum})F_{Spleen\text{-}Serum}$

$\delta_{RBC}F_{RBC\text{-}Spleen} - \Delta_{RBC\ Spleen}F_{RBC\ Spleen} = \delta_{Spleen}F_{Spleen\text{-}Serum} - \Delta_{Spleen\text{-}Serum}F_{Spleen\text{-}Serum}$ $(\Delta_{RBC\text{-}Spleen} \equiv 0)$

$-\delta_{Spleen}F_{Spleen\text{-}Serum} + \delta_{RBC}F_{RBC\text{-}Spleen} = -\Delta_{Spleen\text{-}Serum}F_{Spleen\text{-}Serum}$

LIVER

$\delta_{Serum\text{-}Liver}F_{Serum\text{-}Liver} = \delta_{Liver\text{-}Serum}F_{Liver\text{-}Serum}$

$(\delta_{Serum}-\Delta_{Serum\text{-}Liver})F_{Serum\text{-}Liver} = (\delta_{Liver}-\Delta_{Liver\text{-}Serum})F_{Liver\text{-}Serum}$

$\delta_{Serum}F_{Serum\text{-}Liver}-\Delta_{Serum\text{-}Liver}F_{Serum\text{-}Liver} = \delta_{Liver}F_{Liver\text{-}Serum} - \Delta_{Liver\ Serum}F_{Liver\ Serum}$ $(\Delta_{Liver\text{-}out} \equiv 0)$

$\delta_{Serum}F_{Serum\text{-}Liver}-\delta_{Liver}F_{Liver\text{-}Serum} = \Delta_{Serum\text{-}Liver}F_{Serum\text{-}Liver}$

OTHER

$\delta_{Serum\text{-}Other}F_{Serum\text{-}Other} = \delta_{Other\text{-}Serum}F_{Other\text{-}Serum} + \delta_{Other\text{-}out}F_{Other\text{-}out}$

$(\delta_{Serum}-\Delta_{Serum\text{-}Other})F_{Serum\text{-}Other} = (\delta_{other}-\Delta_{Other\text{-}Serum})F_{Other\text{-}Serum} + (\delta_{Other}-\Delta_{Other\text{-}out})F_{Other\text{-}out}$

$\delta_{Serum}F_{Serum\text{-}Other} - \Delta_{Serum\text{-}Other}F_{Serum\text{-}Other} = \delta_{other}F_{Other\text{-}Serum} - \Delta_{Other\ Serum}F_{Other\ Serum} + \delta_{Other}F_{other\text{-}out}$

$- \Delta_{Other\text{-}out}F_{Other\text{-}out}$ $(\Delta_{Other\text{-}Serum}, \Delta_{Other\text{-}out} \equiv 0)$

$\delta_{Serum}F_{Serum\text{-}Other} - \delta_{Other}F_{Other\text{-}out} - \delta_{Other}F_{Other\text{-}Serum} = \Delta_{Serum\text{-}Other}F_{Serum\text{-}Other}$

SERUM

$\delta_{Absorption}F_{Absorption} + \delta_{Spleen\text{-}Serum}F_{Spleen\text{-}Serum} + \delta_{Other\text{-}Serum}F_{Other\text{-}Serum} + \delta_{Liver\text{-}Serum}F_{Liver\text{-}Serum} = \delta_{Serum\text{-}Bone}F_{Serum\text{-}Bone} + \delta_{Serum\text{-}Liver}F_{Serum\text{-}Liver} + \delta_{Serum\text{-}Other}F_{Serum\text{-}Other}$

$(\delta_{Food}-\Delta_{Absorption})F_{Absorption}+(\delta_{Spleen}-\Delta_{Spleen-Serum})F_{Spleen-Serum}+(\delta_{other}-\Delta_{Other-Serum})F_{Other-Serum}+(\delta_{Liver}-\Delta_{Liver-Serum})F_{Liver-Serum}=(\delta_{Serum}-\Delta_{Serum-Bone})F_{Serum-Bone}+(\delta_{Serum}-\Delta_{Serum-Liver})F_{Serum-Liver}+(\delta_{Serum}-\Delta_{Serum-Other})F_{Serum-Other}$

$\delta_{Food}F_{Absorption}-\Delta_{Absorption}F_{Absorption}+\delta_{Spleen}F_{Spleen-Serum}-\Delta_{Spleen-Serum}F_{Spleen-Serum}+\delta_{other}F_{Other-Serum}-\Delta_{Other\ Serum}F_{Other\ Serum}+\delta_{Liver}F_{Liver-Serum}-\Delta_{Liver\ Serum}F_{Liver\ Serum}=\delta_{Serum}F_{Serum-Bone}-\Delta_{Serum-Bone}F_{Serum-Bone}+\delta_{Serum}F_{Serum-Liver}-\Delta_{Serum-Liver}F_{Serum-Liver}+\delta_{Serum}F_{Serum-Other}-\Delta_{Serum-Other}F_{Serum-Other}$

$\mathbf{\delta_{Food}F_{Absorption}+\delta_{Spleen}F_{Spleen-Serum}+\delta_{other}F_{Other-Serum}+\delta_{Liver}F_{Liver-Serum}-\delta_{Serum}F_{Serum-Bone}-\delta_{Serum}F_{Serum-Liver}-\delta_{Serum}F_{Serum-Other}=\Delta_{Absorption}F_{Absorption}+\Delta_{Spleen-Serum}F_{Spleen-Serum}-\Delta_{Serum-Bone}F_{Serum-Bone}-\Delta_{Serum-Liver}F_{Serum-Liver}-\Delta_{Serum-Other}F_{Serum-Other}}$

WHOLE MOUSE

$\delta_{Absorption}F_{Absorption}=\delta_{Other-out}F_{Other-out}+\delta_{Bleed}F_{Bleed}$

$(\delta_{Food}-\Delta_{Absorption})F_{Absorption}=(\delta_{Other}-\Delta_{Other-out})F_{Other-out}+(\delta_{Blood}-\Delta_{Bleed})F_{Bleed}$

$\delta_{Food}F_{Absorption}-\Delta_{Absorption}F_{Absorption}=\delta_{Other}F_{EXC}-\Delta_{EXC}F_{EXC}+\delta_{Blood}F_{Bleed}-\Delta_{Bleed}F_{Bleed}$ ($\Delta_{Other-out}$, $\Delta_{Bleed} \equiv 0$)

$\mathbf{\delta_{Food}F_{in}-\delta_{Other}F_{Other-out}-\delta_{Blood}F_{Bleed}=\Delta_{Absorption}F_{Absorption}}$

APPENDIX B

SUPPLEMENT TO CHAPTER 6

In order to interpret our results and quantify the rate the of bones loss in bed rest patients, we used the model of Ca isotope fractionation originally presented by Skulan and Depaolo (1999). The simple model is depicted in Figure 1-5.

$$N_b \frac{d\delta_b}{dt} = V_b(\delta_s - \Delta_b - \delta_b) \quad (1)$$

$$N_s \frac{d\delta_s}{dt} = V_d(\delta_d - \delta_s) - V_b\Delta_b + V_l(\delta_b - \delta_s) \quad (2)$$

The model was implemented as a time-dependent system of ordinary differential equations and integrated in MATLAB, yielding time-dependent predictions of soft tissue $^{44}Ca/^{42}Ca$ directly corresponding to measurements in our study. We found the best fit between the model and data could be obtained by include a 4 day lag between the onset of bed rest and the onset of bone loss (negative BMB). We believe this lag corresponds to and is justified by the time required for osteoblastogenesis.

APPENDIX C

HUMAN AND ANIMAL SUBJECT TESTING APPROVAL

ASU Arizona State University
Research and Economic Affairs

Office of Research Integrity and Assurance

To:	Ariel Anbar PSF
From:	Carol Johnston, Chair Biosci IRB
Date:	12/11/2009
Committee Action:	**Renewal**
Renewal Date:	12/11/2009
Review Type:	Expedited F2
IRB Protocol #:	0812003532
Study Title:	Rapid Measurements of Bone Loss using Tracer-less Ca Isotope Analysis of Blood and Urine
Expiration Date:	12/10/2010

The above-referenced protocol was given renewed approval following Expedited Review by the Institutional Review Board.

It is the Principal Investigator's responsibility to obtain review and continued approval of ongoing research before the expiration noted above. Please allow sufficient time for reapproval. Research activity of any sort may not continue beyond the expiration date without committee approval. Failure to receive approval for continuation before the expiration date will result in the automatic suspension of the approval of this protocol on the expiration date. Information collected following suspension is unapproved research and cannot be reported or published as research data. If you do not wish continued approval, please notify the Committee of the study termination.

This approval by the Biosci IRB does not replace or supersede any departmental or oversight committee review that may be required by institutional policy.

Adverse Reactions: If any untoward incidents or severe reactions should develop as a result of this study, you are required to notify the Biosci IRB immediately. If necessary a member of the IRB will be assigned to look into the matter. If the problem is serious, approval may be withdrawn pending IRB review.

Amendments: If you wish to change any aspect of this study, such as the procedures, the consent forms, or the investigators, please communicate your requested changes to the Biosci IRB. The new procedure is not to be initiated until the IRB approval has been given.

Please retain a copy of this letter with your approved protocol.

ASU Knowledge Enterprise Development

Office of Research Integrity and Assurance

To:	Ariel Anbar PSF
From:	Carol Johnston, Chair Biosci IRB
Date:	12/06/2010
Committee Action:	**Renewal**
Renewal Date:	12/06/2010
Review Type:	Expedited F2
IRB Protocol #:	0812003532
Study Title:	Rapid Measurements of Bone Loss using Tracer-less Ca Isotope Analysis of Blood and Urine
Expiration Date:	12/05/2011

The above-referenced protocol was given renewed approval following Expedited Review by the Institutional Review Board.

It is the Principal Investigator's responsibility to obtain review and continued approval of ongoing research before the expiration noted above. Please allow sufficient time for reapproval. Research activity of any sort may not continue beyond the expiration date without committee approval. Failure to receive approval for continuation before the expiration date will result in the automatic suspension of the approval of this protocol on the expiration date. Information collected following suspension is unapproved research and cannot be reported or published as research data. If you do not wish continued approval, please notify the Committee of the study termination.

This approval by the Biosci IRB does not replace or supersede any departmental or oversight committee review that may be required by institutional policy.

Adverse Reactions: If any untoward incidents or severe reactions should develop as a result of this study, you are required to notify the Biosci IRB immediately. If necessary a member of the IRB will be assigned to look into the matter. If the problem is serious, approval may be withdrawn pending IRB review.

Amendments: If you wish to change any aspect of this study, such as the procedures, the consent forms, or the investigators, please communicate your requested changes to the Biosci IRB. The new procedure is not to be initiated until the IRB approval has been given.

Please retain a copy of this letter with your approved protocol.

APPENDIX D

PERMISSION TO REPRINT FIGURES

ELSEVIER LICENSE
TERMS AND CONDITIONS

Mar 23, 2011

This is a License Agreement between Jennifer L. L. Morgan ("You") and Elsevier ("Elsevier") provided by Copyright Clearance Center ("CCC"). The license consists of your order details, the terms and conditions provided by Elsevier, and the payment terms and conditions.

All payments must be made in full to CCC. For payment instructions, please see information listed at the bottom of this form.

Supplier	Elsevier Limited The Boulevard,Langford Lane Kidlington,Oxford,OX5 1GB,UK
Registered Company Number	1982084
Customer name	Jennifer L. L. Morgan
Customer address	2405 S. 107th Dr Avondale, AZ 85323
License number	2631400619934
License date	Mar 17, 2011
Licensed content publisher	Elsevier
Licensed content publication	International Journal of Mass Spectrometry
Licensed content title	High precision Fe isotope measurements with high mass resolution MC-ICPMS
Licensed content author	S. Weyer, J. B. Schwieters
Licensed content date	1 May 2003
Licensed content volume number	226
Licensed content issue number	3
Number of pages	14
Start Page	355
End Page	368
Type of Use	reuse in a thesis/dissertation
Portion	figures/tables/illustrations
Number of figures/tables/illustrations	4
Format	both print and electronic
Are you the author of this Elsevier article?	No

ELSEVIER LICENSE
TERMS AND CONDITIONS

Mar 23, 2011

This is a License Agreement between Jennifer L. L. Morgan ("You") and Elsevier ("Elsevier") provided by Copyright Clearance Center ("CCC"). The license consists of your order details, the terms and conditions provided by Elsevier, and the payment terms and conditions.

All payments must be made in full to CCC. For payment instructions, please see information listed at the bottom of this form.

Supplier	Elsevier Limited The Boulevard,Langford Lane Kidlington,Oxford,OX5 1GB,UK
Registered Company Number	1982084
Customer name	Jennifer L. L. Morgan
Customer address	2405 S. 107th Dr Avondale, AZ 85323
License number	2631400730854
License date	Mar 17, 2011
Licensed content publisher	Elsevier
Licensed content publication	International Journal of Mass Spectrometry
Licensed content title	High precision Fe isotope measurements with high mass resolution MC-ICPMS
Licensed content author	S. Weyer, J. B. Schwieters
Licensed content date	1 May 2003
Licensed content volume number	226
Licensed content issue number	3
Number of pages	14
Start Page	355
End Page	368
Type of Use	reuse in a thesis/dissertation
Intended publisher of new work	other
Portion	figures/tables/illustrations
Number of figures/tables/illustrations	1
Format	both print and electronic

Dear Jennifer

The Royal Society of Chemistry hereby grants permission for the use of the material specified below in the work described and in all subsequent editions of the work for distribution throughout the world, in all media including electronic and microfilm. You may use the

material in conjunction with computer-based electronic and information retrieval systems, grant permissions for photocopying, reproductions and reprints, translate the material and to publish the translation, and authorize document delivery and abstracting and indexing services. The Royal Society of Chemistry is a signatory to the STM Guidelines on Permissions (available on request).

Please note that if the material specified below or any part of it appears with credit or acknowledgement to a third party then you must also secure permission from that third party before reproducing that material.

Please ensure that the published article carries a credit to The Royal Society of Chemistry in the following format:

[Original citation] – Reproduced by permission of The Royal Society of Chemistry

and that any electronic version of the work includes a hyperlink to the article on the Royal Society of Chemistry website. The recommended form for the hyperlink is http://dx.doi.org/10.1039/*DOI suffix*, for example in the link http://dx.doi.org/10.1039/b110420a the DOI suffix is 'b110420a'. To find the relevant DOI suffix for the RSC paper in question, go to the Journals section of the website and locate your paper in the list of papers for the volume and issue of your specific journal. You will find the DOI suffix quoted there.

Regards

Gill Cockhead
Contracts & Copyright Executive

Gill Cockhead (Mrs), Contracts & Copyright Executive
Royal Society of Chemistry, Thomas Graham House
Science Park, Milton Road, Cambridge CB4 0WF, UK
Tel +44 (0) 1223 432134, Fax +44 (0) 1223 423623
http://www.rsc.org

BIOGRAPHICAL SKETCH

JENNIFER L. L. MORGAN
CURRICULM VITAE

Chemistry and Biochemistry
Arizona State University
jennifer.l.morgan@asu.edu
Tempe, AZ 85287-1404
www.JenniferLLMorgan.com
Cell: 602-214-8312

EDUCATION

2011	Ph.D.	Arizona State University	Chemistry and Biochemistry

Thesis: Non-Traditional Stable Isotope Variations: Applications for Biomedicine

2007	M.S.	Arizona State University	Chemistry and Biochemistry
2005	B.S.	Baylor University	Chemistry and Biochemistry

APPOINTMENTS

2008 - 2011	Graduate Research Assistant Dept. of Chemistry and Biochemistry Arizona State University
2005 - 2008	Teaching Assistant Dept. of Chemistry and Biochemistry Arizona State University
2003 – 2005	Undergraduate Research Fellow Dept. of Chemistry and Biochemistry Baylor University

PEER-REVIEWED PUBLICATIONS

Jennifer L. L. Morgan, Laura E. Wasylenki, Jochen Neuster, Ariel D. Anbar; Fe isotope fractionation during Equilibration of Fe-Organic Complexes; *Environ. Sci. Technol.*, 2010, 44 (16), pp 6095-6101

Patricia E. Carigan, Joseph G. Hentz, Gwyneth Gordon, Jennifer L. L. Morgan, Massimo Raimondo, Ariel D. Anbar, and Laurence J. Miller (2007). Distinctive Heavy Metal Composition of Pancreatic Juice in Patients with Pancreatic Carcinoma. *Cancer Epidemiol Biomarkers Prev*, 16(12). 2656 – 2663.

J.W. Karban, J. L. Morgan, J.M. Dees, and K.K. Klausmeyer (2004). 2-(4-tert Butylbenzyl)-3-phenylinden-1-one. *Acta Cryst.* E60, o2304-o2305.

MANUSCRIPTS IN PREPARATION OR REVIEW

Jennifer L. L. Morgan, Gwyneth W. Gordon, Ruth C. Arrua, Joseph L. Skulan, Ariel D. Anbar; High precision measurement of variations in calcium isotope ratios in biomedical materials by multiple collector inductively coupled plasma mass spectrometry (MC-ICP-MS); *Analytical Chemistry*; (Submitted February 2011)

Jennifer L. L. Morgan, Gwyneth W. Gordon, Stephen J. Romaniello, Joseph L. Skulan, Ariel D. Anbar; Whole organism Fe isotope mass balance: implications for the study of Fe metabolism in vivo; *Biometals*; (in preparation)

Glass JB, R Raiswell, JLL Morgan, GA Hamilton, JA Shipp, KM Noonan, RL Mestek, S Neuer, HE Hartnett, AD Anbar. Growth of an Arctic diatom with nanoparticulate iron: implications for the supply of bioavailable iron from icebergs. In review at *Marine Chemistry (*Submitted January 2011)

Jennifer L. L. Morgan, Gwyneth W. Gordon, David H. Abbott, Ricki J. Colman; Joseph L. Skulan, Ariel D. Anbar; Rapid changes in bone mineral balance in response to estrogen depletion in Rhesus Monkeys detected using tracer-less calcium stable isotope technique; *Journal of Clinical Endocrinology*; (in preparation)

Jessie Shipp, George A. Hamilton, Jennifer L. L. Morgan, Yevgeniy Marusenko, Michael Keebaugh, Hansina Hill, Arnab Dutta, Xiaoding Zhuo, Nabin Upadhyay, James Hutchings, Pierre Herckes, Ariel Anbar, Everett Shock, Hilairy Hartnett; Bioavailability of Nanoparticulate Hematite to *Arabidopsis thaliana*; *Journal of Environmental Monitoring*; (Submitted March 2011)

CONTRIBUTED PRESENTATIONS* AND POSTERS

J.L.L. Morgan, D.H. Abbott, A.D. Anbar, G. Gordon, J.L. Skulan, R.J. Colman (2010) Rapid Changes in Bone Mineral Balance in Response to Estrogen Depletion in Rhesus Monkeys Detected Using Tracer-less Calcium Stable Isotope Technique. ASU-Mayo Research Symposium. Scottsdale, AZ

J.L.L. Morgan, D.H. Abbott, A.D. Anbar, G. Gordon, J.L. Skulan, R.J. Colman (2010) Rapid Changes in Bone Mineral Balance in Response to Estrogen Depletion in Rhesus Monkeys Detected Using Tracer-less Calcium Stable Isotope Technique. BioMetals. Tucson, AZ

J.L.L. Morgan, D.H. Abbott, A.D. Anbar, G. Gordon, J.L. Skulan, R.J. Colman (2010) Rapid Changes in Bone Mineral Balance in Response to Estrogen Depletion in Rhesus Monkeys Detected Using Tracer-less Calcium Stable

Isotope Technique. ENDO. San Diego, Ca

J.L.L. Morgan, L.E. Wasylenki, J. Nuester, A.D. Anbar (2010). Fe isotope fractionation during equilibration of Fe-organic complexes. Gordon Research Conference: Environmental Bioinorganic Chemistry. Newport, RI.

***J.L. Morgan**, G. Gordon, J. Skulan, A. D. Anbar (2010) Development of Fast Throughput Method using MC-ICP-MS to measure Ca Isotopes as a Maker of Bone Mineral Balance. NASA Human Research Program Investigators Workshop. Houston, TX.

S. Smith, J. Skulan, **J.L. Morgan**, G. Gordon, T.D. Bullen, A.D. Anbar (2009) Rapid Measurement of Bone Loss Using Tracer-less Calcium Isotope Analysis of Blood and Urine. NASA Human Research Program Investigators Workshop. Houston, TX.

J.L. Morgan, L.E. Wasylenki, A.D. Anbar (2008). Effect of organic ligand chelation on iron isotope fractionation. Gordon Research Conference: Environmental Bioinorganic Chemistry. Waterville Valley, NH.

***J.L. Morgan**, L.E. Wasylenki, A.D. Anbar (2008). Effect of organic ligand chelation on iron isotope fractionation. Southern California Geobiology Symposium. Los Angeles, CA.

J.L. Morgan, L.E. Wasylenki, A.D. Anbar (2007). Effect of organic ligand chelation on iron isotope fractionation. Southern California Geobiology Symposium. Pasadena, CA.

F. Wolfe-Simon**, J. Morgan**, J.J. Elser, and A. D. Anbar (2006). Metallomic plasticity of cyanobacteria induced by iron availability. Gordon Research Conference: Environmental Bioinorganic Chemistry. Andover, NH.

G.W. Gordon, P. Carrigan, **J.L. Morgan**, J. Elser, L. Miller, A.D. Anbar (2006). Metals, Medicine and Mass Spectrometry. Interdisciplinary science symposia. Tempe, AZ

RESEARCH AND INSTRUMENTATION EXPERIENCE

Research experience with trace-metal-free clean lab operations, X-Series ICP-MS, Neptune MC-ICP-MS, sterile technique, BSL-2 operations, and wet chemistry including IC and LC.

Experience with AA, CV, GS/MS, LC/MS, HPLC, NMR, X-ray crystallography, organic synthesis, cell cultures, and plant cultures.

HONORS, AWARDS AND FUNDING

Graduate Research Travel Grant, ASU Graduate College, 2008

SERVICE

Departmental

2006-2007 Vice-President. Chemistry Graduate Student Council
2005-2006 First year rep. on Graduate Admissions committee. Chemistry Graduate Student Council

Community

2009-Present Vice-President. Valley Dogs Rescue
2005-2009 Intake Coordinator, Valley Dogs Rescue

TEACHING EXPERIENCE

Spring 2008 Teaching Assistant: CHM 326 Analytical Chem. Lab (ASU)
Designed experiments and syllabus

Fall 2007 Teaching Assistant: CHM 113 General Chem. (ASU)
Weekly lab and recitation sections

Spring 2007 Teaching Assistant: CHM 453 Inorganic Chem. (ASU)
CHM 325 Analytical Chem. (ASU)
Grader and one-on-one tutor

Fall 2006 Teaching Assistant: CHM 101 Introductory Chem. (ASU)
Weekly lab and recitation sections

Spring 2006 Teaching Assistant: CHM 113 General Chem. I (ASU)
Weekly lab and recitation sections

Fall 2005 Teaching Assistant: CHM 114 General Chem. (ASU)
Weekly lab and recitation sections

STUDENT MENTORING

2007-Present Michael Wimmer (ASU), Chemistry Undergraduate Research Thesis 2011

PROFESSIONAL DEVELOPMENT

Phlebotomy Certification 16 hour training, PACE, 2009

Professional Development Strategies for success workshop, Graduate College Arizona State University (4 Workshops attended)

Fundamental Intellectual Property, ASU Special Course, 2006

LANGUAGE PROFICIENCY

American Sign Language (Fluent)

GRADUATE ADVISOR* AND DISSERTATION COMMITTEE

Ariel D. Anbar*, Anne K. Jones, Laura E. Wasylenki and Everett Shoc